NTNU
Norwegian University of
Science and Technology

# Recycling and Utilisation of Secondary Aluminium Products

Ingrid Meling

Materials Science and Engineering (MTMT)
Submission date: June 2018
Supervisor: Gabriella Tranell, IMA
Co-supervisor: Anne Kvithyld, Sintef

Norwegian University of Science and Technology
Department of Materials Science and Engineering

# Preface

This report is a Master´s thesis concerning recycling of aluminium and utilisation of aluminium by-products. The thesis has been written for the Department of Materials Science and Engineering at NTNU, Trondheim during the spring of 2018. The work was carried out in cooperation with Hydro Aluminium Rolled Products´ aluminium recycling plant in Holmestrand, Norway. Their objectives were highly considered when designing the contents of the thesis, and materials were chosen in close cooperation with them.

Trondheim, 2018-06-10

Ingrid Meling

# Acknowledgment

Firstly, I would like to thank my supervisors professor Gabriella Tranell and senior research scientist Anne Kvithyld for their great help, motivation and guidance along the way. In addition, the insights from Mertol Gökelma are much appreciated.

I would further like to thank André Granå from Hydro Aluminium Rolled Products for being very helpful and contributing to interesting discussions.

The practical help of Arne Nordmark, Kurt Sandaunet, Dmitry Slizovskiy, Irene Bragstad and Jonas Einan Gjøvik is also much appreciated. Thank you also to Torild Krogstad for preparing my ICP-MS samples, Syverin Lierhagen for performing the ICP-MS analyses, and Morten Peder Raanes for conducting EPMA analyses. In addition, the help from Kai Erik Ekstrøm concerning FactSage calculations was immensely helpful.

The work was funded by SFI Metal Production and the BEST project, and I am thankful for having been able to conduct the work through their financial contribution.

I.M.

# Abstract

Efficient utilisation of secondary aluminium products is increasingly important as the energy consumption and $CO_2$ emissions are greatly reduced by recycling compared to primary production. The aim of this study was to compare the recyclability of used beverage cans to incinerator metal, and investigate the efficiency of an environmentally friendly salt flux. In addition, an alternative to traditional recycling was executed to potentially increase the utilisation of dross.

Used beverage can scrap and incinerator metal were melted under two different salt fluxes in two different induction furnaces – one 20 cl. crucible and one 500 cl. crucible. For the small-scale experiments the coalescence was measured by sieving the resulting metal pieces. In the larger scale experiments, the yield was measured through a mass balance and the metal was analysed through inductively coupled plasma mass spectrometry and electron probe analyser.

Furthermore, clean aluminium and dross were charged into a pre-prepared molten CaO-$SiO_2$ slag at 1600°C for the purpose of aluminothermic reduction of $SiO_2$. The resulting metal and slag phases were chemically analysed by inductively coupled plasma mass spectrometry and electron probe analyser, and compared to results obtained by thermodynamic modelling.

The results indicate that the incinerator metal is highly recyclable, as it is easily coalesced and produce yields in the same region as used beverage cans. However, lead contaminations are present in the raw material leading to relatively high lead contents in the resulting metal, which could be detrimental for the finished product.

As for the salts, the operating temperature seems to be of importance for their performance. Temperatures close to the salts' solidification temperature result in low yield, which is also confirmed by theory. In the small-scale experiments, the recycled salt seemed to perform very well, while the two salts perform approximately equal in the larger scale experiments.

Moreover, from the preliminary experiments on aluminothermic reduction, dross seems like a suitable reducing material for aluminothermic reduction, as the chemical composition is very close to that obtained for clean aluminium. However, the obtained chemical compositions deviate from the theoretical composition, most likely due to the solidification procedure.

# Sammendrag

Effektiv utnyttelse av sekundære aluminiumsprodukter er av økt viktighet ettersom energiforbruk og $CO_2$-utslipp kan reduseres kraftig ved resirkulering sammenlignet med primærproduksjon. Målet med oppgaven var å sammenligne resirkulerbarheten til brukte brusbokser og forbrennigsmetall, og undersøke effekten av en miljøvennlig saltflux. I tillegg har et alternativ til tradisjonell resirkulering blitt gjennomført for å potensielt øke utnyttelsen av dross.

Brukte brusbokser og forbrenningsmetall ble smeltet med to forskjellige saltfluxer i to forskjellige induksjonsovner – en 20 cl. digel og en 500 cl. digel. I småskalaforsøkene ble koagguleringen målt ved sikting av de resulterende metallbitene. I de større forsøkene ble utbytte målt ved en massebalanse, og metallet ble analysert ved induktivt koblet plasma massespektrometri og elektronsondeanalysator.

Videre ble rent aluminium og dross tilsatt til en forhåndspreparert smeltet CaO-$SiO_2$ slagg ved 1600°C med hensikt å redusere $SiO_2$ aluminotermisk. De resulterende metall- og slaggfasene ble kjemisk analysert ved induktivt koblet plasma massespektrometri og elektronsondeanalysator, og sammenlignet med resultater fra termodynamisk modellering.

Resultatene indikerer at forbrenningsmetallet er høyst resirkulerbart, ettersom det er lett å koagulere og produserer omtrent samme utbytte som brukte brusbokser. Blykontaminering er tilstede i forbrennigsmetallet som fører til relativt høye blyinnhold i det resulterende metallet, som kan være ødeleggende for det ferdige produktet.

For saltene virker temperaturen å være viktig for deres virkning. Temperaturer nær saltenes størkningstemperatur resulterer i lavt ubytte, som også blir bekreftet av teorien. I småskalaforsøkene virker det resirkulerte saltet å fungere veldig bra, mens de to saltene virker omtrent like bra i de større forsøkene.

Fra de innledende aluminotermiske forsøkene virker dross å være et passende materiale for aluminotermisk reduksjon, ettersom den kjemiske komposisjonen er veldig nær den kjemiske komposisjonen oppnådd ved bruk av rent aluminium. Allikevel varierer de kjemiske komposisjonene fra teortiske verdier, mest sannsynlig på grunn av størkningsforløpet.

# Contents

# List of Figures

# Chapter 1

# Introduction

Aluminium is an important material for the world society. It is widely used due to its good isolating and conducting properties, flexible structure, high corrosion resistance and ability to be shaped into all kinds of products [1, 2]. It is used extensively in cars, constructions and food packaging to mention a few. Pure aluminium is a soft material, but it can be hardened by alloying. It is also a light material, having a density of 2700g/cm$^3$ compared to approximately 8000g/cm$^3$ for steel [3], making it a good option for use in vehicles, planes and buildings.

## 1.1 Primary production of aluminium

Primary aluminium is produced through an electrolysis process known as the Hall-Héroult process. A typical electrolysis cell can be seen in Figure 1.1. Alumina ($Al_2O_3$) is dissolved in cryolite ($Na_3AlF_6$) and reduced to metallic aluminium according to reaction 1.1 by carbon anodes and cathodes. Producing one tonne of aluminium theoretically consumes 334kg C, accumulating over 1200kg $CO_2$. In addition, 13-15 kWh of electricity is needed to produce one tonne of aluminium [3], making primary production of aluminium the most power-consuming industry in Norway [4]. Furthermore, the Bayer process, where alumina is produced from bauxite ore, is an energy demanding process which produces red mud as a by-product [3].

$$\frac{1}{2}Al_2O_3(diss) + \frac{3}{4}C(s) = Al(l) + \frac{3}{4}CO_2(g) \tag{1.1}$$

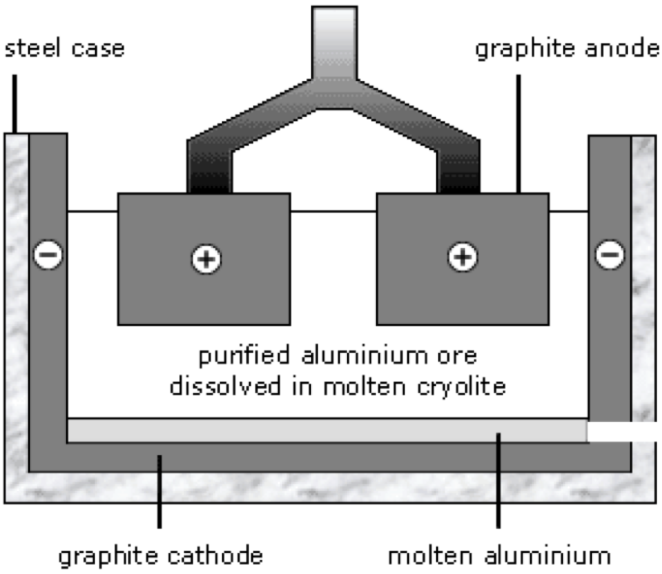


Figure 1.1: Schematic drawing of a typical aluminium electrolysis cell [5]

## 1.2 Secondary production of aluminium

Recycling aluminium, known as secondary production, can reduce the energy consumption by 95% compared to primary production [6, 7, 8]. As environmental aspects and $CO_2$ emissions are of high global interest, efficient methods for recycling aluminium are becoming increasingly important.

In addition to the energy savings, there exist several other benefits to recycling. Firstly, waste is reduced as the scrap goes back into the value chain instead of being landfilled and disposed [8]. Secondly, less aluminium will have to be produced primarily. This results in less bauxite mining, reducing the amount of red mud which creates challenges due to contamination of the local population and landfilling [3]. Furthermore, $CO_2$ emissions can be greatly reduced. As mentioned in Section 1.1, using carbon as anode for reduction of $Al_2O_3$ leads to high $CO_2$ emissions. According to Henryson and Goldman [9], the $CO_2$ emissions can be reduced by 10 tons per ton aluminium by recycling compared to primary production.

Another important aspect is the increasing demand of aluminium worldwide. Especially the car industry, where more and more parts are made of aluminium, increases the demand. From 1990 to 2012, the aluminium content in cars increased by 180% [10]. According to Ducker Worldwide [11], a further increase of 25% is expected from today until 2025. This increased demand will create more aluminium scrap, as well as an increased demand for bauxite mining if the materials are not recycled.

The recycling process should be a continuous and closed loop, as illustrated in Figure 1.2.

It is important that the losses are held to a minimum, even though some losses of metal are inevitable in each step. As shown in Figure 1.2, there are three main losses in the process.


Figure 1.2: Recycling loop [12]

Firstly, we will never be able to collect all the scrap. Scrap collection is essential for the recycling rate, and is in large part up to the consumer. The next step is sorting the scrap before remelting, which will generate some aluminium waste. The scrap ought to be well separated and cleaned before melting, to get a good yield and high quality. Recycled aluminium has the same quality demands as primary aluminium, which makes it important that few impurities are introduced into the melt [8]. Finally, there are some losses in the actual remelting process. Some aluminium will be skimmed off when removing the oxide layer on top of the metal bath, called slag. Oxidation of the aluminium will also occur to a varying degree, lowering the metal recovery.

Due to the losses in the recycling process, it is not given that recycling is the most efficient way of utilising the generated scrap. Some scrap types generate high losses due to non-metallic compounds complicating the remelting procedure. Therefore, exploring alternatives to recycling is highly relevant.

## 1.3 Objectives

This thesis consists of two main parts. The first part deals with traditional recycling of aluminium scrap. Experiments varying salt and scrap types have been investigated through

coalescence and yield experiments. The objectives of the work were to compare the coalescence behaviour and metal yield of different salts and scraps, and investigate alternatives to the scraps and salts being used in Norway today. Therefore, a recycled salt and aluminium from an incineration facility were studied to see how these performed in comparison to materials being used in the Norwegian industry.

The second part of the thesis consists of investigating an alternative way of utilising aluminium scrap, as traditional recycling might not be the most suitable way of utilising all types of scraps and by-products. The method chosen was aluminothermic production of silicon, using clean aluminium and dross as the reducing materials. The aim was to see how well dross performed compared to clean aluminium, and if dross is a suitable material for this use. To answer these questions, chemical analyses and equilibrium calculations have been executed and compared to theoretical data from FactSage [13].

# Chapter 2

# Theoretical background

In this chapter, the theoretical background behind the experimental work is presented. The chapter presents the general material flow of aluminium and includes several aspects of recycling of aluminium, in particular salt fluxing and recycling of used beverage cans and incinerator metal. In addition, production of silicon both carbothermically and aluminothermically is explained. The section goes into detail about the CaO-$SiO_2$-$Al_2O_3$ slag system, possible reduction materials and comparing the two production routes. Relevant literature on the topics is presented.

## 2.1 Material flow

As evident from Figure 2.1, the world production of aluminium has increased rapidly since 1995, as the blue line shows. From Figure 2.2, it is clear that the observed growth is mainly due to the increased production in China. For the other countries and continents the production has been quite stable over the past decades, including Western Europe [14].

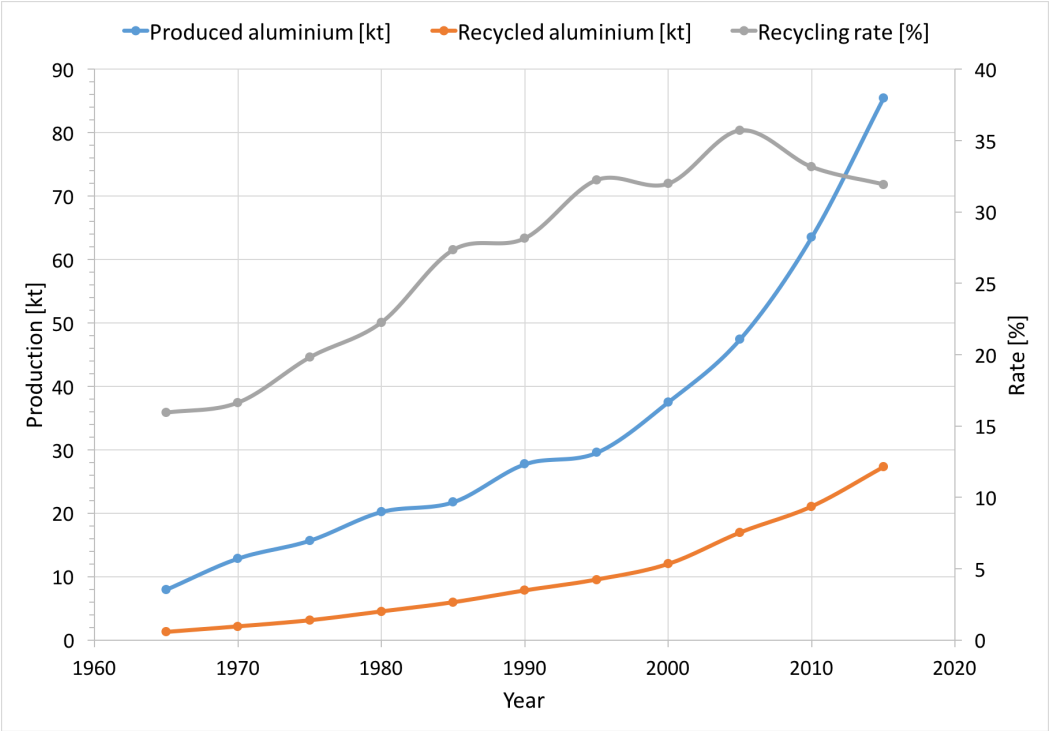


Figure 2.1: World production of aluminium from 1965 to 2015 [15]

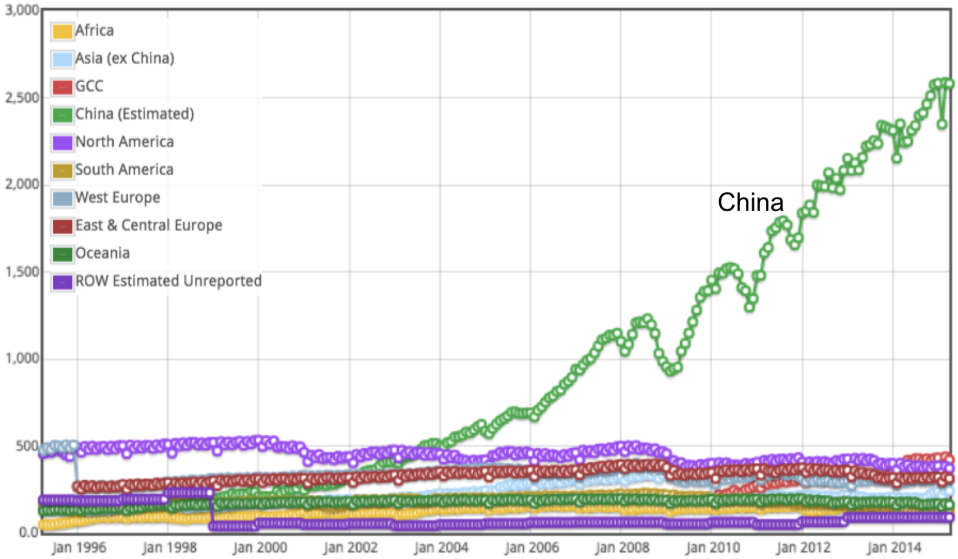


Figure 2.2: World production of aluminium according to geographical location [14]

Figure 2.1 also shows the amount of recycled aluminium, which has increased from under 20% in 1965 to over 30% in 2015 [15]. The world production of aluminium in 2015 was 85.4 kt. Of this, 27.3 kt was recycled aluminium, corresponding to 31.9% of the total production. Of the recycled aluminium, 65% came from end-of-life products, while the rest was recovered from different processing steps [15]. 21.4% of the collected scrap was disposed or incinerated, corresponding to 5.4% of the worldwide produced aluminium [10]. In Europe,

the disposal and incineration rate is three times higher per capita than for the rest of the world [16].

Figure 2.3 shows the import and export rates for various parts of the aluminium life cycle, from production to end-of-life (EOL) management. As the blue poles indicate, Europe imports quite a lot in the early processing steps, while the export rates are high for manufacturing and scrap management [16]. According to numbers from 2016, over 80% of the exported scrap ends up in Asia, mainly China and India [17]. A desire from the European Commission is to obtain a circular economy within Europe, making Europe less dependent on other countries [18]. For this to be possible, it is important that the scrap produced is handled within Europe, and not exported.

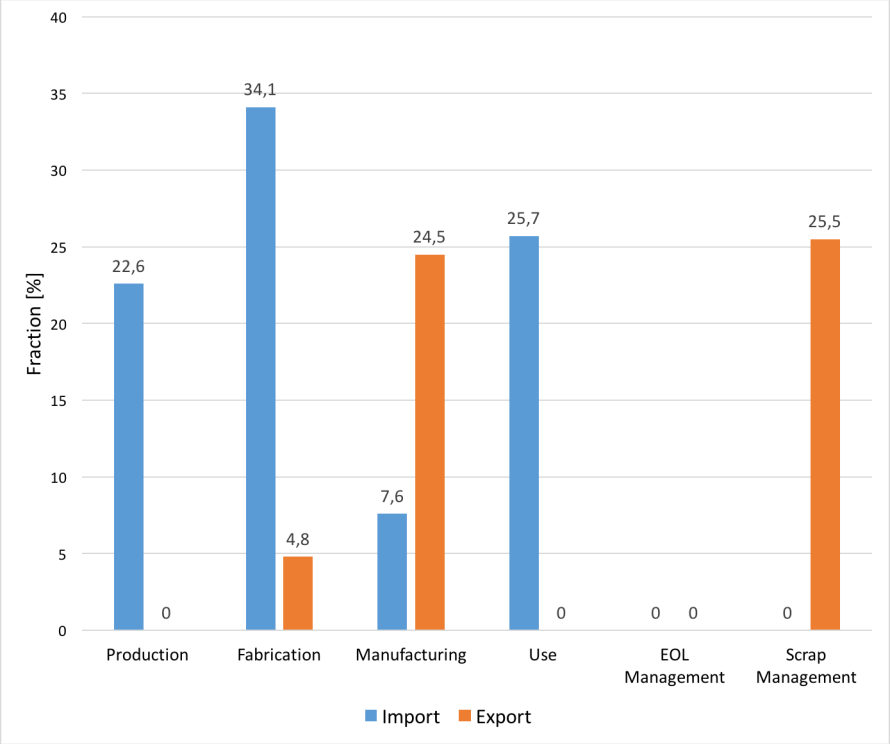


Figure 2.3: Import and export rates for different steps of the aluminium flow [16]

## 2.2 Route for recycling of aluminium

As an alternative to the primary production route, recycling aluminium scrap is an energy saving option. Figure 2.4 shows the energy consumption of primary production (blue poles) and recycling (yellow pole). Clearly, primary production is a lot more energy demanding, with electrolysis being the largest contributor to the high energy consumption. Over 80% of the energy needed is in fact used during the electrolysis step. On the other hand, recycling aluminium only uses a fraction of the energy (approximately 4.5%) compared to primary production [19].

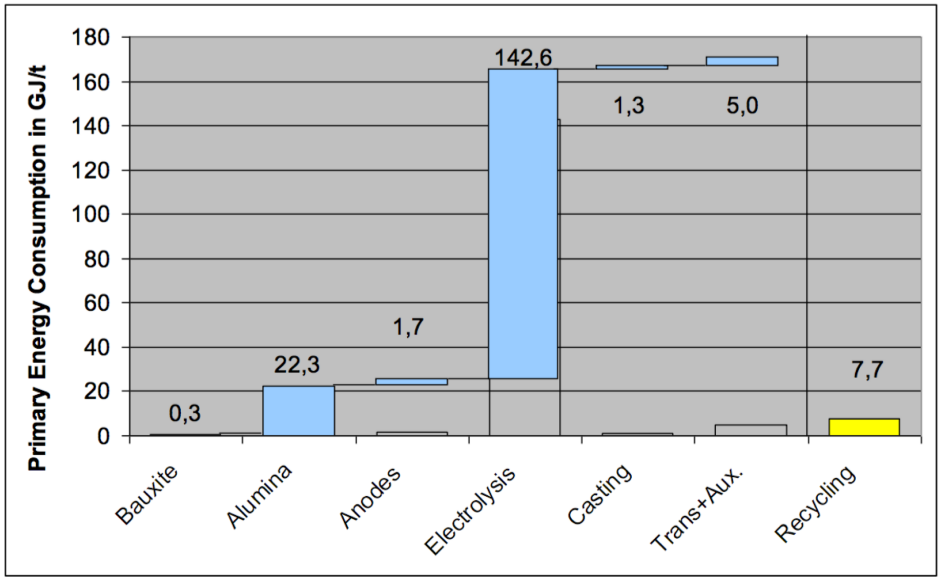


Figure 2.4: Energy consumption of different steps in primary production versus recycling [19].

### 2.2.1 Scrap remelting technologies

There exist several furnaces used for recycling aluminium depending on geometry and size of the scrap, and degree of contamination. Some furnaces are for relatively clean and homogeneous scraps, while others deal with heavily contaminated scraps. Figure 2.5 shows different types of scraps and how easily recyclable they are. Large products with low degree of contamination are the easiest, while small, highly contaminated products are the most difficult. If the products are highly contaminated, shredders, dryers and delacquerers might be used as a pre-step before melting to remove various contaminants [20, 21].

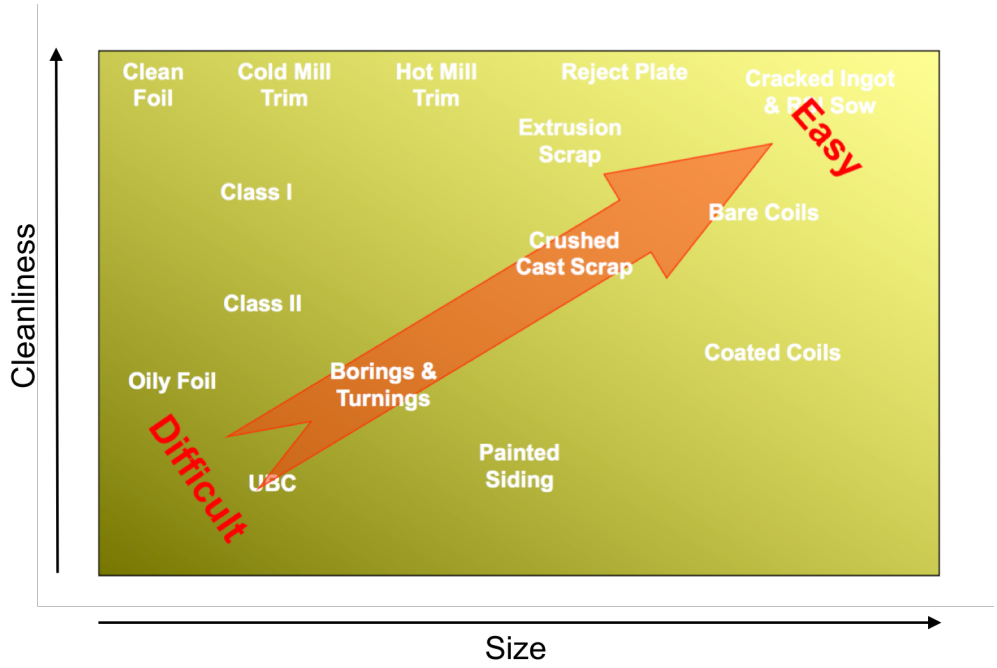


Figure 2.5: Representation of different scrap materials and their recyclability [21].

## The rotary furnace

For recycling of heavily contaminated scraps, a rotary furnace is normally used. A sketch of a typical rotary furnace is shown in Figure 2.6. The furnace rotates around its own axis, in addition to being tilted at a chosen angle. The rotation speed and angle are controlled by the furnace operators, which vary from plant to plant. By utilising a rotary furnace, the energy consumption can be lowered by up to 15%, while the metal recovery can be increased by up to 5% [22] compared to conventional remelting furnaces. The furnace is operated using a salt flux, which prevents oxidation of the melt. The heat source is called a burner, which burns natural gas with oxygen to produce the necessary heat to melt the materials [23].

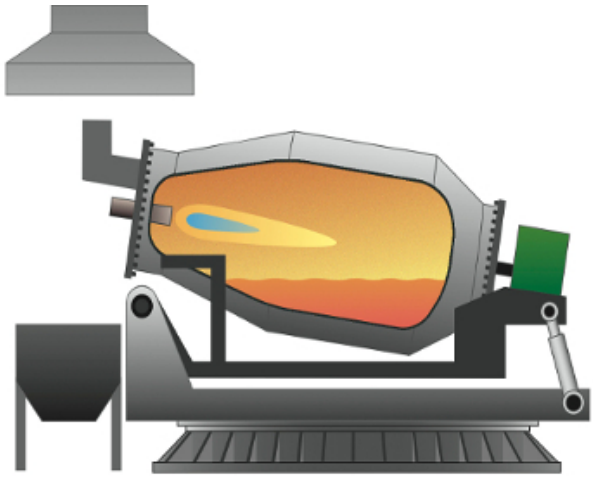

Figure 2.6: Schematic drawing of a typical rotary furnace [24]

Figure 2.7 shows the general melting cycle. It is a batch process, so one batch of material is melted and emptied before the next batch is charged. The material with blue color is the metal, while the red is the slag. First, the furnace is charged with scrap and salt (Step 1), and the materials are melted while the furnace rotates around its own axis (Step 2). When melting is complete, the liquid aluminium is poured out, while the slag is left in the furnace (Step 3). The furnace is rotated further to tap the remaining aluminium in the slag (Steps 4 and 5), before the slag is tapped in a separate container (Step 6) [22].

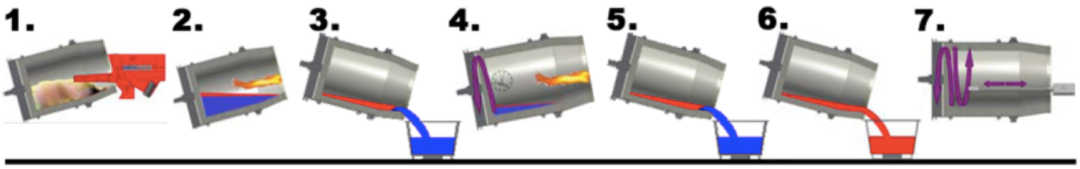


Figure 2.7: Melting process in a rotary furnace [22]

Figure 2.8 shows the inside of the rotary furnace under operation. The rotation leads to good mixing, resulting in solid pieces mixing with the molten metal making the scrap easier to melt. As seen from the figure, the molten metal lies on the bottom, while the salt will form a slag together with the oxides from the scrap on top of the metal bath. This slag is called dross [25]. The dross will contain both metallic aluminium and oxidised aluminium, i.e. $Al_2O_3$. Oxidation of aluminium mainly happens according to reactions 2.1, 2.2 and 2.3 [26]. Boin et al [26] calculated that the oxidation rate of aluminium in the rotary furnace lies between 2 and 4.5%, depending on scrap materials.

$$2Al + \frac{3}{2}O_2 = Al_2O_3 \tag{2.1}$$

$$2Al + \frac{3}{2}CO_2 = Al_2O_3 + \frac{3}{2}C \tag{2.2}$$

$$2Al + 3H_2O = Al_2O_3 + 3H_2 \tag{2.3}$$

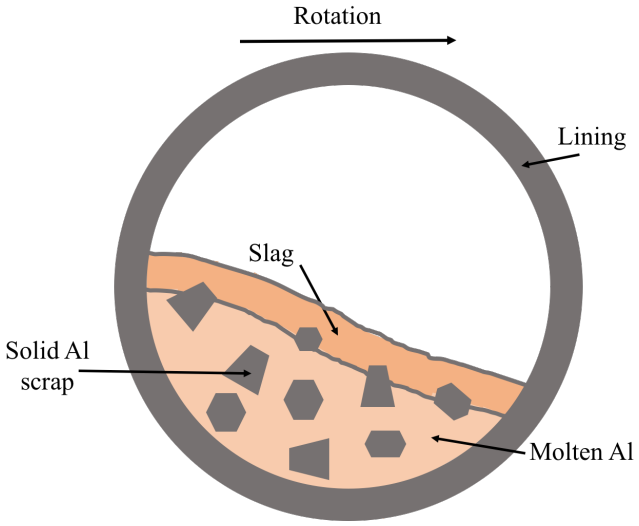


Figure 2.8: Illustration of metal and dross in the rotary furnace. Sketch made by the author.

### 2.2.2 Thermal decoating of aluminium scrap

A challenge when recycling end-of-life aluminium products, is the presence of surface oxides and coatings [27]. So to speak all aluminium products sold as everyday commercial merchandise, are coated in one way or another. The coatings contain non-metallic compounds, often oxides and polymers, which make the scrap difficult to process, and impurities are introduced. Figure 2.9 shows thickness of various products and their coating thicknesses. Obviously, thin products with thick coating layers are difficult to recycle efficiently [28].

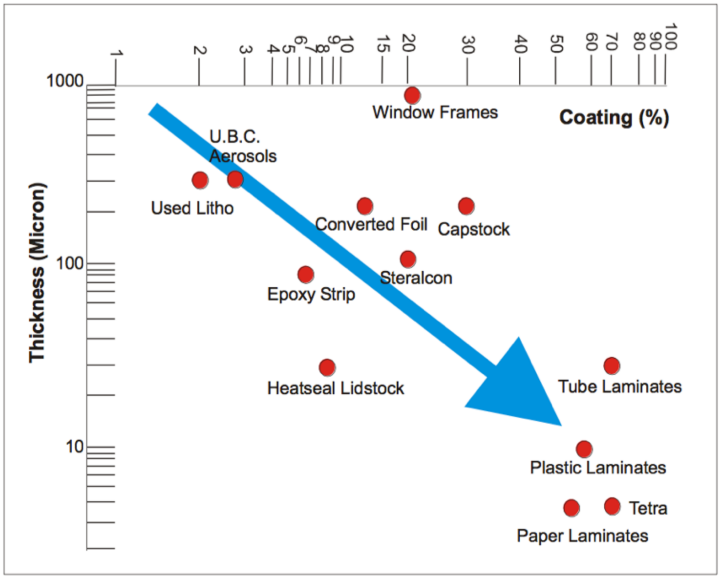


Figure 2.9: Thickness of various aluminium products as function of coating amount [28]

The organic coatings are usually made of waterborne epoxy, polyester and acrylic polymer resins, which are all organically based [29]. These organic compounds lead to gas-melt reactions when the scrap is melted, resulting in increased dross formation and decreased metal yield [30]. Therefore, a pre-treatment step to remove this coating could be feasible to avoid the occurrence of gas-melt reactions. One pre-treatment technique is thermal de-coating, which is performed by heating the materials to a certain temperature for a certain time, to decompose the coating. The decomposition depends on amount of oxygen present, which will create different hydrocarbon reaction products [31]. Table 2.1 shows which products will be generated with different amounts of oxygen. The three reactions are called combustion, gasification and pyrolysis [32]. According to Jaroni et al. [31], the de-coating will happen in a closed chamber, leading to a low oxygen concentration, meaning pyrolysis is the most significant reaction during de-coating. Here, $\lambda$ is the amount of oxygen present compared to the oxygen needed for total combustion. The same has been shown by Kvithyld et al. [33], who studied decomposition of organic coatings on aluminium scrap. They was found that the coating starts to decompose at 200-400°C and releases hydrocarbons ($C_xH_y$) in gaseous form, meaning a pyrolysis reaction takes place.

Table 2.1: Decomposition reactions and reaction products of thermal decoating. Modified from [32].

| | Process parameter | Ideal reaction products |
|---|---|---|
| Combustion | $\lambda > 1$ | $CO_2$, $H_2O$ |
| Gasification | $0 < \lambda < 1$ | CO, $H_2$ |
| Pyrolysis | $\lambda = 0$ | $C_xH_y$, $C_{fix}$ |

The coalescence of coated and un-coated aluminium discs were investigated by Capuzzi et al. [34]. By melting 100 8mm diameter aluminium pieces under a molten salt flux, they found that the un-coated aluminium is clearly easier to coalesce, meaning a thermal de-coating step removing the coating will most probably increase the metal yield for this material.

Further, Danbolt [35] investigated thermal de-coating of aluminium food tubes at different temperatures and times. Figure 2.10 shows the mass loss as a function of temperature and time. De-coating temperatures below 400°C seem to have little effect, while 500 and 600°C achieve the same result after 60 minutes. A reasonable conclusion is therefore that at approximately 9% weight loss the de-coating is complete, and both 500 and 600°C can be used to de-coat this product. Meanwhile, de-coating at 600°C is more efficient, and complete mass reduction is obtained after 10 minutes.

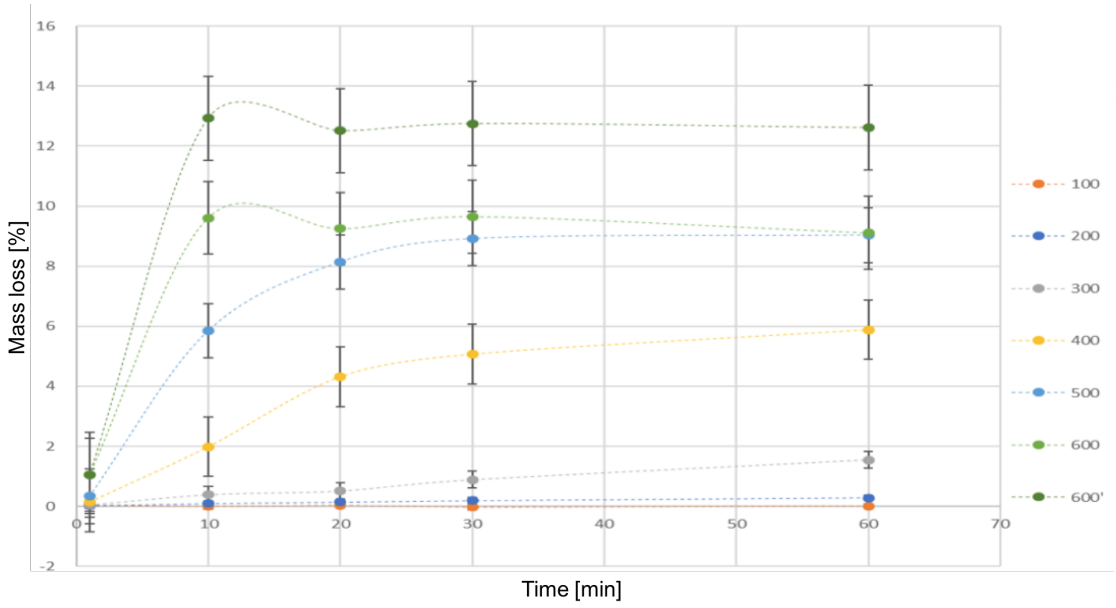


Figure 2.10: Mass loss at different times and temperatures after decoating aluminium food tubes [35]

However, from Figure 2.11 it is not necessarily so that de-coating steps will reduce the dross formation. Steglich et al. [29] found that the dross formation using non-treated used beverage cans ("A Raw" and "B Raw") lies in the same range as the pre-treated materials. In addition, not de-coating the UBCs does not lead to more generation of non-metallic particles (NMP).

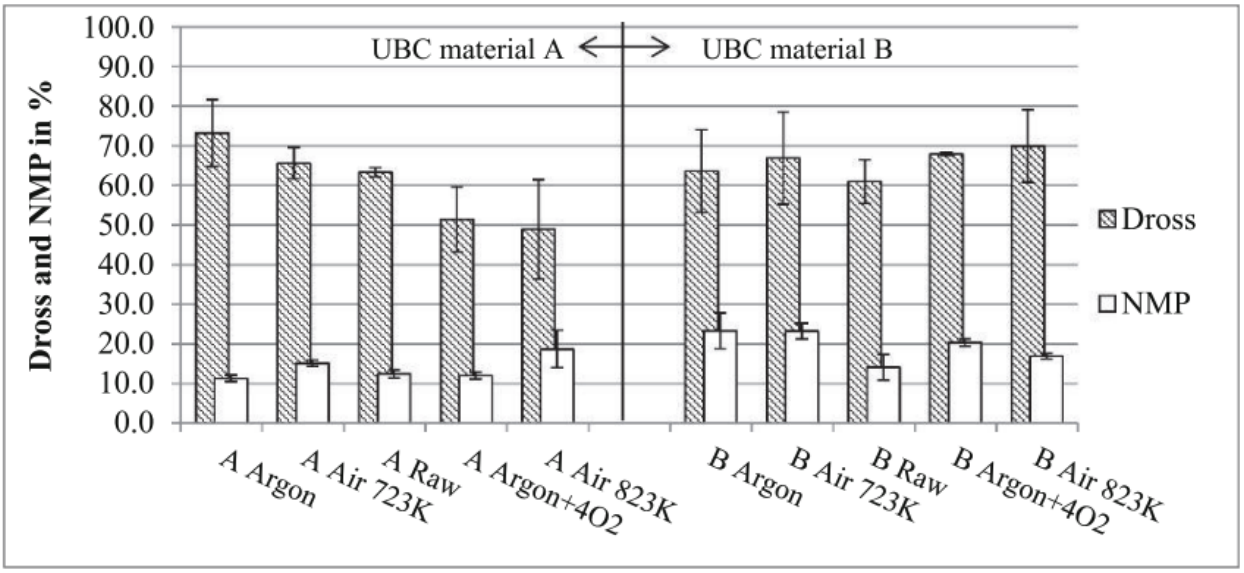


Figure 2.11: Dross formation for different UBC materials and heat treatment procedures [29]. NMP = Non-metallic particles

### 2.2.3 Salt fluxing

Fluxing is a term used to describe chemical additions and treatments that are applied to molten aluminium. Often, a salt is used as the flux. The salts usually contain mainly NaCl and KCl, in addition to small amounts of fluorine to promote coalescence [36].

Salt fluxes are used for several purposes. Mainly, they physically cover the metal, preventing oxidation at the surface of the metal bath by hindering the metal from being in contact with the atmosphere [37, 8], as mentioned in Section 2.2.1. The oxide layer created when liquid aluminium is exposed to air will make the metal difficult to cast, and give decreased yield due to aluminium being present as $Al_2O_3$ [27].

In addition, the flux should contribute to stripping away the $Al_2O_3$ oxide layer which surrounds the metal particles. It is always desirable to decrease the aluminium content in the dross, which can be done by having a flux encouraging coalescence of the aluminium droplets entrapped in the dross. To be able to recover the droplets, they need to settle back into the molten aluminium. The probability of them doing so increases with increasing droplet radius [38], meaning bigger droplets are more likely to return into the bath and be tapped as metal, i.e. increasing the metal yield. The fact that each individual aluminium droplet will be surrounded by an oxide layer when suspended in a liquid flux hinders the droplets from coalescing [39].

Furthermore, the fluxes should contribute to reduction of impurities in the melt [39, 40, 38, 8]. Alkali- and alkaline earth metals are removed by chemically reacting with the salt flux. The anions formed from the flux react with compounds in the liquid melt to decrease the

amount of impurities [37]. For instance, magnesium will preferentially react with the $Cl^-$ component in NaCl and KCl of the molten salt flux to form $MgCl_2$, in accordance with Equations 2.4 and 2.5 [36].

$$2NaCl + Mg = 2Na + MgCl_2 \tag{2.4}$$

$$2KCl + Mg = 2K + MgCl_2 \tag{2.5}$$

There are several parameters affecting how well the salt fluxes execute their mentioned purposes. The efficiency of the processes is affected by the flux´s chemical composition, particle size, amount, fluxing time and temperature, and density [40].

### Chemical composition

The chemical composition of the flux depends mainly on two parameters. Firstly, the melting point of the flux is determined by the relative amounts of NaCl and KCl to one another [41]. The NaCl-KCl phase diagram is shown in Figure 2.12. A low melting point is preferable due to decreased viscosity and surface tension, leading to better fluidity of the melt. A low salt viscosity leads to better mobility of the metal droplets entrapped in the dross, increasing their likelihood of finding other droplets and coalesce [41]. From Figure 2.12, eutectic composition leads to the lowest melting point, which is found at approximately 50mol% NaCl and 50mol% KCl. Therefore, the optimal NaCl-KCl ratio from a theoretical point of view is close to equimolar composition. However, since NaCl is cheaper than KCl, higher amounts of NaCl are normally used [42].

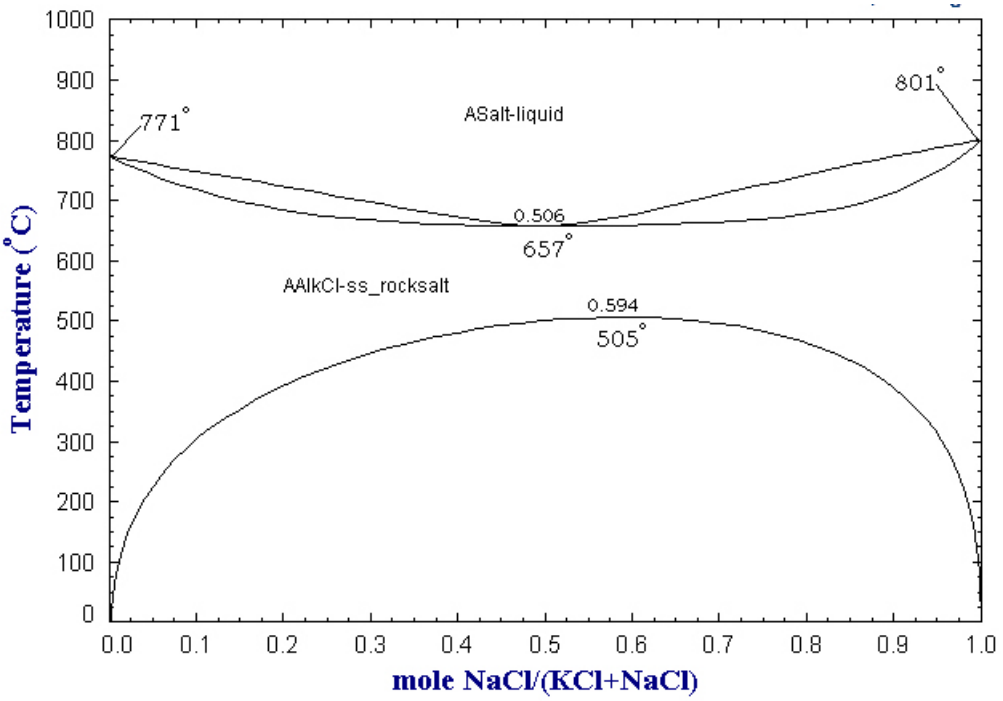


Figure 2.12: NaCl-KCl phase diagram [43]

Secondly, oxide stripping properties of the flux have to be considered. Friesen and Utigard [39] have shown that pure NaCl-KCl systems have little effect on removal of the oxide layer. Therefore, small amounts of other compounds are added. Friesen and Utigard [39] tested an equimolar NaCl-KCl salt with additions of 5wt% of several different chlorides ($AlCl_3$, $MgCl_2$, $BaCl_2$, $CaCl_2$, LiCl) and fluorides ($MgF_2$, $CaF_2$, $AlF_3$, LiF, $Na_3AlF_6$, NaF, KF), and assessed them according to their ability to coalesce aluminium droplets. Their results indicate that $Na_3AlF_6$, NaF and KF are the most effective oxide removers, while chloride salts does not enhance coalescence. Besson et al. [38] have obtained similar results. They investigated the coalescence ability as function of cryolite ($Na_3AlF_6$) content, and found that only small additions of cryolite has a significant effect on the coalescence behaviour of the flux. Figure 2.13 shows that only 1wt% cryolite increases the coalescence efficiency from approximately 15% to over 60%. As a consequence, small amounts of fluorine containing compounds are usually added to the salt fluxes, as it is believed that the fluorine has the ability to strip the oxide layer. [41, 38].

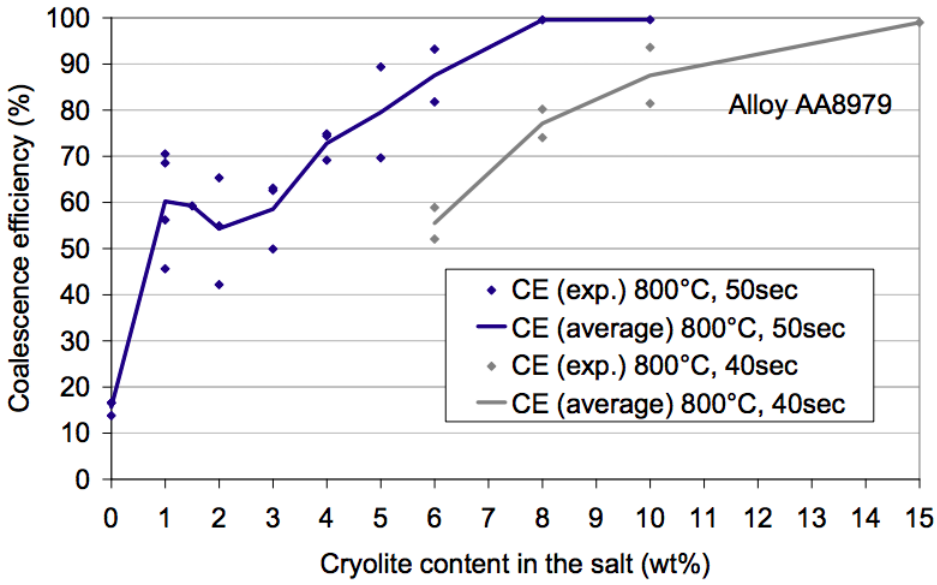


Figure 2.13: Coalescence efficiency as function of cryolite content in the salt [38]. CE = Coalescence efficiency

Klug et al. [44] have illustrated how the fluorine strips away the oxide layer. Figure 2.14 shows that the fluorine anions surround the oxide and crack it. The cracked oxide and salt will float towards the top, while the aluminium will stay in the metal phase [44].

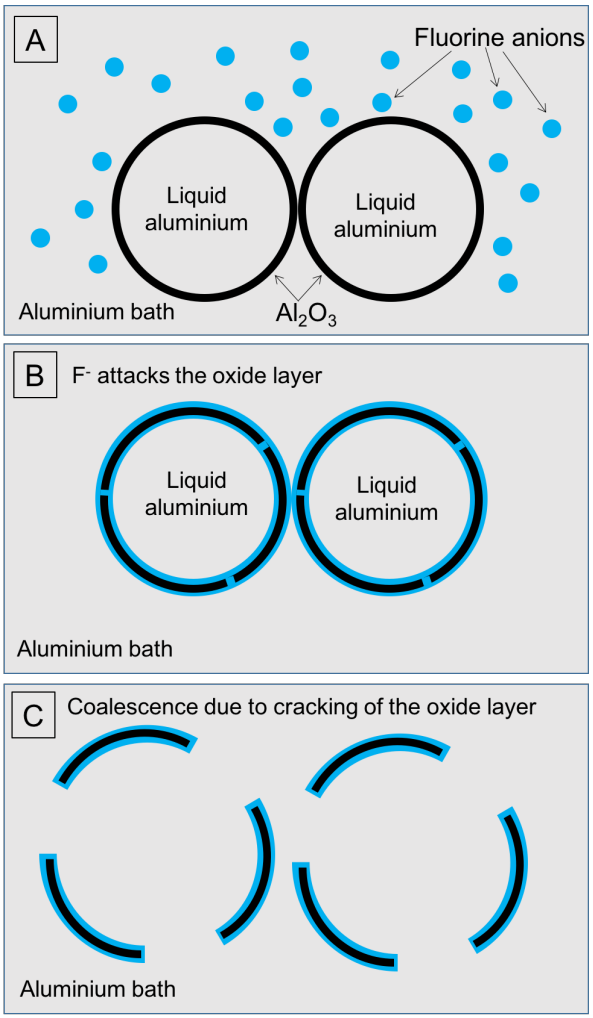


Figure 2.14: Illustration of how $F^-$ strips the $Al_2O_3$ layer (adapted from [44])

Capuzzi [34] investigated the coalescence behaviour of several salts. He tested three different salts used to a varying degree in industry. One salt contained cryolite as the fluroine component, one was recycled as explained as in Section 2.3.3, and the last one is the salt used by Hydro Holmestrand containing $CaF_2$. Capuzzi ran experiments varying type of salt, holding time and fluroine content. He found that the salt containing cryolite performs the best, which is in compliance with the results obtained by Friesen et al. [39] and Besson et al. [38].

Meling [45] also ran coalescence tests with the same three salts as Capuzzi, in addition to one other salt. Also here, the salt with cryolite performed best, while the $CaF_2$ containing salt performed worst and did not manage to coalesce any of the aluminium droplets. The recycled salt performed somewhere in-between the above mentioned salts.

### Particle size

The particle size distribution of the salts are of importance for their performance. A narrow size distribution is important to avoid segregation, resulting in higher melting temperatures of the salts [46].

The particle size and size distribution of the three salts described above were characterised by Meling [47]. Figure 2.15 shows that the salt containing $CaF_2$ i.e. the salt used by Hydro Holmestrand, have larger particles and a wider size distribution that the other two salts. This might be a contributing factor to the salt's bad performance in the above mentioned coalescence experiments.

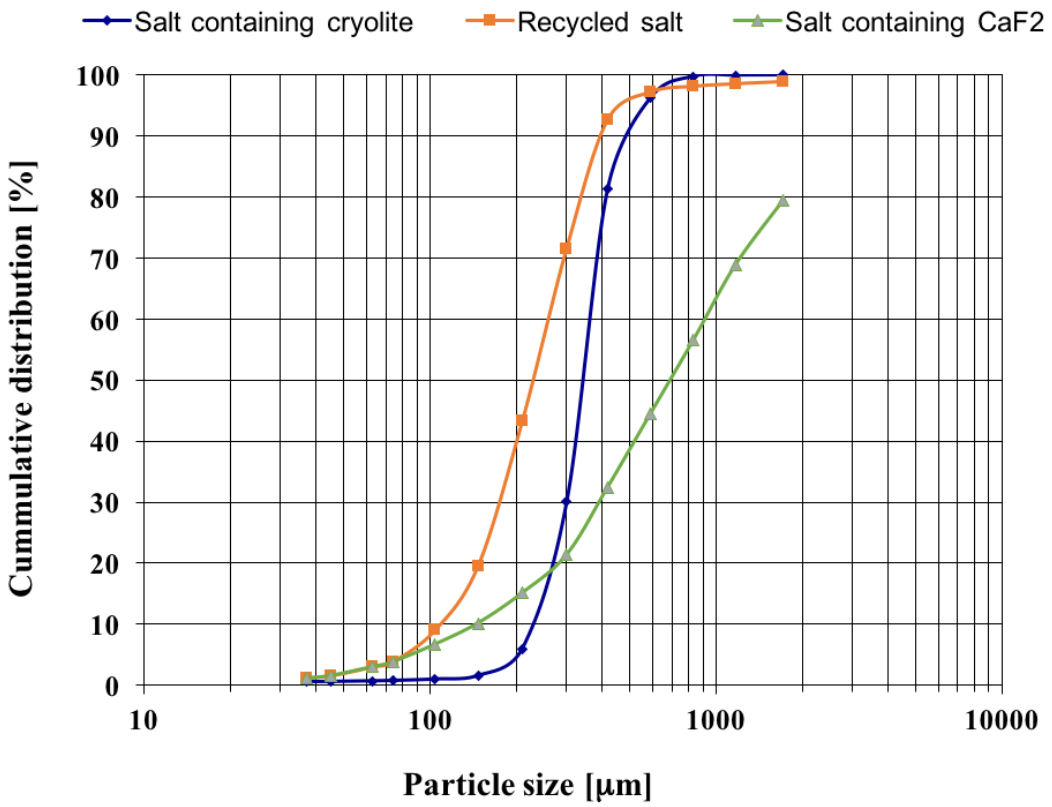


Figure 2.15: Cumulative size distribution of three different salts (adapted from [47])

### Salt amount

In the aluminium recycling industry, around 15% of the total weight of the charge is salt. More salt should favour coalescence and oxide stripping, in addition to covering more of the metal bath. Results obtained by Capuzzi [34], shows that increasing the salt to scrap ratio from 0.5 to 2 increases the sphericity but not the coalescence of the entrapped metal droplets.

#### Fluxing temperature and time

When it comes to fluxing temperature, it is important that the temperature is neither too high nor too low. Firstly, the salt needs to be molten. As explained using Figure 2.12, the melting point of the salt depends on its chemical composition. If the flux has very high or low NaCl:KCl ratios, the melting temperature becomes high, even exceeding $800^0$C. This means that the operating temperature needs to be high, as well as the mentioned decreased fluidity of the molten salt. In addition, high fluxing temperatures have the tendency to increase the hydrogen absorption into molten aluminium. Too low temperatures are not desirable either. The refining properties of the flux will not be very efficient if the temperature is too close to the solidification temperature [40].

Capuzzi [34] also tested coalescence at different holding times. In theory, longer times should favour coalescence, as the particles need time to fine each other. Meanwhile, Capuzzi´s results show that holding time does not affect the results, suggesting coalescence happens shortly after the metal pieces are added.

#### Density

It is also of importance that the molten flux has a low density, to make it easier to separate the flux and the metal [48], which has a high density compared to the salt. If the salt is good at stripping the oxide layer, the oxides will be entrapped in the salt. This increases the metal recovery, and is desirable in theory. However, an increased amount of oxides in the salt, increases the density of the molten salt [38], making the salt more difficult to separate from the metal phase due to decreased fluidity.

## 2.3 Recyclable materials

In theory, all aluminium-based products are recyclable. However, some products are easier to recycle than others, as explained through figure 2.5.

### 2.3.1 Internal scrap

The aluminium plants will always produce some internal scrap, in the form in cut-offs and material which has not passed various quality controls. As Figure 2.16 indicates, the amount of internal scrap is significant. "Dross and Fabricator Scrap" is internal scrap from the producing plant, while "Traded New Scrap" is the internal scrap from the processing plants. Adding these, the amount of internal scrap exceeds primary metal. [49]. This scrap is usually

relatively easily recyclable, due to low contamination and known composition. The products often reside in the top right corner of figure 2.5, meaning they are quite big and clean.

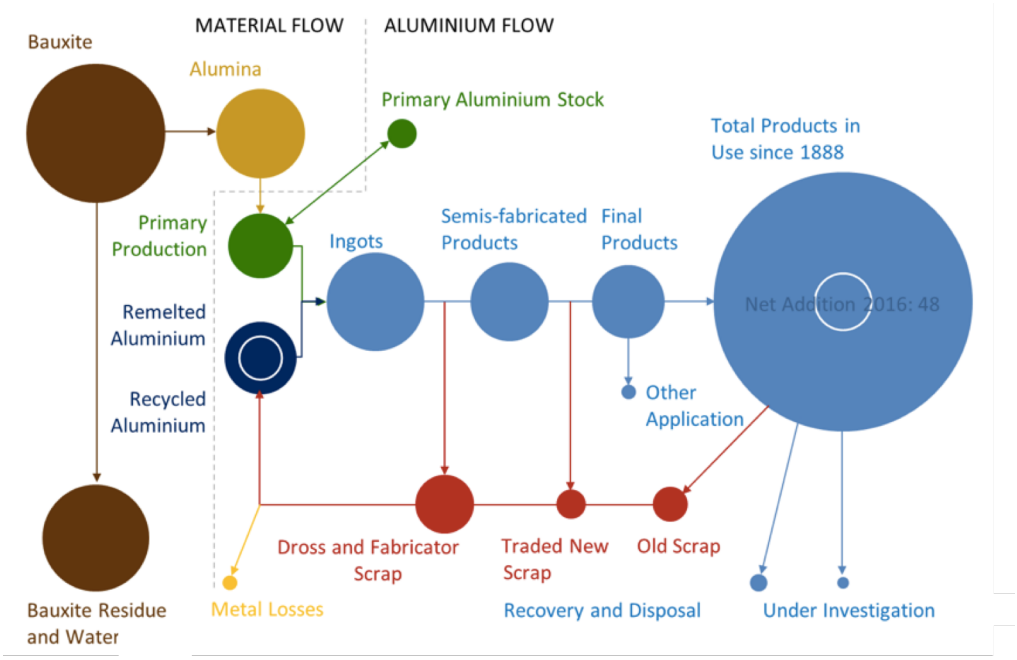


Figure 2.16: Global aluminium mass flow for 2016 [49]

### 2.3.2 Large constructions

Large constructions like buildings, cars and airplanes usually contain significant amounts of aluminium. According to Henryson and Goldman [9], approximately 60% of the produced aluminium in Europe is utilised in large constructions. The recycling rate of these products is often high. In Europe, approximately 95% of the aluminium in cars is recycled, while this number is 90% for buildings. For cars, a deposit-refund system is used, which most likely contribute largely to the high recycling rates. For buildings, the companies responsible for the destruction are obliged to handle the scrap, resulting in high recycling rates [50].

### 2.3.3 Dross

The dross produced during primary production is different to that produced during recycling. Common for both is that the dross contains considerable amounts of aluminium. According to Utigard et al. [37], the dross contains up to 60-80% aluminium. Friesen et al. [39] states that "one of the most important objectives in recycling is to reduce metal losses within the 'dross layer'". Herbert [46] emphasises this by stating that increasing the metal recovery from the dross by 3%, a plant producing 500 tonnes of dross monthly can save $460,000 annually. As a consequence, the recycling plants strive to improve their dross processing to

increase the metal recovery. According to Herbert [46], 60–70% of the aluminium can be recovered by efficient dross management processes.

### Dross from primary production

The dross formed in the electrolysis cell mainly contains oxides, non-metallic compounds and aluminium. After the dross has been skimmed, it is usually handled on sight.

The simplest and least efficient way of processing the dross is floor cooling, meaning cooling the dross at room temperature and physically removing visible aluminium pieces. By this process, approximately 30% of the aluminium can be recovered, corresponding to approximately half the recovery of modern dross management processes [46].

Other dross processing procedures are stirring, rotary cooling and pressing. The most efficient of these is pressing, where the dross is pressed to make the liquid metal flow to the sides [46]. Figure 2.17 shows the metal recovery obtained for different dross processing procedures.

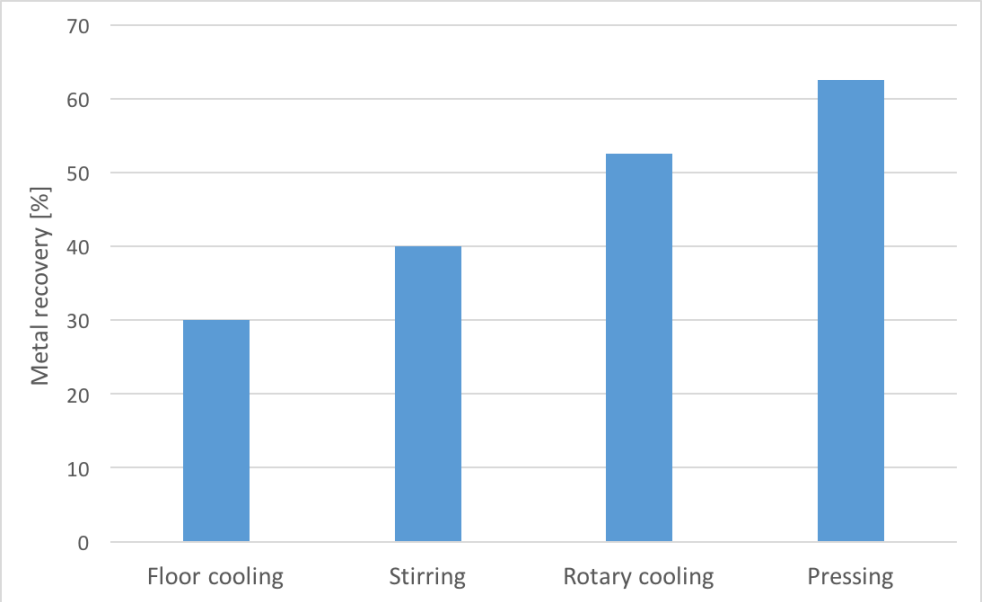


Figure 2.17: Metal recovery obtained for various dross processing procedures [46]

### Dross from secondary production

The dross from the recycling plants often contains high amounts of salt in addition to oxides, non-metallic compounds and aluminium. Many recycling plants charge their dross back into the rotary furnace, and run the process as described in Section 2.2.1 with the furnace containing only dross to extract as much metal as possible. The remaining dross is sent to companies specialising on recycling the dross. Here, the aluminium and salt fractions are

separated and recycled. To separate the salt, the dross is crushed and dissolved in water, before the salt particles are crystallised to obtain a mixture of NaCl and KCl which can be sold to the remelting plants as salt fluxes [51].

### 2.3.4 Post-consumed scrap

The scrap generated by the consumers as post-consumed scrap (Old Scrap in Figure 2.16), is often the most challenging and where the biggest losses occur. The scrap is usually heavily contaminated and consists of a wide variety of alloys. However, from Figure 2.16 it is clear that the post-consumed scrap accounts for a significant amount of the remelted scrap [49].

In Norway, the collection of post-consumed scrap is divided into three, see Figure 2.18. A deposit system is available for a narrow range of aluminium scrap, while the rest should be thrown in the glass and metal waste. If the scrap is thrown in the residual waste it will end up at the incinerators, being burnt with other waste [52].

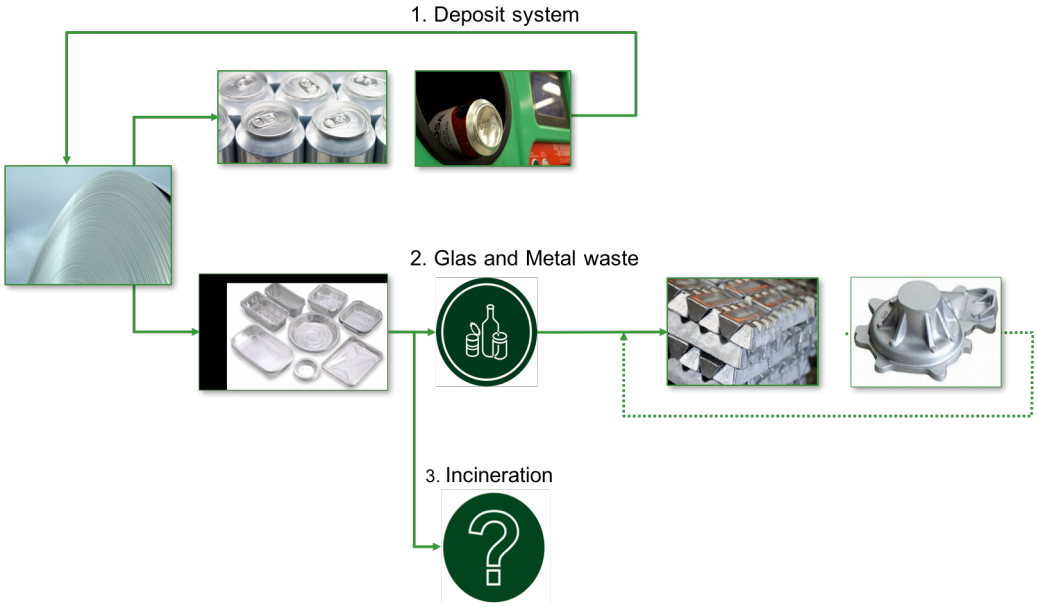


Figure 2.18: Waste systems in Norway [53]

#### Used beverage cans

There exists a deposit system for used beverage cans (UBCs) in Norway, where consumers buy the cans for a slightly higher price and get this amount refunded when handing them in for recycling. In 2014, almost 494 million aluminium beverage cans were sold in Norway. With one can weighing approximately 14g, over 7400 tons of aluminium is needed to produce the cans. As seen in figure 2.19, the recycling rate of the UBCs was 95% in 2014, making

Norway among Europe´s leading countries when it comes to recycling the UBCs, only surpassed by The Netherlands, Germany and Finland [50].

UBCs are being recycled at Hydro Aluminium Rolled Products' plant in Holmestrand today. Before they arrive at the remelting plant, they are collected by the deposit system and compressed by Infinitum AS. Obviously, to get 95% recycling rate, it is crucial that consumers hand in their UBCs, which is the main contributor to losses in the recycling of UBCs. Even though a recycling rate of 95% is high, the remaining 5% corresponds to four cans per person in Norway, containing considerable amounts of aluminium. Infinitum´s goal is therefore to have a 100% recycling rate of the UBCs in Norway [50].

Examining the recycling rates in Europe, only 70% of the UBCs are collected on average, ranging from approximately 30-99% for the different countries [10], as can be seen in Figure 2.19. Most likely, a contributing factor to the high recycling rate in Norway is the deposit system. Figure 2.20 shows the recycling system for UBCs in several countries around the world. There is an obvious coherence between the countries having a deposit system and having high recycling rates. Most European countries have an extended producer responsibility (EPR) system, often in combination with other systems, meaning that producers are given incentives to make products that are easier to recycle and are more environmentally friendly [1].

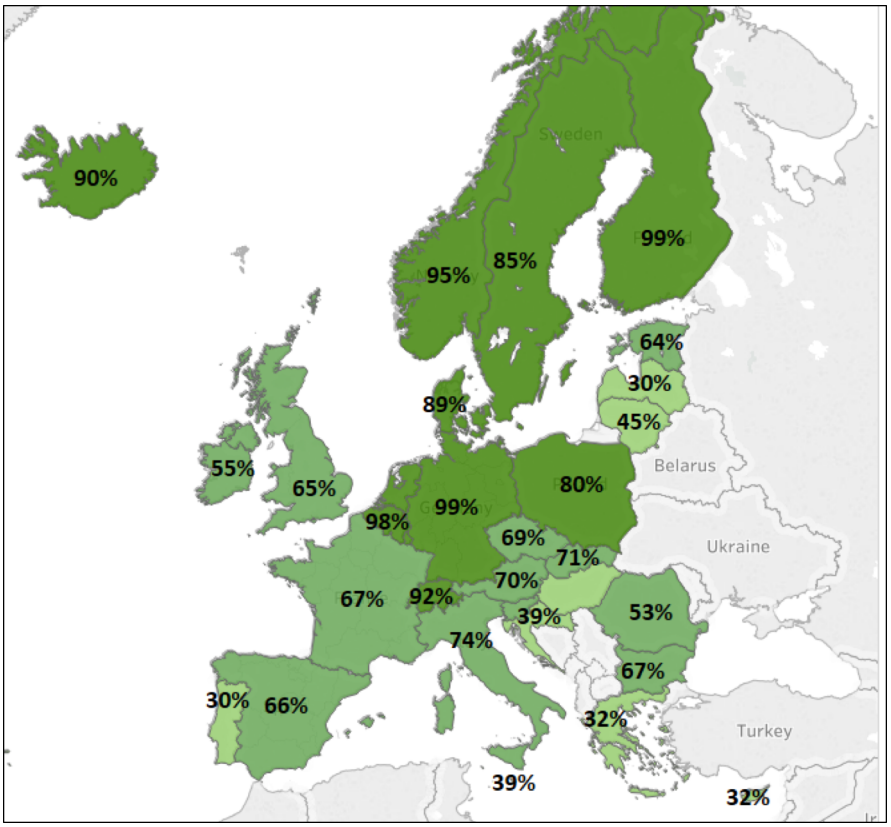


Figure 2.19: Recycling rate of UBCs in Europe [1]

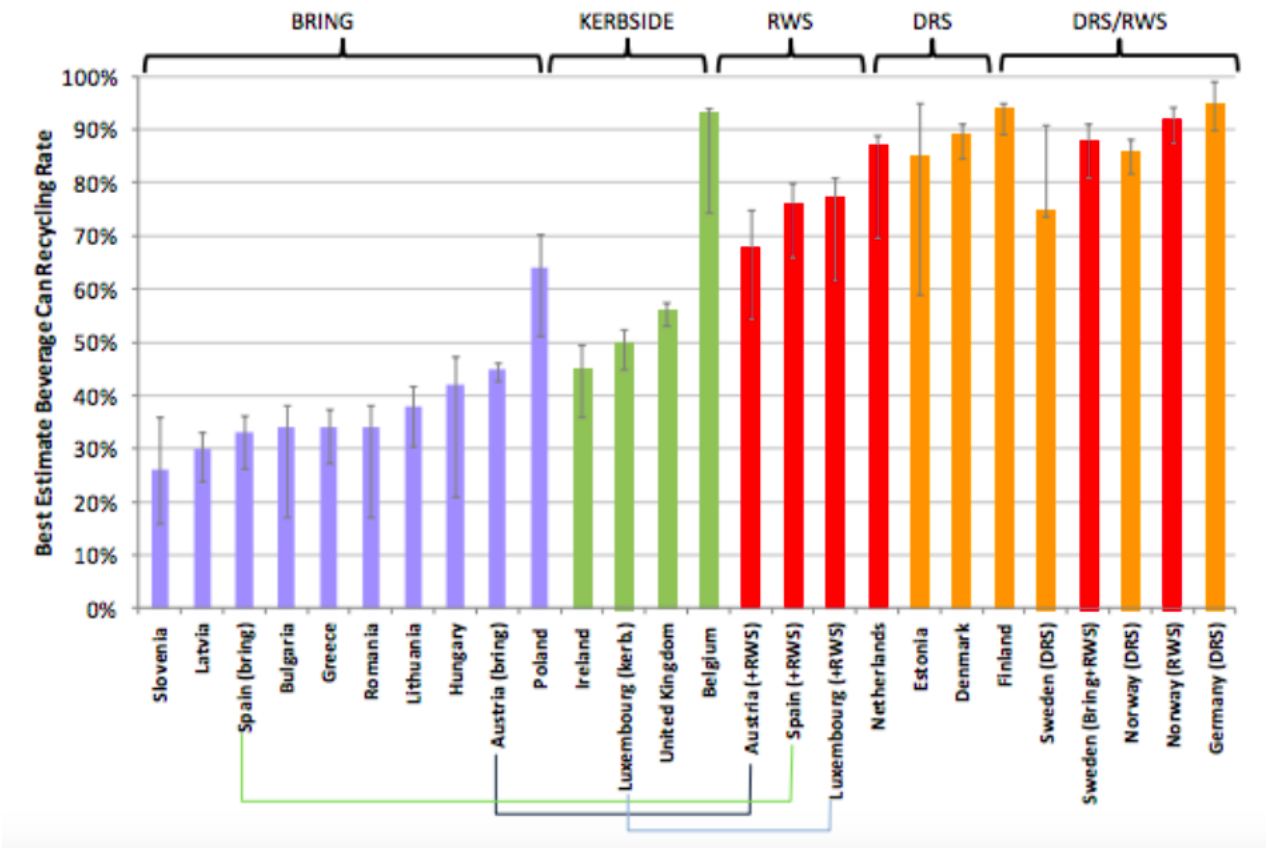


Figure 2.20: UBC collection rates for different countries. DRS = Deposit Reward System, RWS = Residual Waste Sorting [54].

According to Raadal et al. [55], who studied the environmental impact of handing UBC to the deposit system instead of it ending up at incinerators, a recycling yield of 97.1% can be obtained for the UBCs. This is assuming that the collected cans are 100%, meaning that the collection rate is not included. 2.4% of the losses are accounted for in the recycling process, while the remaining 0.5% occurs in other parts of the processing system.

An observed trend, shown by Doutre [56], is that the thickness of the beverage cans is decreasing, as illustrated in Figure 2.21. The thickness has decreased by almost 40% from 1980 to 2004, resulting in a significant mass decrease of the can (Figure 2.22). The decreased thickness leads to less aluminium consumption, but the cans become increasingly difficult to recycle with decreasing aluminium thickness.

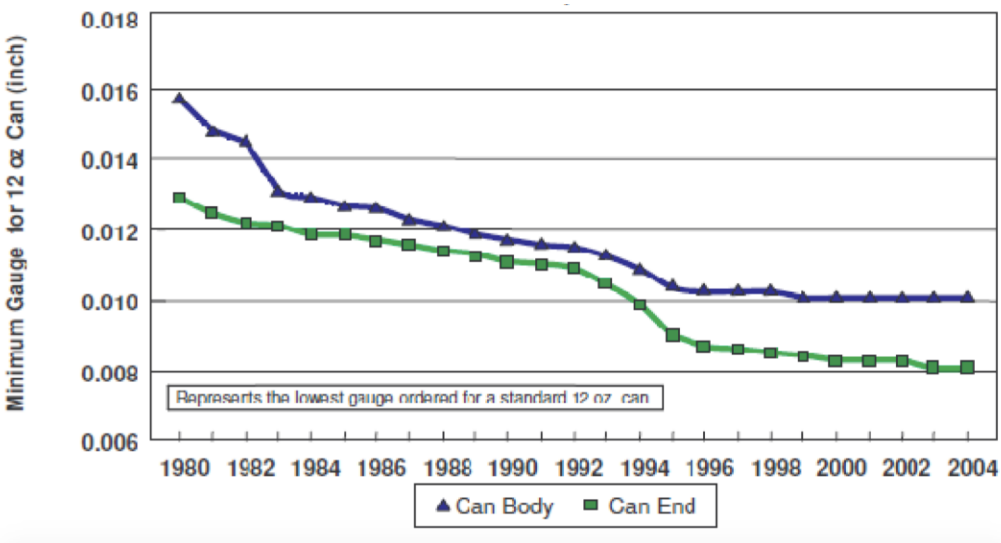


Figure 2.21: Thickness of the beverage can as function of time [56]

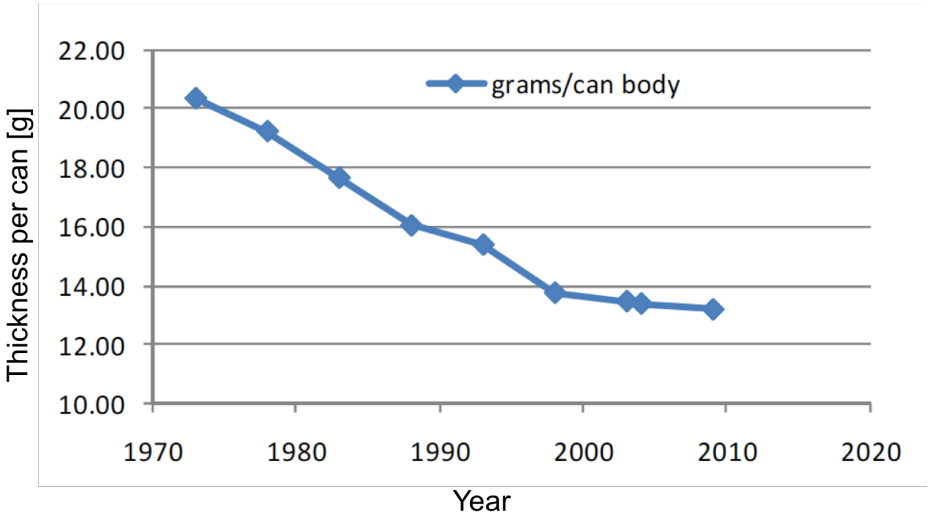


Figure 2.22: Weight of the beverage can in grams as function of time [56]

**Everyday consumer products**

Many everyday consumer products are made of aluminium. Usually these products are made of soft alloys, most commonly 1xxx and 3xxx alloys. It is estimated that 10,800 tons aluminium were used for these types of products in Sweden in 2005 [9]. A common thing for all these products is that they do not have a separate recycling system, like the UBCs. These materials are, hopefully, thrown in the metal and glass waste by the consumers, and are treated and remelted together. This causes challenges due to many different alloys being mixed. In addition, since these products do not have a deposit system like the one explained in Section 2.3.4, they have a significantly lower collection rate. In Sweden, only 27% of the

aluminium in these products was recycled in 2005, compared to 86% for the UBCs [9]. Many consumers throw them in the residual waste bin, and they end up at incinerators or landfills. Another challenge is the organic compounds. A large amount of these products contain coatings, plastics and food residues, which make them difficult to process.

In previous work, Meling [47] has investigated aluminium food tubes containing cream cheese. It was found that food residues and plastic have a negative effect on the metal yield, as shown in Figure 2.23. The value denoted metal yield is the weight of metal and coatings before remelting compared to cast metal, meaning the metal yield includes the organic coating but not plastic caps and food residues.

However, it is not necessarily so that the organic compounds decrease the metal quality. The same experiments resulted in a decreased bifilm index for tubes containing food residues, as illustrated in Figure 2.24. A low bifilm index indicates a good metal quality with low amounts of hydrogen and inclusions [57].

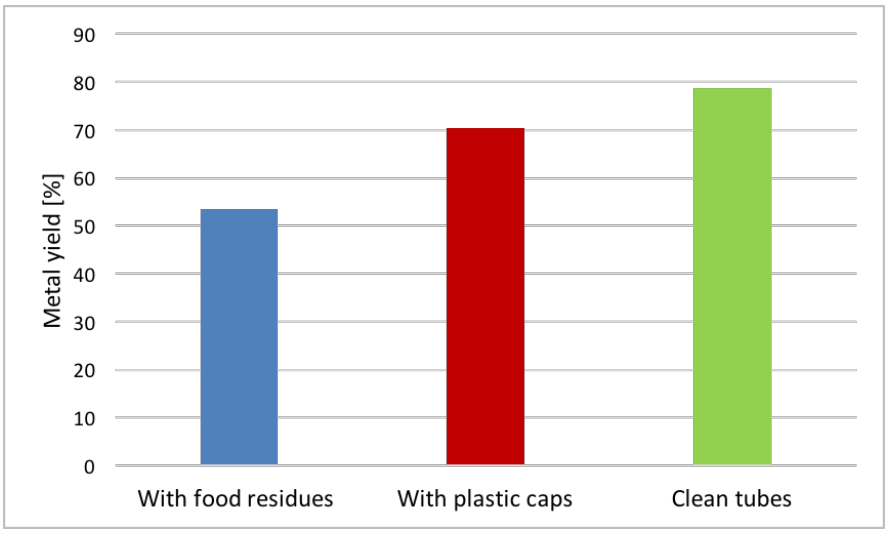


Figure 2.23: Metal yield of aluminium food tubes with various contaminations [47].

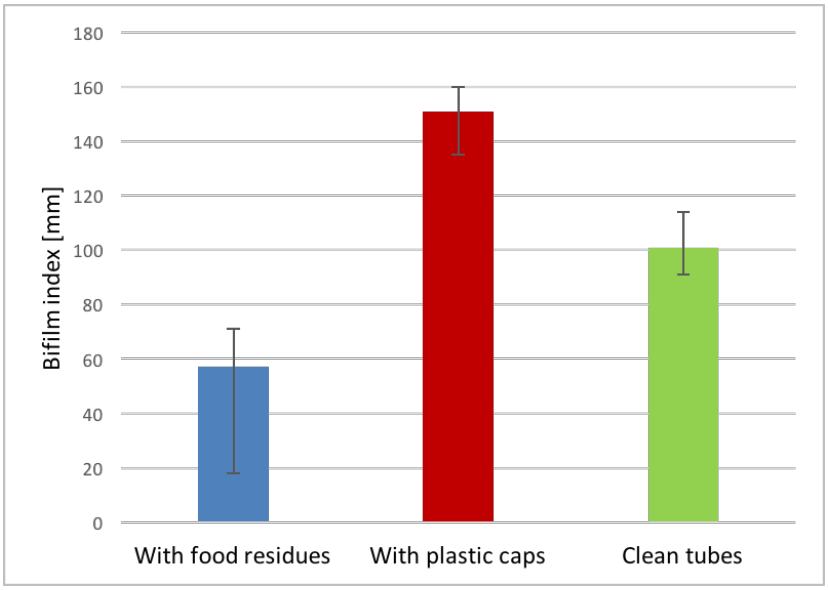


Figure 2.24: Bifilm index of aluminium food tubes with various contaminations [47].

### Incinerator metal

As mentioned, the aluminium not collected ends up at incinerators or landfills together with other waste. There are 21 incinerators in Norway, which burn scrap to recover energy which can be used as heat or production of electricity [58]. In 2007, 40% of all district heating was supplied by incinerators in Norway. The total incinerated scrap this year was 922.000 tons. In 2013 this number had increased to 4.3 million tons, corresponding to 40% of all household waste [59]. The amount has increased dramatically the past 20 years, with a doubling of incinerated scrap from 1998 to 2007 [58]. A considerable amount of the scrap arriving at the incinerators is metal scrap thrown away by consumers. According to Chandler et al. [60], the residual waste from consumers consists of approximately 5% metals on average. Figure 2.25 shows the metal fraction for eight different countries, varying from 3 to 9%.

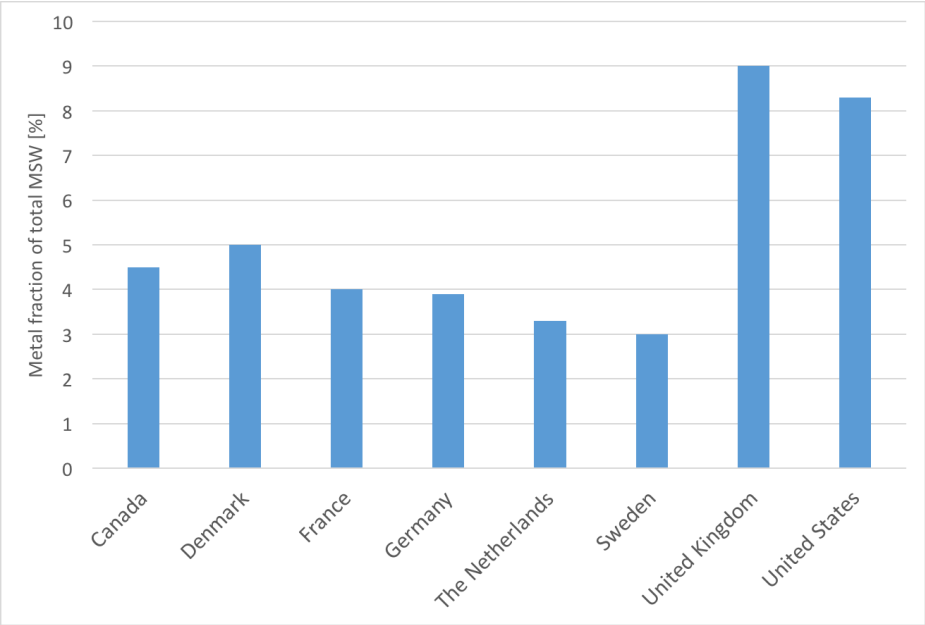


Figure 2.25: Metal fraction in the incinerated waste for eight different countries [60]

The metal fraction is separated after incineration, and the burning leads to oxidation of the aluminium metal. According to Raadal et al. [55], 10% of the metal in UBCs is oxidised during incineration. After incineration, the aluminium fraction is sorted, where another 10% oxidation occurs during the storage of the metal while 10% is lost during the actual sorting step. Further, 10% of the metal is landfilled before the remaining fraction is sent for recycling. During the recycling step, a yield of 80% is attained, see Figure 2.26. Adding all the losses, a yield of 52.5% is attained from recycling the incineration metal, compared to 97.1% for the UBCs collected through the deposit system. Figure 2.27 shows number of recyclable UBCs as a function of recycling loops for UBCs going through incineration and the deposit system, assuming an initial mass of 100kg. As seen from the figure, there is almost no aluminium left after recycling incinerator metal seven times, while 84% of the initial mass is left after recycling through the deposit system seven times.

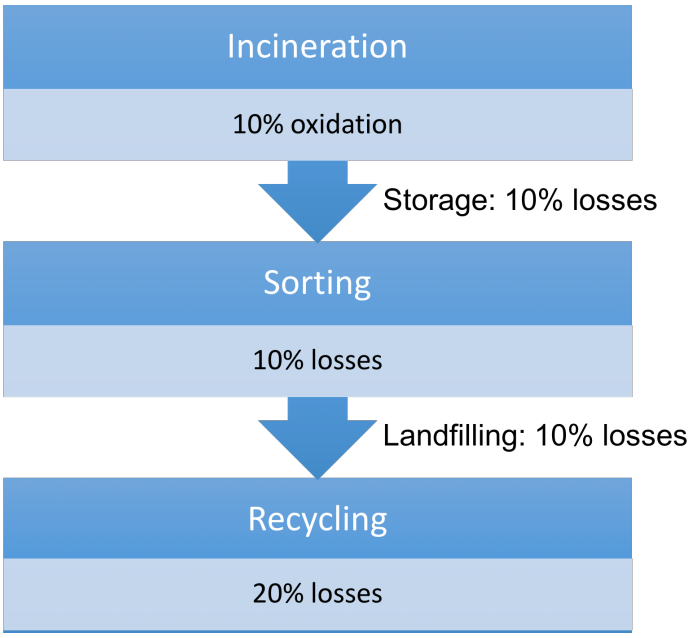


Figure 2.26: The complete incineration process with corresponding losses for every step [55]

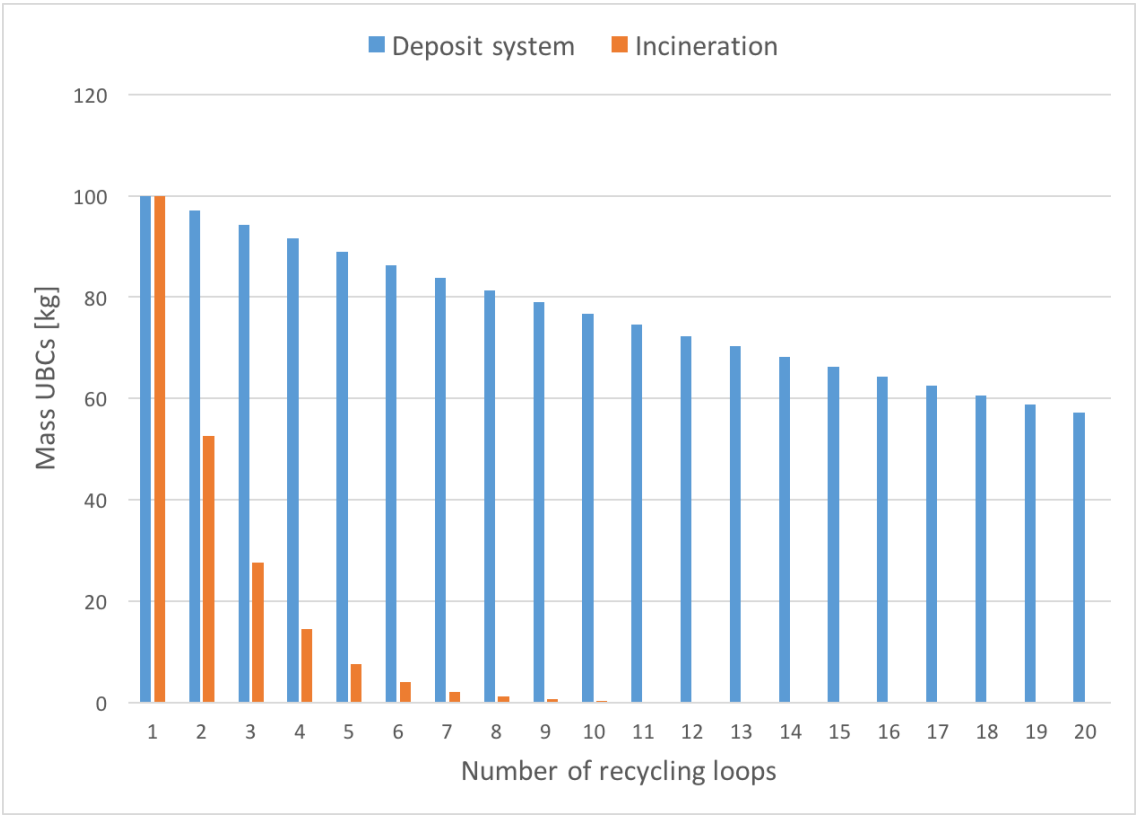


Figure 2.27: Number of recyclable UBCs as function of recycling loops. Adapted from [55]

## 2.4 Alternative utilisation of aluminium scrap

Recycling aluminium scrap is a complex process. Therefore, alternative ways of utilising end-of-life scrap and dross are sought. An alternative investigated in this study is utilisation of aluminium scrap and dross as reductant for quartz to produce silicon, i.e. aluminothermic production of silicon.

### 2.4.1 The element silicon

Silicon is an important element with a wide range of applications. Due to the special electrical properties, silicon is used to make electronic components and solar panels. In addition, it is an important alloying element in aluminium and steel, and used to make silicones [3].

The earth's crust contains high amounts of silicon, most commonly found in the form of silicon dioxide ($SiO_2$) and silicates [61]. It has been estimated that the earth's crust contains approximately 25 wt% silicon, which makes it the second most abundant element on earth [3]. Despite this, the European Commission [62] placed silicon on their list of Critical Raw Materials in 2014. Their definition of a critical raw material is "raw materials with a high supply-risk and a high economic importance" [62]. The reason silicon has been in the list since 2014 is that the recycling rate and substitutability are low. In addition, China accounts for over 50% of the global production, while the EU only accounts for 6%. Counting Norway as part of the European collaboration, the European countries produce 14% of the worldwide silicon [62]. The low production rate in Europe means that silicon has to be imported mainly from Brazil and China to cover the European supply [63, 62]. As mentioned in Section 2.1, it is unfavourable for the circular economy of Europe to be dependent on other countries to get the needed supply. Therefore, methods for increasing the production rate of critical raw materials within Europe are wanted.

### 2.4.2 Carbothermic production of silicon

Even though silicon is abundant, it is not easily separated from oxygen. The covalent bonds in the $SiO_2$ molecule are strong, meaning a lot of energy has to be provided to break the bonds [64]. Today silicon is usually produced through a carbothermic reaction, meaning $SiO_2$ is reduced with carbon, usually coal, to produce liquid silicon and CO gas [3]. The ideal overall metal producing reaction is shown in Equation 2.6.

$$SiO_2(s) + 2C(s) = Si(l) + 2CO(g) \qquad \Delta G = 623.1 \frac{kJ}{mol} \tag{2.6}$$

Figure 2.28 shows a typical submerged arc furnace (SAF) used for carbothermic production

of silicon. $SiO_2$ and carbon are added as raw materials and melted in the furnace. The process is very energy demanding, due to the fact that the reaction is very endothermic, shown by the Gibbs free energy, $\Delta G$. It is estimated that approximately 12 MWh of electric power is necessary to produce on tonne of silicon through this process [3].

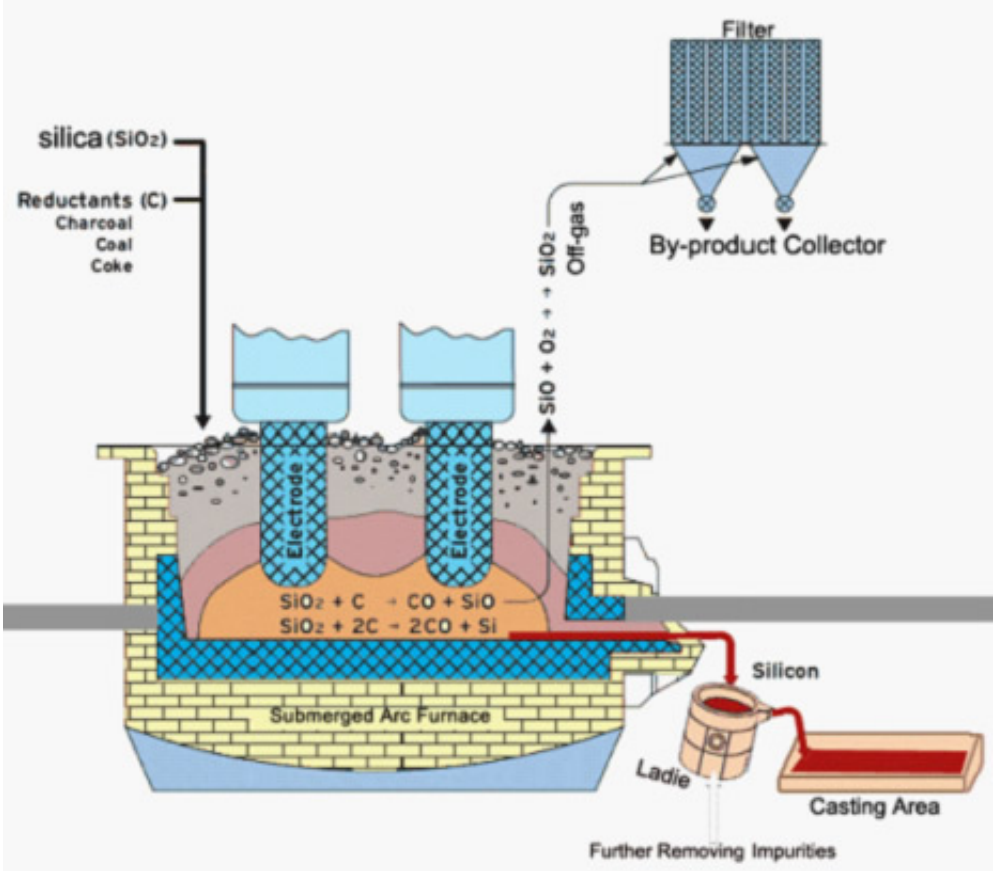


Figure 2.28: Schematic drawing of a submerged arc furnace (SAF) [65]

A lot of carbon is needed to reduce the $SiO_2$. Theoretically, 0.85 tonnes of carbon are required to produce one tonne of silicon. However, the yield is not 100%, as some carbon will be used to run other reactions, like producing SiO gas [61]. The total reaction equation including the production of SiO is shown in Equation 2.7 [61]. Counting a typical carbon yield of 80%, 1.03 tonnes of carbon are necessary to produce one tonne of silicon, corresponding to 2 tonnes of CO gas according to reaction 2.6. This gas will react with oxygen in the air to produce $CO_2$ upon outlet, according to Equation 2.8. 2 tonnes of CO gas produce approximately 3.1 tonnes of $CO_2$, meaning producing one tonne of silicon emits 3.1 tonnes of $CO_2$.

$$(1+x)SiO_2 + (2+x)C = Si + xSiO + (2+x)CO \tag{2.7}$$

$$CO(g) + \frac{1}{2}O_2(g) = CO_2(g) \qquad \Delta G = -257.2\frac{kJ}{mol} \tag{2.8}$$

The rate in which $SiO_2$ reacts with carbon to form SiO gas highly depends on the size of the $SiO_2$ particles. As shown by Ozturk and Fruehan [66], small $SiO_2$ particles react much faster to produce SiO according to reaction 2.9, which is illustrated in Figure 2.29. This means that fine $SiO_2$ particles cannot be used as raw material in the process.

$$SiO_2(s) + CO(g) = SiO(g) + CO_2 \tag{2.9}$$

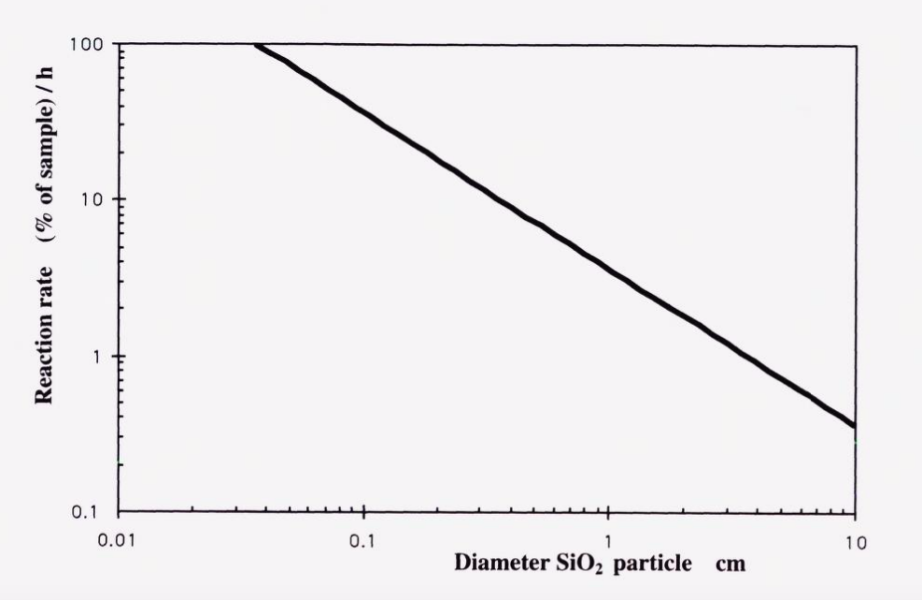


Figure 2.29: Reaction rate of $SiO_2$ particles as fucntion of particle size [61]

### 2.4.3 Aluminothermic production of silicon

An alternative to the carbothermic reaction is aluminothermic reduction of $SiO_2$, meaning aluminium is used as the reduction material instead of carbon. Equation 2.10 shows the ideal reaction. The aluminium will be oxidised while $SiO_2$ will be reduced, to end up with metallic silicon and $Al_2O_3$. The reaction is exothermic, meaning it will generate heat.

$$4Al(l) + 3SiO_2(l) = 3Si(l) + 2Al_2O_3(l) \qquad \Delta G_{1600^oC} = -423.33\frac{kJ}{mol} \tag{2.10}$$

The reason why aluminium will reduce $SiO_2$ is found in the Ellingham diagram shown in Figure 2.30. The line for aluminium (green line) is further down in the diagram than silicon (blue line), meaning aluminium requires less energy to oxidise to $Al_2O_3$ than silicon to $SiO_2$. This means that $Al_2O_3$ is a more stable compound than $SiO_2$. Thus, addition of aluminium metal to molten $SiO_2$ should in theory react as Equation 2.10 shows.

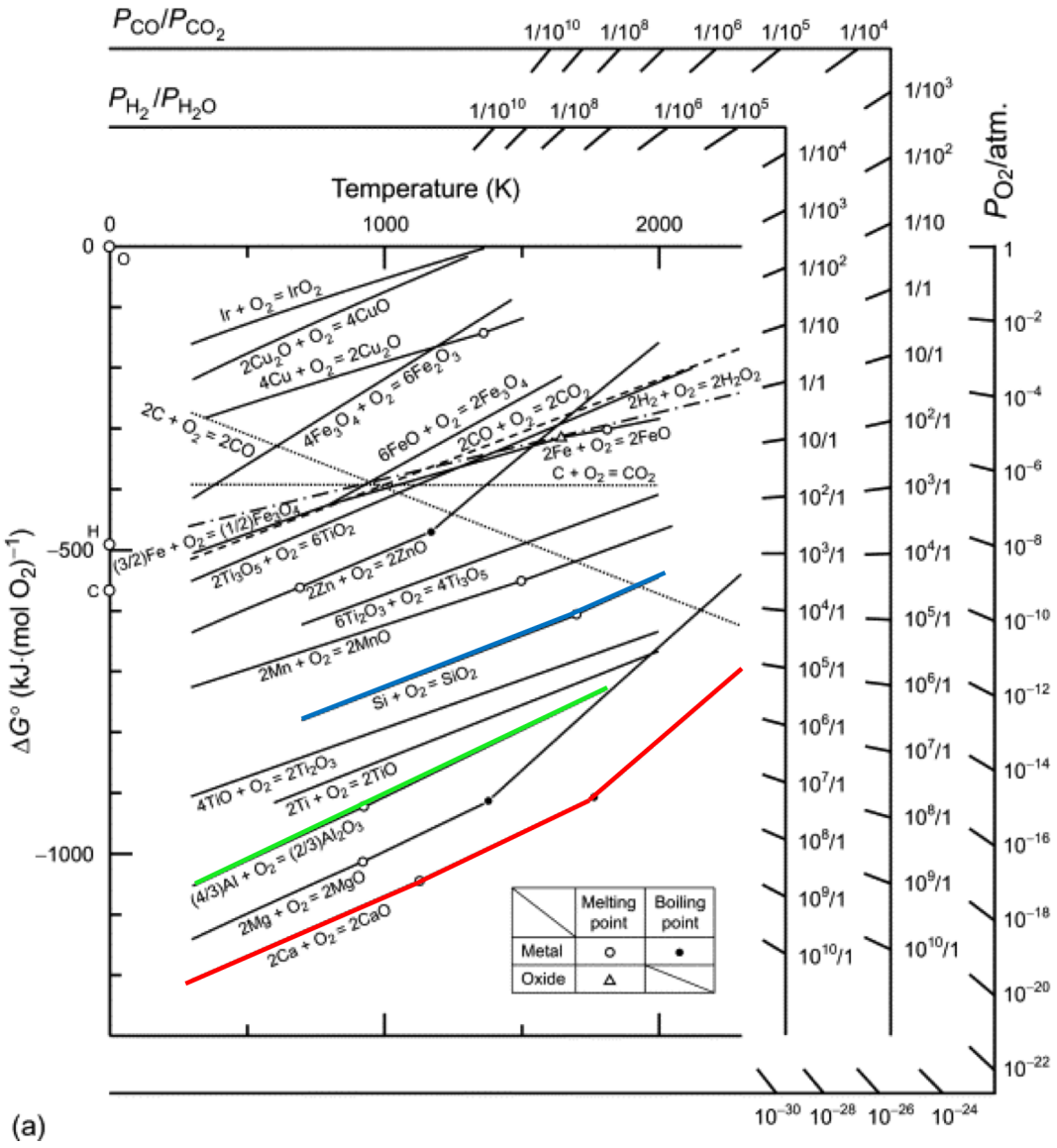


Figure 2.30: Ellingham diagram [67]. Blue line: Si oxidation, Green line: Al oxidation, Red line: Ca oxidation

An equilibrium will be obtained between aluminium and silicon when molten. The Al-Si phase diagram (Figure 2.31) can be used to calculate the resulting metal composition at room temperature. If an operating temperature of 1600°C (1873K) and over-eutectic composition of silicon are assumed, one silicon phase and one eutectic Si-Al alloy will be present at room temperature if the solidification follows the liquidus line. This solidification path is illustrated by the red lines in the figure.

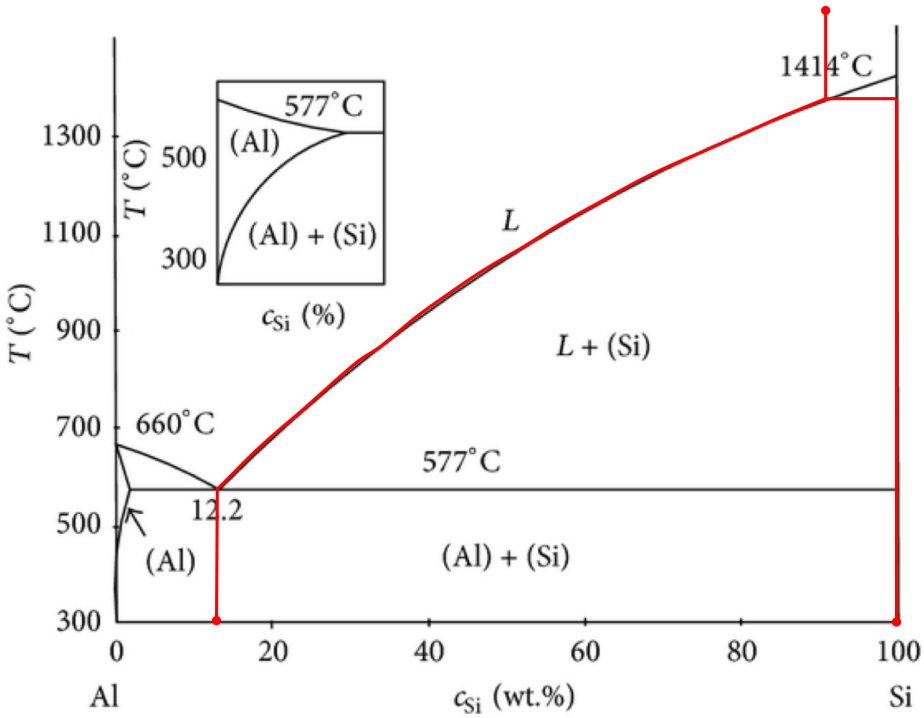


Figure 2.31: The Al-Si phase diagram [68]

The silicon source may be the same as in carbothermic reduction, *i.e.* quartz. Since carbon is not present, the significant SiO generation for small quartz particles is not present, meaning also fine quartz can be used [69]. The availability of high quality quartz sand is high, due to the fact that the traditional silicon plants cannot use the smallest fractions [70].

In addition to the traditional quartz, $SiO_2$ slag systems can be used as the oxidising material. The slag will contain the silicon source, but it can in addition act as a solvent for $Al_2O_3$ [70]. For these systems, it is important that the other oxides in the slag are more stable than $Al_2O_3$. Otherwise, aluminium will be consumed by reducing these oxides instead of $SiO_2$, as seen from the Ellingham diagram in Figure 2.30.

Furthermore, by using slag systems as oxidising materials, *e.g.* a CaO-$SiO_2$ slag, the operating temperature can be lowered compared to using quartz and to carbothermic reduction, which is desirable due to lower energy consumption. In the traditional carbothermic production in a SAF, the temperature needs to be around 2000°C to produce liquid silicon [61]. However, by using a $SiO_2$-CaO slag as the silicon source in an aluminothermic production, the temperature can be lowered to 1500-1600°C since the melting point of the slag is exceeded at such temperatures. As illustrated by the CaO-$SiO_2$ phase diagram in Figure 2.32, the slag melts below 1450°C for certain compositions. Therefore, a slag in the eutectic region is optimal, and the lowest melting temperature is found for a slag containing 60.6at% CaO at 1709K, corresponding to 1436°C. The phase diagram also shows the melting temperature of quartz, which is significantly higher than eutectic CaO-$SiO_2$ slag.

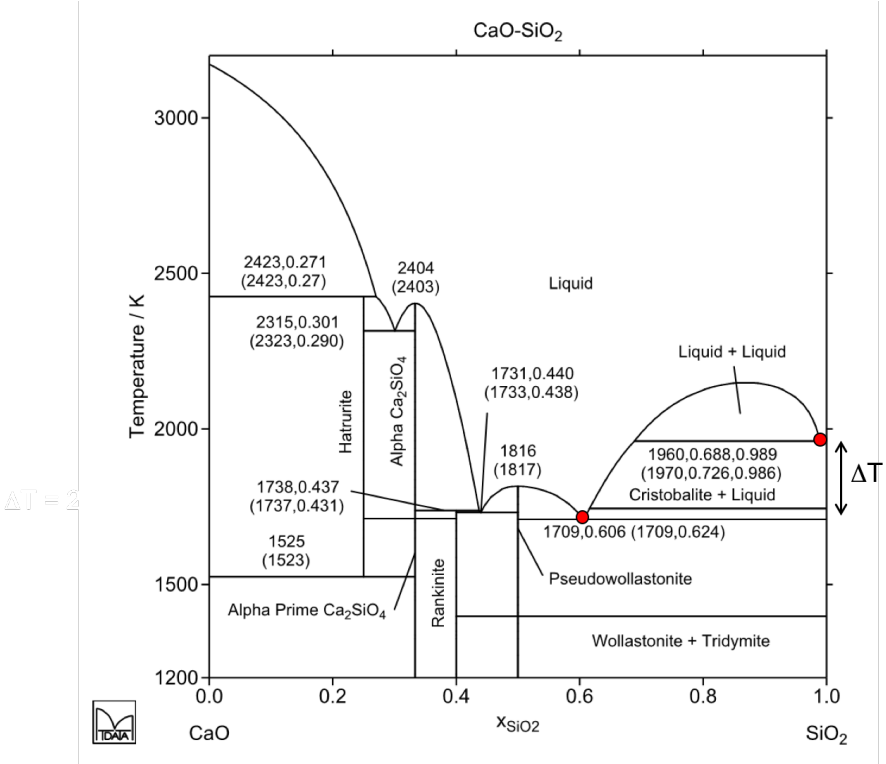


Figure 2.32: CaO-$SiO_2$ phase diagram [71]. The red dots indicate the eutectic point and melting temperature of $SiO_2$

### The $Al_2O_3$-CaO-$SiO_2$ slag system

During oxidative refining of silicon, an $Al_2O_3$-CaO-$SiO_2$ slag is generated when removing calcium and aluminium [61]. This slag is not of value for the silicon plant, and is sold cheaply to silicomanganese producers [69]. For the purpose of aluminothermic production on the other hand, this slag could be utilised as the $SiO_2$ source. As seen from the Ellingham diagram in Figure 2.30, CaO is more stable than both $SiO_2$ and $Al_2O_3$ and will in theory not react upon addition of aluminium to the molten slag.

A slag initially containing 50wt% CaO and 50wt% $SiO_2$ before the addition of aluminium, will have the theoretical composition of 58.7wt% $Al_2O_3$ and 41.3wt% CaO if it is assumed that there is no $SiO_2$ left in the slag after reaction 2.10 has taken place. The $Al_2O_3$-CaO phase diagram is shown in Figure 2.33, with the red line indicating the composition at 1600°C down to room temperature. During solidification, one CaO*$Al_2O_3$ phase and one $CaOAl_2O_3$-$3CaOAl_2O_3$ phase will remain at room temperature.

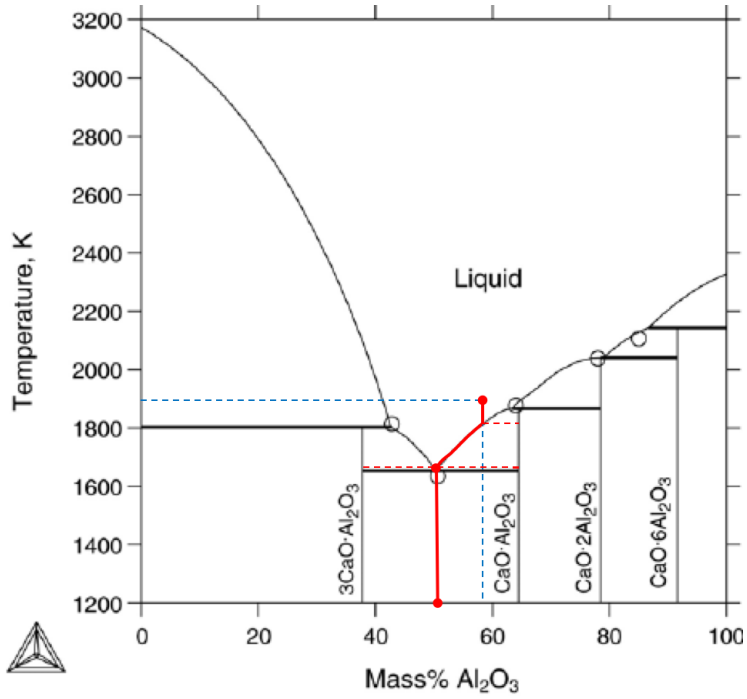


Figure 2.33: $Al_2O_3$-CaO phase diagram [72]. Dashed red lines is the starting composition, while the red lines are the solidification path from 1600°C to room temperature

However, the slag will contain small amounts of $SiO_2$, as an equilibrium will be obtained between the elements in the slag. Figure 2.34 shows the $Al_2O_3$-CaO-$SiO_2$ phase diagram for different temperatures with compositions of the different regions. Figure 2.35 shows the same phase diagram at 1600° with isoconcentration lines for aluminium and calcium. From this diagram, the theoretical slag composition obtained from a specific metal composition can be found. Similarly to the slag, the metal phase will also have an equilibrium composition with silicon as the main element and small amounts of aluminium and calcium at 1600°C. The icoconcentration curves in Figure 2.35 indicate the mass fraction of aluminium (straigt lines) and calcium (dashed lines) in the silicon metal. The Al-Ca-Si phase diagram is shown in Figure 2.36, and shows which alloys are present at various aluminium, calcium and silicon concentrations. According to this phase diagram, a silicon phase will form in addition to aluminium, calcium and silicon alloys depending on initial composition and solidification conditions assuming silicon is the main element.

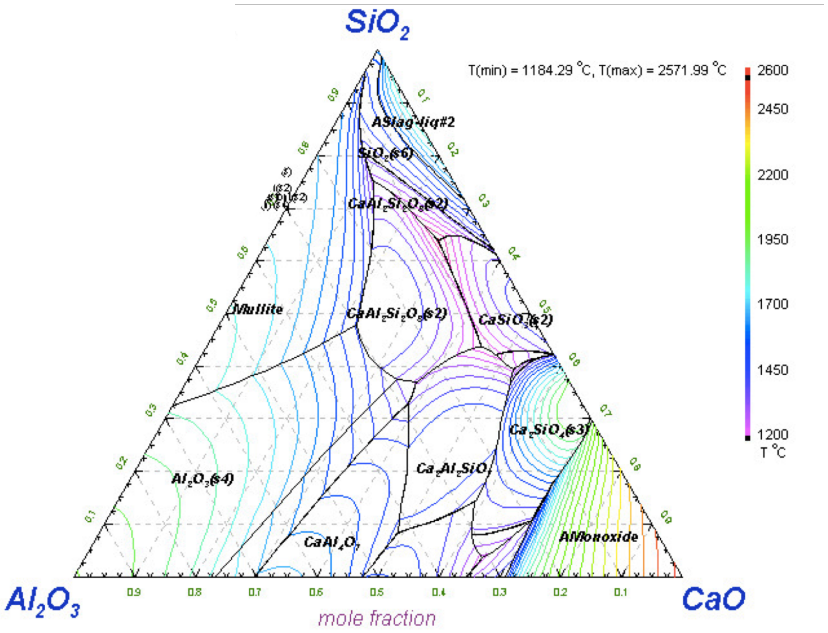


Figure 2.34: $Al_2O_3$-CaO-$SiO_2$ phase diagram [73]

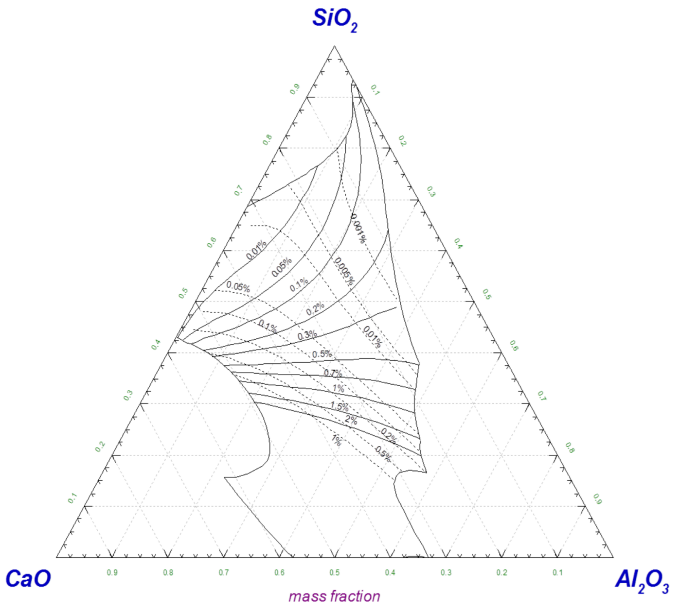


Figure 2.35: $Al_2O_3$-CaO-$SiO_2$ phase diagram at 1600°C with isoconcentration curves for Al and Ca [74]

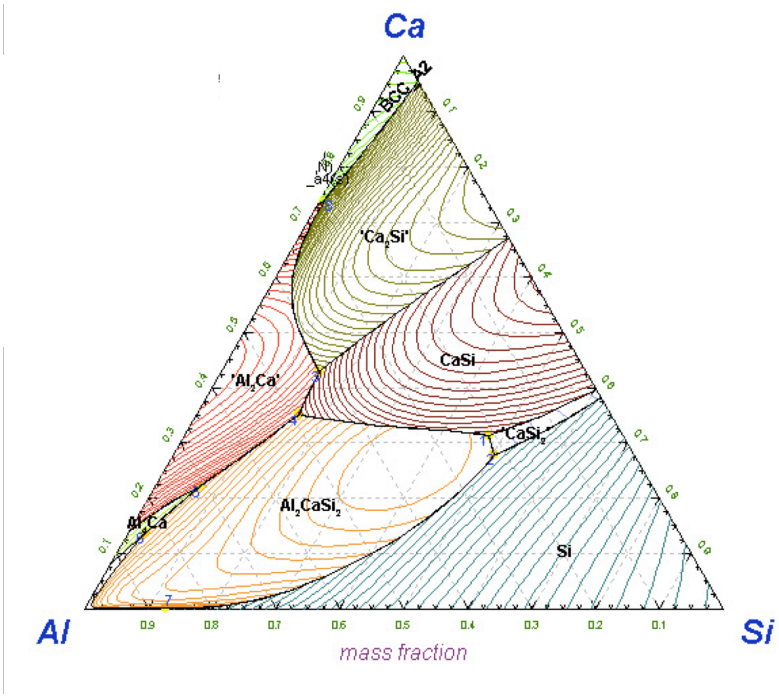


Figure 2.36: Al-Ca-Si phase diagram [73]

## Reducing materials

The reducing materials need to contain metallic aluminium. Of course, primary aluminium can be used for the purpose of aluminothermic reduction, but aluminium scrap and by-products are also usable in theory. As aluminium scrap needs to go through a recycling process as described in detail in Sections 2.2 and 2.3, resulting in aluminium losses, the scraps might be better utilised for this purpose. As explained in Section 2.3, some aluminium scrap products are more difficult to recycled than others. Internal scrap is often pure with known compositions, making them relatively easy to recycle. However, post-consumed scrap is more challenging. Since $Al_2O_3$ dissolves easier in a slag at e.g. 1600°C than a salt at e.g. 800°C [75, 76], the scrap is potentially better utilised for the purpose of aluminothermic production in $SiO_2$ based slags than traditional recycling.

A second potential reducing material is dross. As explained in Section 2.3, dross is always accumulated during primary production of aluminium and contains significant amounts of aluminium. The $Al_2O_3$ in the dross will dissolve in the slag, while the aluminium content will reduce the $SiO_2$ [70].

### 2.4.4 Benefits of aluminothermic production

There are several benefits of producing silicon aluminothermically compared to the traditional carbothermic production. Firstly, producing silicon through aluminothermic reduction compared to the traditional carbothermic reduction can decrease the $CO_2$ emissions significantly. Producing in the traditional SAF with carbon as the reductant, $CO_2$ emissions are over eight times higher than producing through aluminothermic reduction [69].

The reduced $CO_2$ emissions are partly due to the decreased energy consumption. Only one third of the energy needs to be consumed when producing aluminothermically due to the lowered operating temperature [69]. Another reason for the low $CO_2$ emissions is the use of aluminium instead of carbon as reductant. As can be seen from Equation 2.6, the carbothermic reaction emits two moles of CO gas per mole produced silicon.

Another factor is the utilisation of raw materials. In this process, aluminium scrap and by-products can be utilised. Secondly, small quartz particles, which are not used in the SAF today, can be used as the silicon source. Another option for the silicon source is slags. For the instance of a CaO-$SiO_2$ slag, the resulting $Al_2O_3$-CaO slag can be hydrometallurgically processed to obtain $Al_2O_3$ and CaO [61]. The $Al_2O_3$ can be utilised as raw material in the primary production of aluminium, while the CaO can in turn be used to produce CaO-$SiO_2$ slag used as raw material in the aluminothermic process [69].

# Chapter 3

# Experimental

The experimental work was divided into three main parts – coalescence experiments, yield experiments and aluminothermic reduction of silica. In this chapter, the materials and methods used in this study will be presented.

Coalescence and yield experiments were carried out to investigate the recyclability of different scrap materials and how different salts affect the recyclability. The aim of the coalescence experiments was to get an understanding of how different salts affect the coalescence of aluminium pieces, and to compare two scrap materials to one another. The yield experiments aimed to compare the material yield using the same scraps and salts as in the coalescence experiments.

The aluminothermic production of silicon was done to investigate an alternative way of utilising end-of-life aluminium products and dross, aiming to see if clean aluminium and dross can be used to produce silicon aluminothermically. This work is on a preliminary basis, and aims to explore the feasibility of utilising aluminium products in this manner.

Figure 3.1 shows an overview of the experimental work. As seen, coalescence and yield experiments goes under the recycling route, while aluminothermic production is an alternative to traditional recycling. Coalescence and yield experiments are similar in their execution, but use different setups and have slightly different aims. As for the aluminothermic production of silicon, a synthetic slag was prepared beforehand, and used as the silicon source.

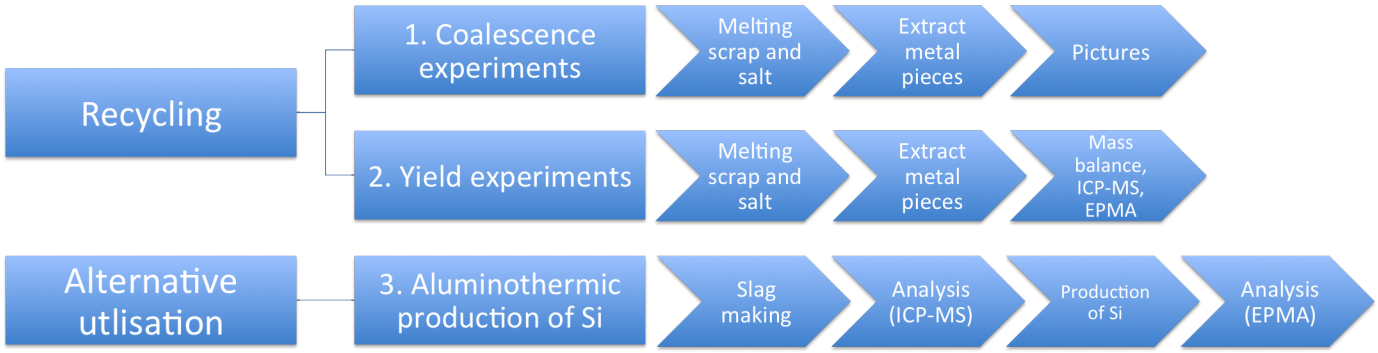


Figure 3.1: Flow sheet of the experimental work performed in the thesis

## 3.1 Materials

### 3.1.1 Recycling experiments

During this work, two different aluminium scrap types have been investigated. The first one is used beverage cans (UBCs), which are aluminium cans containing various types of beverages. The can body is usually made of a 3104 alloy, while the lid is a 5182 alloy [56]. In table 3.1, chemical compositions of the alloys are shown. According to Doutre [56], the can body weighs approximately 3.4 times more than the lid, meaning the 3xxx alloy make up most of the can.

Table 3.1: Chemical compositions of alloys used in the UBC [77]

| | Alloy | Si | Fe | Cu | Mn | Mg | Cr | Zn | Ti |
|---|---|---|---|---|---|---|---|---|---|
| Body | 3104 | 0.6 | 0.8 | 0.05-0.25 | 0.8-1.4 | 0.8-1.3 | - | 0.25 | 0.1 |
| Lid | 5182 | 0.2 | 0.35 | 0.15 | 0.2-0.5 | 4-5 | 0.1 | 0.25 | 0.1 |

As explained in Section 2.3.4, the cans are collected through a deposit system. Since the cans are being recycled on a large scale today, both in Norway and the rest of Europe, they are a good reference material when comparing to other scraps. The UBCs were sent from Hydro Aluminium Rolled Products AS' plant in Holmestrand, who receive the cans already compressed from Infinitum AS [78]. The block received was 40x40x10 cm and weighed 21 kg (Figure 3.2), which corresponds to a bulk density of 1250 kg/m$^3$. As mentioned in Section 1, the density of aluminium is 2700kg/m$^3$, meaning over 50% of the UBC material is air. The block was cut into appropriate sizes and used for various experiments.


Figure 3.2: Compressed block of UBCs

The UBCs were compared to a less extensively studied material – incinerator metal. This material was also received from Hydro Aluminium Rolled Products AS' plant in Holmestrand, and a picture of the material can be seen in Figure 3.3. Chemical analyses by optical emission spectroscopy (OES) and inductively coupled plasma mass spectrometry (ICP-MS) have been executed. A general analysis of the heterogeneous material was done, and the elemental analysis of the incinerator metal is found in Table 3.2.


Figure 3.3: Incinerator metal

Table 3.2: Elemental analysis of incinerator metal in wt%

| | OES | ICP-MS |
|---|---|---|
| Si | 0.93 | 1.91 ± 2.10 |
| Fe | 0.55 | 0.76 ± 0.52 |
| Cu | 0.33 | 0.46 ± 0.52 |
| Mn | 0.35 | 0.24 ± 0.13 |
| Mg | 0.04 | 0.04 ± 0.03 |
| Cr | 0.02 | 0.01 ± 0.01 |
| Zn | 0.29 | 0.37 ± 0.37 |
| Ti | 0.02 | 0.03 ± 0.01 |
| Pb | - | 0.015 ± 0.019 |
| Al | 97.43 | 88.96 ± 1.81 |

Table 3.3 shows a comparison of the two scrap materials. Since the incinerator metal is a mixture of the aluminium thrown in residual waste, it probably has a varying composition, also indicated by the deviations in the Table 3.2. The bulk density of the two materials were measured. The UBCs block was weighed as is, while an amount of incinerator metal was charged into a container with known volume and weighed. The bulk density of UBCs is higher than for the incinerator metal, as the table also shows.

Table 3.3: Materials used for coalescence and off gas experiments

| Material | Alloy | Compacted | Average weight of one piece [g] | Bulk density [kg/m$^3$] |
|---|---|---|---|---|
| UBC | 3xxx/5xxx | Yes | 13.8* | 1250 |
| Incinerator metal | - | No | 0.64** | 918 |

*one empty can of 0.33l CocaCola, **average of 112 pieces

In addition to scrap materials, two different salts were used in the recycling experiments. The first salt is the one used by Hydro Aluminium Rolled Products AS today, which is denoted Industrial. This salt has the largest particle size and highest NaCl content. The other salt, denoted Recycled, is a salt that has been recycled as explained in Section 2.2.3. Table 3.4 shows some characteristics of the two salts.

Table 3.4: Salts used for coalescence and off gas experiments

| Salt type | Avg. particle size [$\mu$m] | NaCl:KCl | Added $CaF_2$ | Producer |
|---|---|---|---|---|
| Industrial | 844 | 77:23 | 2wt% | Montanal |
| Recycled | 257 | 55:45 | 2wt% | Befesa |

### 3.1.2 Alternative utilisation of aluminium scrap

For the aluminothermic production of silicon, the CaO-$SiO_2$ slag was made melting CaO lumps with $SiO_2$ powder (Figure 3.4) in an induction furnace. The produced slag can be seen in Figure 3.5. The aluminium source was either clean aluminium or dross. The clean aluminium was cut from a block of 1xxx alloy, and it was assumed to contain 100% aluminium. For the dross, two different types were used. Dross 1 contained 89.2% aluminium, while the second one had an unknown aluminium content. It was therefore assumed to contain 50% aluminium for the calculations. The materials used in these experiments are listed in Table 3.5.

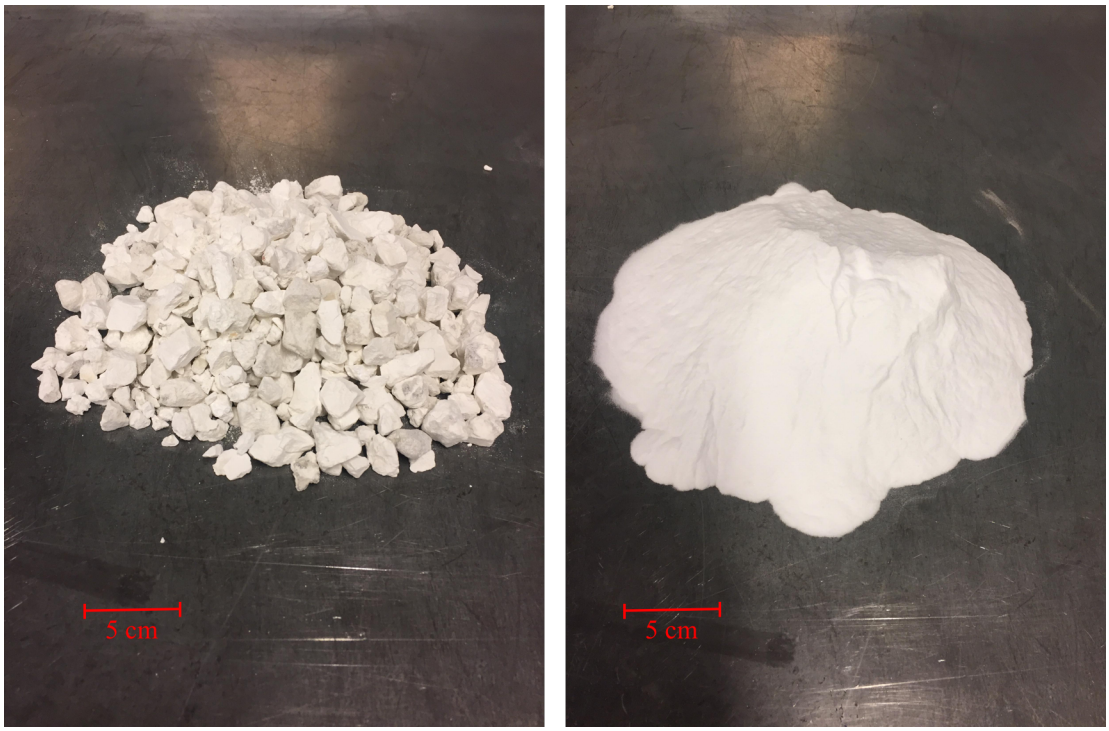


Figure 3.4: CaO lumps (left) and $SiO_2$ powder (right) used to make the slag


Figure 3.5: Produced slag used as the silicon source

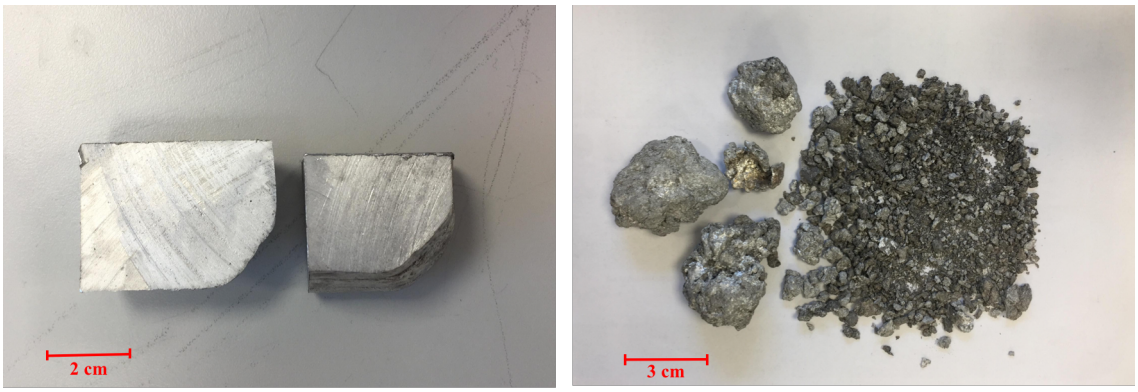


Figure 3.6: Aluminium pieces (left) and dross (right) added as the aluminium sources

Table 3.5: Materials used for aluminothermic production of silicon

| Material | Particle size | Purity [%] |
|---|---|---|
| CaO | 2 cm | 97 |
| $SiO_2$ | Powder | >99 |
| Clean Al | Bulk | 100 (assumed) |
| Dross 1 | Varying | 89.2 |
| Dross 2 | Varying | 50 (assumed) |

## 3.2 Experimental setups

### 3.2.1 Investigation of coalescence behaviour

The coalescence behaviour of UBCs and incinerator metal was investigated by melting the materials under a salt flux. This will give an indication of how easily recyclable the materials are, and how much metal can be recovered during recycling.

In Table 3.6, the experiments are listed. I.M. is an abbreviation for incinerator metal, while UBC stands for used beverage cans. Trials with varying amounts of $CaF_2$ were executed.

Table 3.6: Coalescence experiments

| Experiment no. | Scrap material | Weight scrap [g] | Salt type | Weight salt [g] | $CaF_2$ [%] |
|---|---|---|---|---|---|
| 1 | I.M. | 39.9 | Industrial | 80.0 | 2 |
| 2 | I.M. | 40.2 | Industrial | 80.1 | 2 |
| 3 | UBC | 40.0 | Industrial | 80.0 | 2 |
| 4 | I.M. | 40.2 | Recycled | 80.2 | 0 |
| 5 | I.M. | 40.0 | Industrial | 80.2 | 4 |
| 6 | I.M. | 40.1 | Industrial | 80.0 | 4 |
| 7 | UBC | 40.8 | Industrial | 80.3 | 4 |
| 8 | UBC | 40.6 | Industrial | 79.9 | 4 |
| 9 | I.M. | 39.9 | Recycled | 79.9 | 2 |
| 10 | I.M. | 40.2 | Recycled | 80.0 | 2 |

The aperture was an induction coil heating an 8 cm diameter graphite crucible with mica isolation around and above the crucible. The setup can be seen in Figure 3.7a), while the crucible can be seen in Figure 3.7b)


a) Aperture b) Graphite crucible

Figure 3.7: Experimental setup for coalescence tests

Approximately 40 g of scrap was charged into the bottom of the crucible, while 80 g of salt was charged on top. In advance, the desired amount of $CaF_2$ was added to the salts and mixed properly. The crucible with charge was heated to 800°C at 10 kW before the furnace was turned off and the crucible was removed to cool in air. The experiments took approximately 30 minutes from the furnace was turned on until the crucible was removed. When cooled to room temperature, the crucibles were filled with water to leach the salt and extract the metal pieces.

As mentioned, UBCs and incinerator metal were used as the scrap materials. Compacted and cut UBC pieces of approximately 6-7 grams and 1x1 cm each were used. For each experiment, six pieces were used, shown in Figure 3.8.

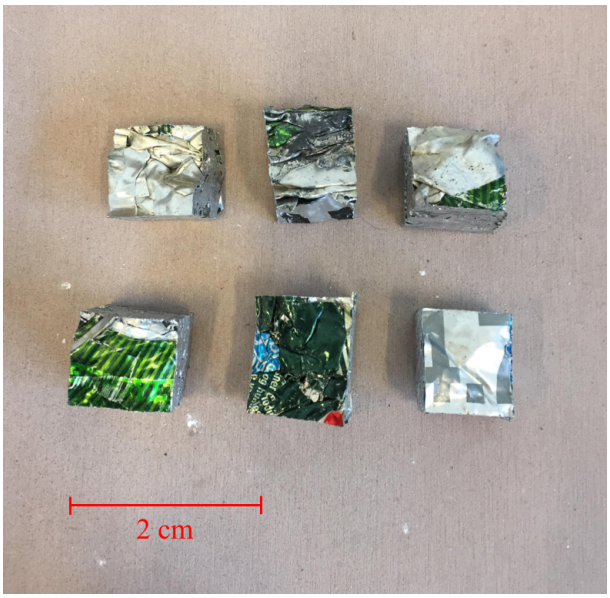


Figure 3.8: UBC pieces used for coalescence experiments

### 3.2.2 Melting aluminium scrap under a salt flux

In addition to small coalescence experiments described in Section 3.2.1, remelting the same scrap under a salt flux was performed in a 5 liter crucible to measure the yield of the scraps using different salts. An induction furnace (IF75) was used to get efficient stirring of the materials. Also here, the scrap was charged in the bottom of the crucible, and the salt covered the scrap to prevent oxidation of the metal. Unlike the coalescence experiments however, one whole piece of compacted UBCs was charged instead of several smaller pieces, shown in Figure 3.9.

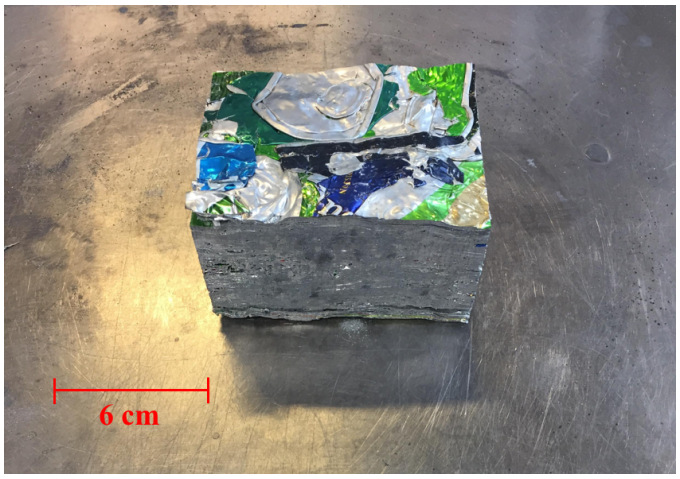


Figure 3.9: Block of UBC used in the experiments

Table 3.7 shows the experimental matrix. Approximately 820 g of scrap and 1640 g of salt

was used, i.e. twice as much salt as scrap. The charged weight of UBCs varied a little due to the lumps not weighing exactly the same. 2wt% $CaF_2$ was mixed into the recycled salt before charging. $CaF_2$ was not added to the industrial salt since it had already been added at Hydro Aluminium Rolled Products AS' plant in Holmestrand before it was received. The crucible was heated to approximately 875°C under an isolating lid and held until everything was molten. The materials were then cast, first pouring the salt into one container, while a different container was used to cast the metal. This setup is shown in Figure 3.10, where the salt was poured into the right container, while the metal was poured into the left container. Some non-metallic compounds were left in the crucible after casting, which was cast separately into the sand as shown in the figure. It is worth noting that the fractions are not clean, meaning metal lumps are found in the salt and non-metallic fraction, and vice versa. After the cast materials were cooled, the metal was extracted by leaching the salt in water. It was characterised by mass balances, EPMA and ICP-MS analyses.

Table 3.7: Remelting experiments under a salt flux

| Experiment no. | Scrap material | Mass scrap [g] | Salt type | Mass salt [g] | Added $CaF_2$ [g] |
|---|---|---|---|---|---|
| 1 | UBC | 820 | Recycled | 1641 | 33 |
| 2 | UBC | 710 | Recycled | 1421 | 28 |
| 3 | UBC | 746 | Industrial | 1492 | 0 |
| 4 | UBC | 742 | Industrial | 1484 | 0 |
| 5 | I.M. | 828 | Recycled | 1640 | 33 |
| 6 | I.M. | 822 | Recycled | 1639 | 33 |
| 7 | I.M. | 820 | Industrial | 1640 | 0 |
| 8 | I.M. | 812 | Industrial | 1624 | 0 |

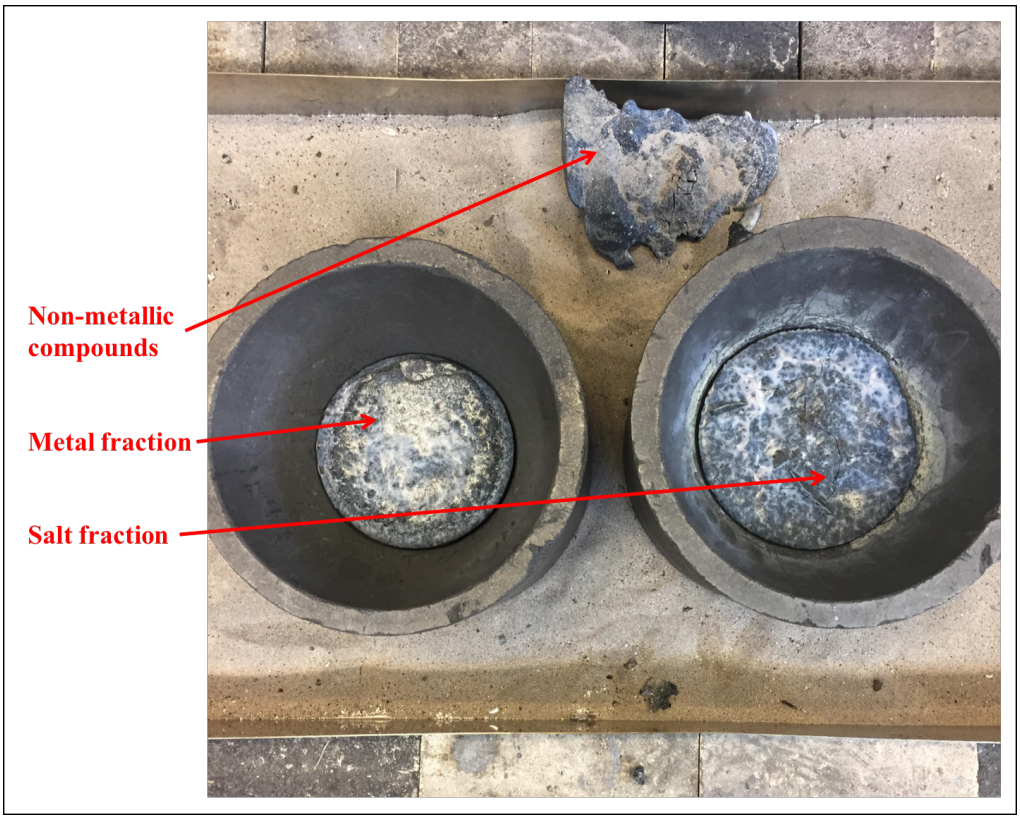


Figure 3.10: Casting procedure

### 3.2.3 Aluminothermic production of silicon

#### Slag production

The CaO-$SiO_2$ slag used in these experiments was prepared beforehand. 1.5kg of CaO was mixed with 1.5 kg $SiO_2$. With equal weights of CaO and $SiO_2$, the slag will in theory consist of 51.7mol% $SiO_2$ and 48.3mol% CaO. The materials were heated to approximately 1700°C in an induction furnace (IF75) in a 12 cm diameter graphite crucible until it was fully molten. The slag was then cast, and crushed into smaller lumps in an agate mortar. It was then remelted again to get a more homogeneous slag. After the second casting, the slag was first crushed in an agate mortar before a small amount of approximately 60 g was crushed in a ring mill with a tungsten carbide chamber. A fraction of the crushed slag was sent for ICP-MS analysis to get a chemical analysis of the slag which could be used to calculate the mass balances for the further experiments. The result of the ICP-MS analysis shows that the slag contains 52.1wt% silicon and 46.6wt% calcium, corresponding to 61.5mol% $SiO_2$ and 38.5mol% CaO. The complete analysis can be found in Appendix B.

**Aluminothermic reduction procedure**

Further, the prepared slag was charged into an 8.5 cm diameter graphite crucible. This crucible was placed inside a crucible like the one used to prepare the slag (12 cm diameter), and heated to 1600°C. A sketch of the experimental setup can be seen in Figure 3.11. Due to the crucible size, it was decided to use 300g of slag. In all experiments the same amount of aluminium was charged, and was calculated using the $SiO_2$ content of the synthetic slag, Equation 2.10, and aluminium content of the drosses.

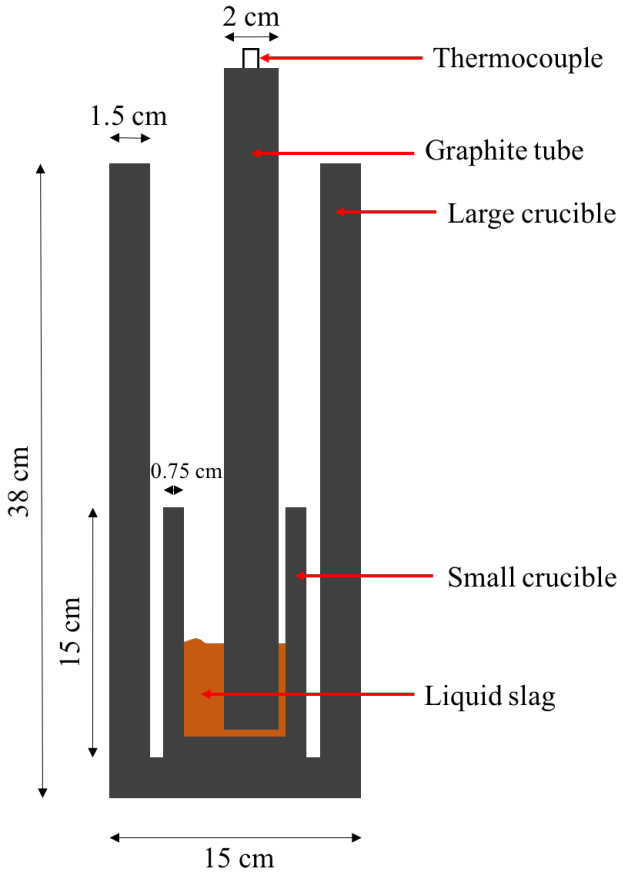


Figure 3.11: Cross-section of the crucible setup

When the slag was completely molten, aluminium was added into the slag. As explained, two different aluminium containing products were used – clean aluminium (1xxx alloy) and dross. The clean aluminium was cut so that two pieces were added into the slag, while the dross was added as is, see Figure 3.6.

In Table 3.8 the experiments are listed. Two parallels were run for each setup. In addition to setups using only clean aluminium and only dross, a third setup using 50/50 clean aluminium and dross was performed. Here, two different drosses were used as can be seen from the table.

Table 3.8: Aluminothermic production of silicon

| Exp. no. | Aluminium source | Weight clean aluminium [g] | Weight dross [g] | Weight slag [g] |
|---|---|---|---|---|
| 1 | Clean | 111 | 0 | 300 |
| 2 | Clean | 113 | 0 | 302 |
| 3 | Dross 1 | 0 | 128 | 299 |
| 4 | Dross 1 | 0 | 126 | 302 |
| 5 | Clean + Dross 1 | 55 | 63 | 299 |
| 6 | Clean + Dross 2 | 56 | 111 | 299 |

Charging the clean aluminium pieces was done by adding one piece at the time manually, while the dross was wrapped in aluminium foil and charged in one piece to keep the small pieces together. Immediately after charging, stirring was performed with the graphite tube to cover the aluminium to prevent oxidation. After charging, the crucible was held at 1600°C for 30 minutes before the crucible was removed from the furnace to cool in air. The charge was stirred after 15 and 30 minutes, in addition to immediately after charging.

When cooled, the crucible was cut into smaller pieces, and the slag, aluminium and silicon phases were analysed using EPMA and ICP-MS.

# Chapter 4

# Results

In this chapter, the results obtained from the experimental work are presented. The aim of the experimental work on recycling was to investigate the recyclability of two different scrap materials and how different salts affect this recyclability. In the results presented here, the two scrap materials and salts will be compared to one another to be able to draw some conclusions from the work. In addition, an alternative way of utilising aluminium scrap was attempted through a preliminary experimental study of aluminothermic production of silicon. The aim of this was to see if the results could say anything about the feasibility of such an option, and testing to see if a by-product like dross can be used for this purpose.

In the recycling experiments, yield has been used to present the results. Here, it is important to differentiate between material yield and metal yield. Material yield is defined as the extracted metal compared to charged material, while metal yield is the extracted metal compared to charged metal. Material yield was used in the yield experiments during recycling under salt fluxes. This means that the calculated yield is based on the mass of charged scrap, rather than the mass of charged aluminium, i.e. coatings, organics, non-metallics etc. are included in the yield calculations.

For the chemical analyses obtained by EPMA and ICP-MS, deviations calculated through a t distribution with a confidence interval of 95% are presented as deviations to the average values. An example calculation can be found in Appendix E.

## 4.1 Investigation of coalescence behaviour

Figure 4.1 shows the extracted metal pieces from the experiments where incinerator metal was melted with the industrial salt. None of the four trials produced significant coalescence, and the increase of $CaF_2$ seems to have little effect on the coalescence behaviour.

What can be observed from Figure 4.1 though, is that the first experiment (left picture) shows less coalescence than the other three. A reason for this could be that the scrap and salt were charged simultaneously into the crucible, while for the remaining trials the scrap was charged on the bottom underneath the salt.

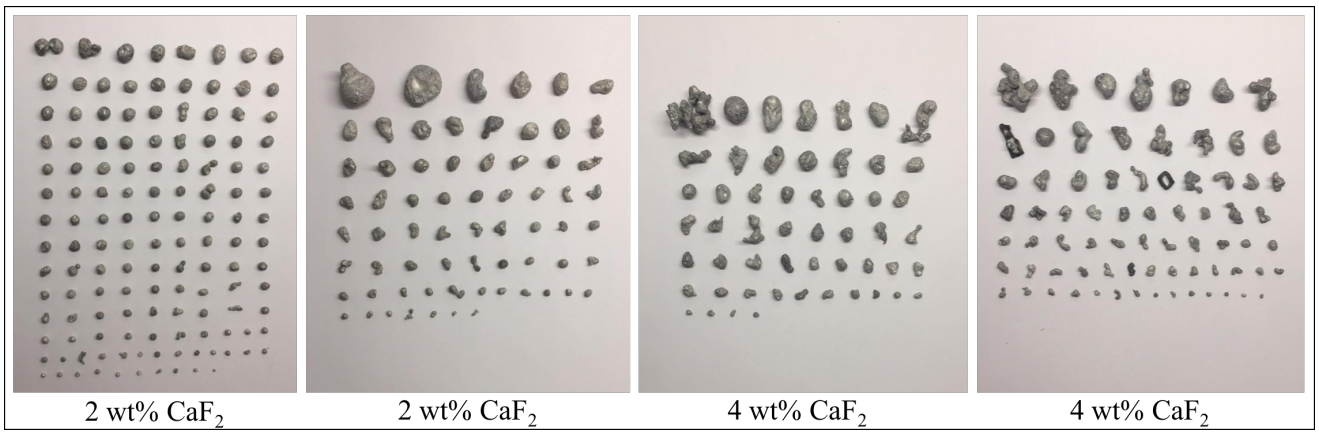


Figure 4.1: Incinerator metal under industrial salt

Figure 4.2 shows incinerator metal melted with recycled salt instead of industrial salt. A comparison of Figures 4.1 and 4.2 clearly shows that the incinerator metal is better coagulated when melted with the recycled salt containing $CaF_2$. However, if $CaF_2$ is not added, a good coalescence effect is not observed. This shows that the fluorine component has a large effect on the coalescence performance of the salt.

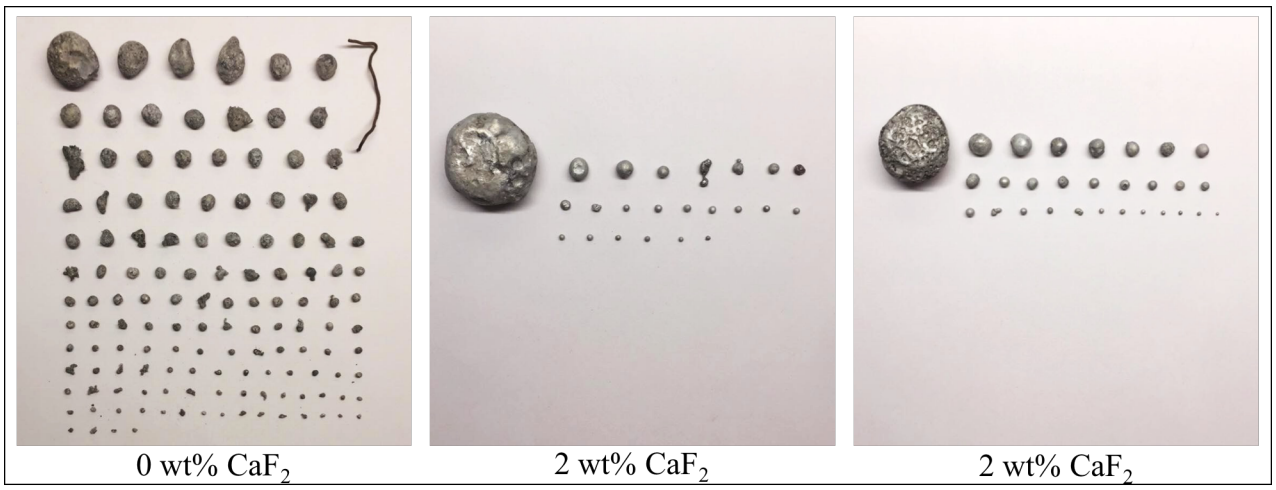


Figure 4.2: Incinerator metal under recycled salt

Figure 4.3 shows pictures of the extracted pieces from the experiments using UBCs and industrial salt. Clearly, the results are not satisfactory, as the UBCs have not coalesced at all. Some small spherical aluminium pieces are observed, but mainly whole pieces or flakes of UBCs are left after extraction. It was observed during the experiments that the UBC scrap

floated on top of the molten salt. The UBCs were molten, but the coating hindered the pieces from coalescing. It is believed that weak stirring was the reason for the unsatisfactory results, as the metal pieces are not able to find each other when it is not stirred. Obviously, stirring is vital when recycling these coated scraps, and no further trials were executed using UBCs due to this problem.

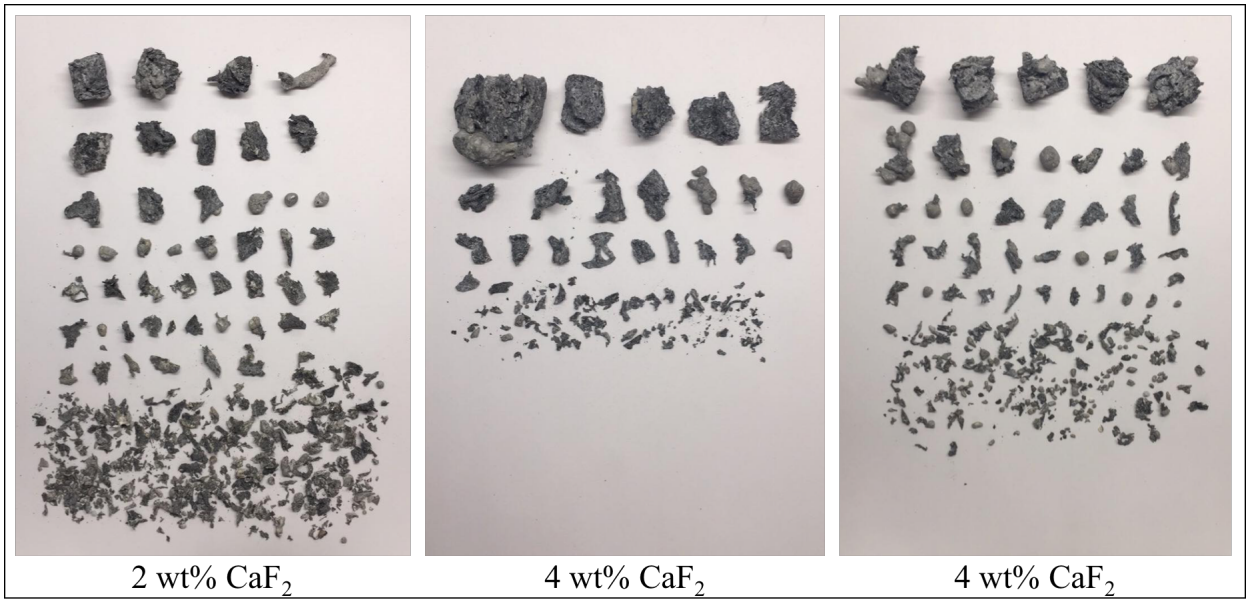


Figure 4.3: UBCs under industrial salt

In Figure 4.4, the number of extracted metal pieces are plotted for incinerator metal containing 0 and 2wt% $CaF_2$. Evidently, the effect of adding 2wt% $CaF_2$ is big, as fewer pieces are extracted indicating more coalescence.

If the salts are compared, the recycled salt seems to perform better than the industrial salt. In Figure 4.5, the trials melting incinerator metal with salts containing 2wt% $CaF_2$ are plotted, and shows that the recycled salt produces bigger metal pieces.

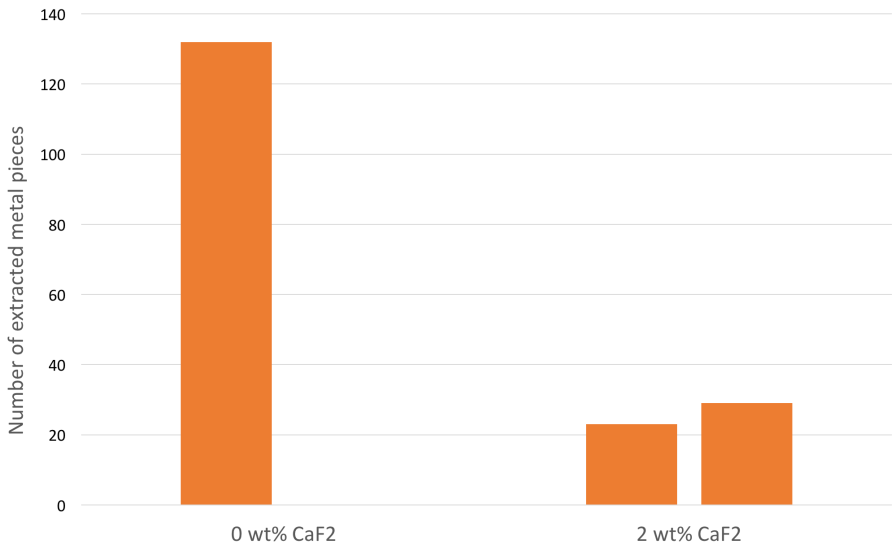


Figure 4.4: Number of extracted metal pieces of the incinerator metal using recycled salt containing 0 and 2 wt% $CaF_2$, showing that $CaF_2$ promote coalescence

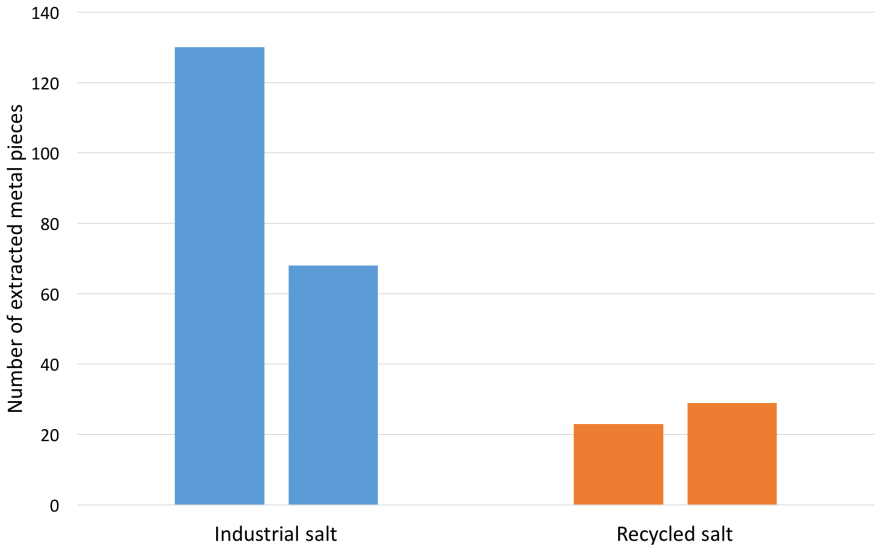


Figure 4.5: Number of extracted metal pieces of the incinerator metal for trials containing 2wt% $CaF_2$, showing that recycled salt promote coalescence

In addition to counting the extracted metal pieces, the pieces were also sieved and characterised according to weight of each fraction. Cumulative distribution curves can be seen in Figures 4.6, 4.7 and 4.8. The incineration metal has a narrower size distribution than the UBCs, shown in Figure 4.6. Further, the recycled salt produces much larger particles than the industrial salt. As can be seen from Figure 4.7, over 85% of the extracted weight of particles are over 20 mm using the recycled salt, while no pieces over 20 mm are found using the industrial salt. Finally, adding 2wt% $CaF_2$ also increases the size drastically, see Figure 4.8.

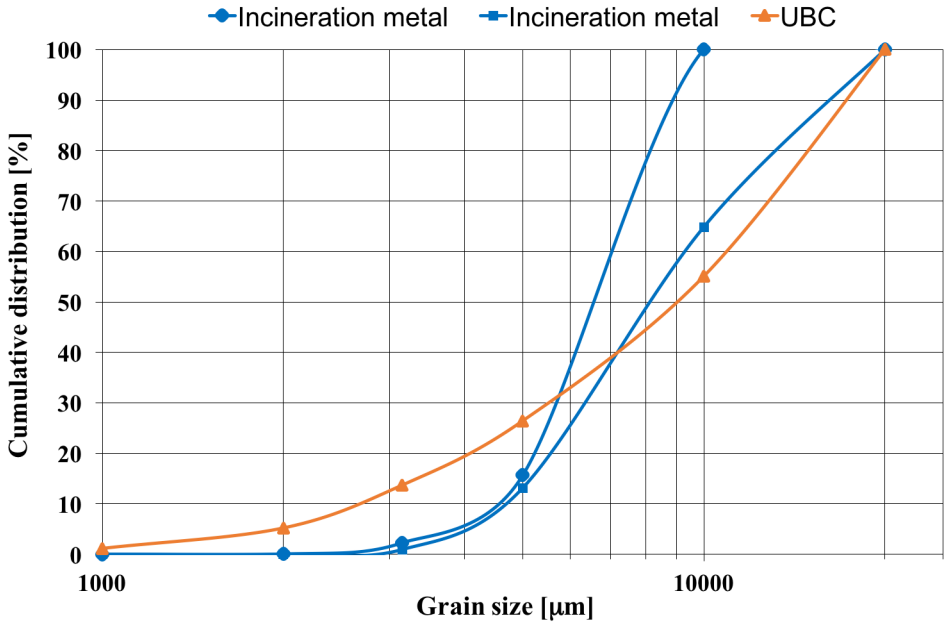


Figure 4.6: Cumulative size distribution of extracted metal pieces using industrial salt with 2wt% $CaF_2$

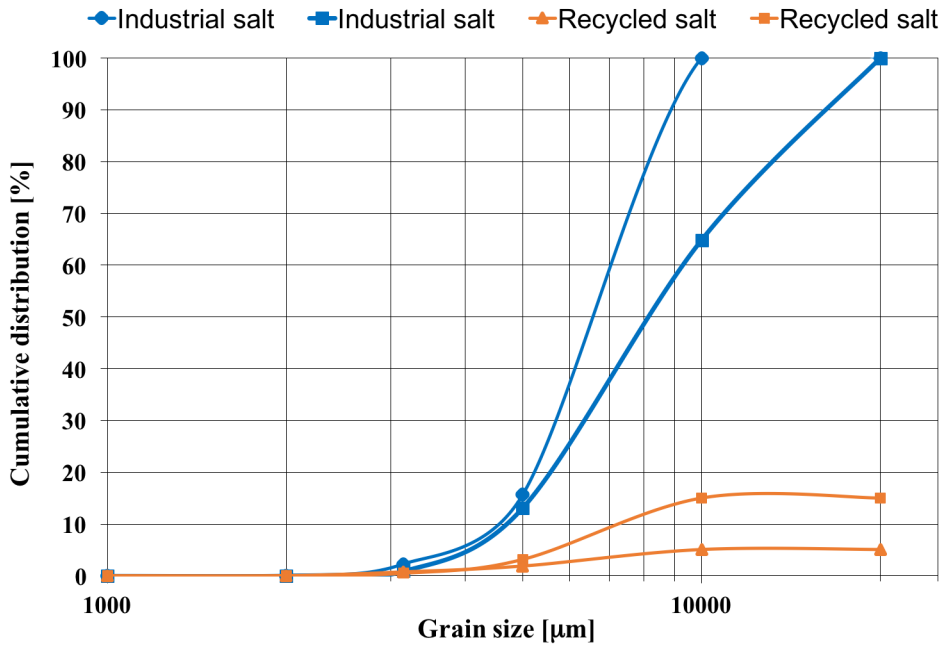


Figure 4.7: Cumulative size distribution of extracted metal pieces after melting incinerator metal with salts containing 2wt% $CaF_2$

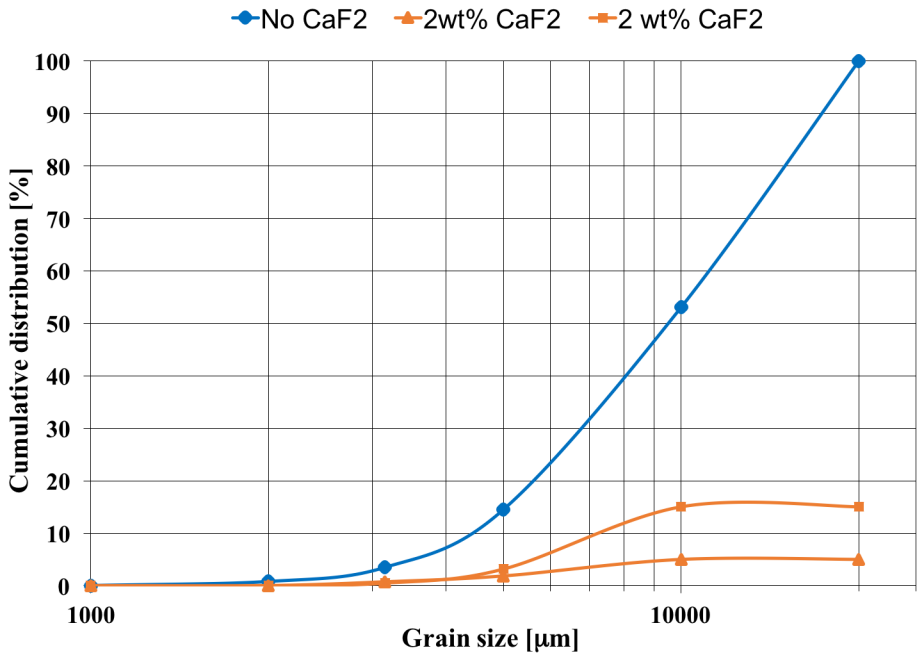


Figure 4.8: Cumulative size distribution of extracted metal pieces after melting incinerator metal under recycled salt

## 4.2 Melting aluminium scrap under a salt flux

In Figure 4.9, the material yields for the eight experiments are shown. The yields range from over 85% to 56%. The UBCs melted with recycled salt gives the lowest material yield, while the UBCs with industrial salt and incinerator metal with recycled salt gives high yields for both parallels. For the incinerator metal melted under industrial salt, the deviation between the two parallels is large.

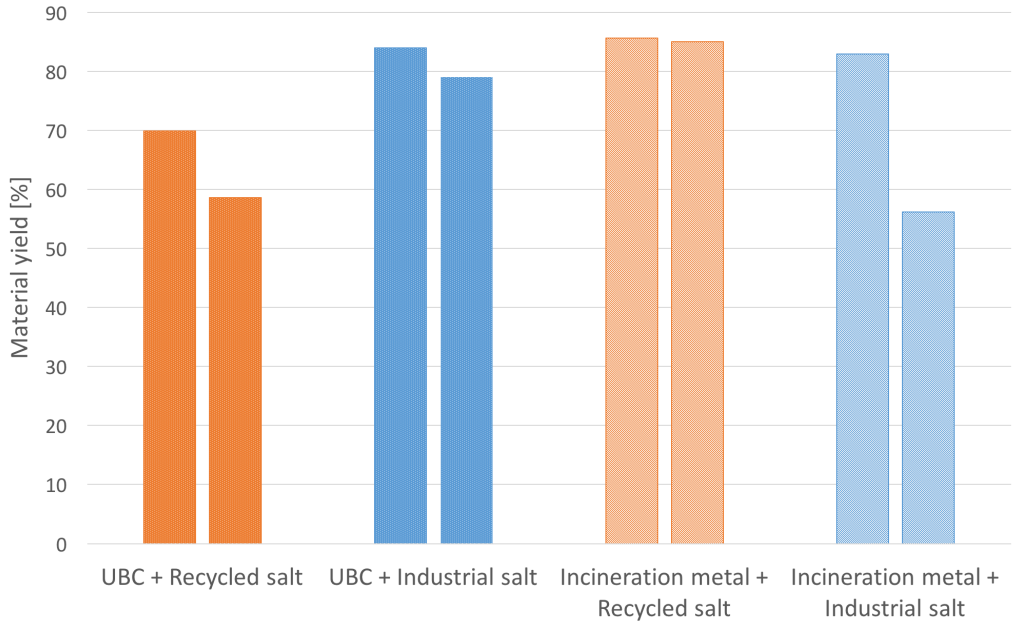


Figure 4.9: Material yield presented according to scrap and salt materials

The metal phases were analysed using EPMA. From Figure 4.10, the metal clearly consists of two main phases. Volume fractions, which is assumed to be equal to the area fractions, were calculated using ImageJ [79], and chemical compositions of both phases in addition to volume fractions of the phase are presented in Table 4.1. The results show that the dark phase contains very high amounts of aluminium, while the light phase, which is probably an intermetallic phase, contains up to 75% aluminium. As Table 4.2 shows, the iron content in the light phase is significant, making up the most of the remaining contents. However, the light phase make up less than 5% of the volume, found in Appendix C. The complete chemical analysis is found in Appendix A.

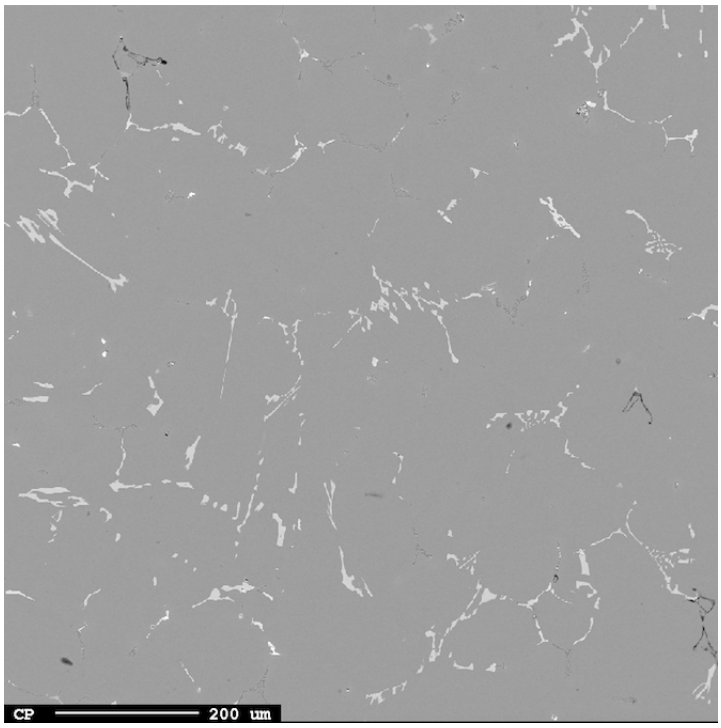


Figure 4.10: SEM image of metal phase from experiment 1 (UBC + Recycled salt) at 100X magnification

Table 4.1: Volume fraction and %Al of the metal phases from EPMA analysis

| Scrap material | Salt type | Volume fraction dark phase [%] | %Al in dark phase | %Al in light phase |
|---|---|---|---|---|
| UBC | Recycled | 96.4 ± 3.41 | 98.0 ± 0.45 | 75.4 ± 0.29 |
| UBC | Industrial | 95.3 ± 3.82 | 97.5 ± 0.57 | 74.0 ± 5.35 |
| I.M. | Recycled | 97.1 ± 2.34 | 98.2 ± 0.03 | 60.6 ± 0.88 |
| I.M. | Industrial | 96.3 ± 2.34 | 97.9 ± 0.4 | 58.3 ± 28.97 |

Table 4.2: Iron content of light phase from EPMA

| Scrap material | Salt type | %Fe [wt%] |
|---|---|---|
| UBC | Recycled | 15.4 ± 2.01 |
| UBC | Industrial | 15.4 ± 1.25 |
| I.M. | Recycled | 23.6 ± 1.80 |
| I.M. | Industrial | 22.7 ± 0.41 |

## 4.3 Aluminothermic production of silicon

Figure 4.11 shows pictures of the cut crucibles from the first experiment using clean aluminium and the experiment using clean aluminium plus Dross 2 as the aluminium sources.

From the left picture it is clear that reaction 2.10 has taken place, and the fact that no aluminium is observed indicates that the reaction has been completed. On the right picture on the other hand, where clean aluminium was added together with Dross 2, some metallic aluminium is left in the crucible.

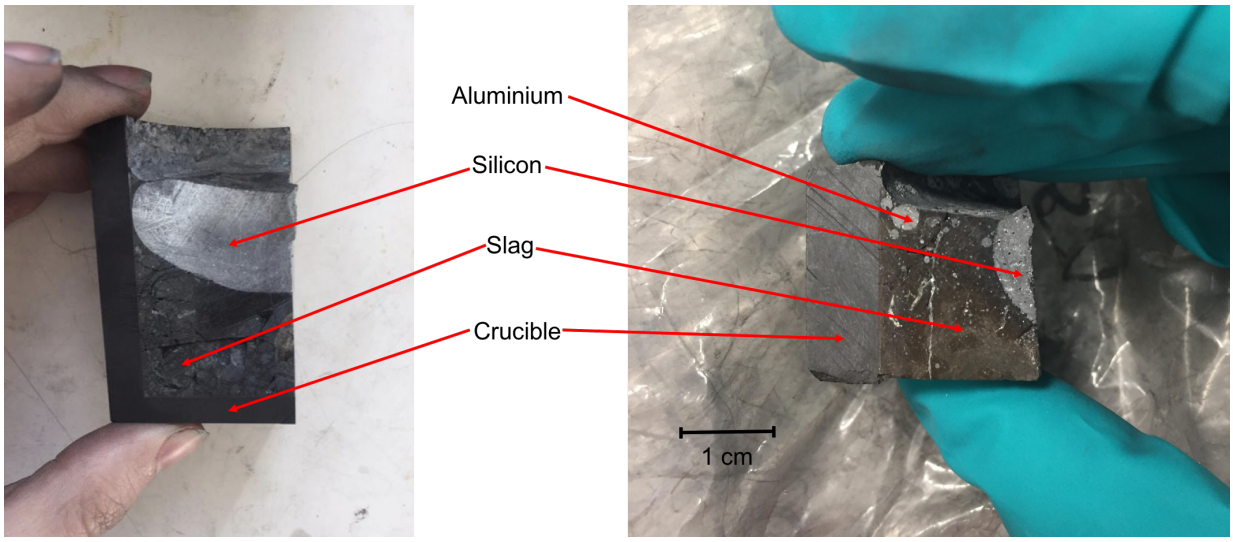


Figure 4.11: Cut crucibles showing the phases after experiments with clean aluminium (left) and clean aluminium + Dross 2 (right)

Since the furnace was turned off during charging of the aluminium, a temperature drop was observed straight after charging. One example is shown by the red dot in Figure 4.12, which shows the temperature profile for the first experiment using clean aluminium. The other temperature profiles can be found in Appendix D. The temperature drops for all six experiments are shown in Table 4.3, where the lowest temperatures after aluminium addition at 1600°C are listed.

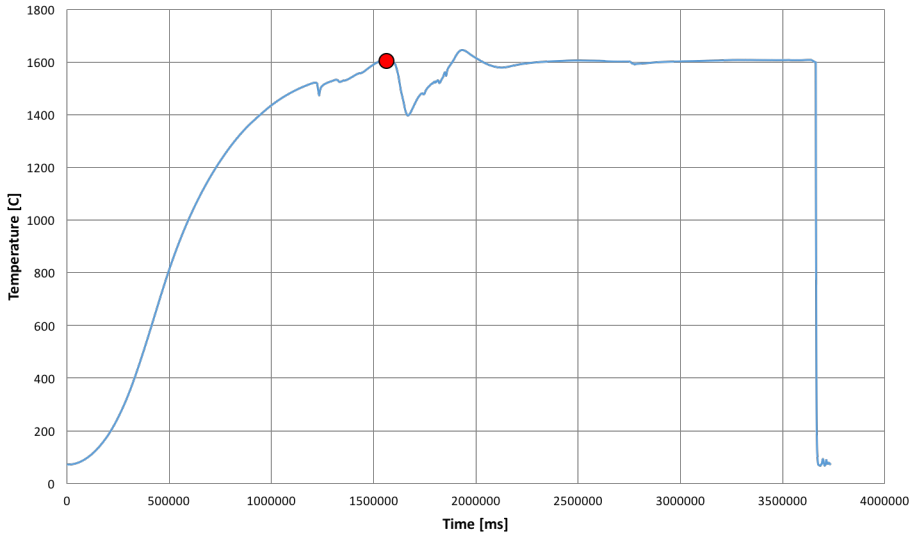


Figure 4.12: Temperature profile for second experiment using clean aluminium. The red dot indicates where aluminium was added

Table 4.3: Temperature drops after charging of aluminium

| Experiment | Reducing material | Temperature after addition of Al [°C] |
|---|---|---|
| 1 | Clean aluminium | 1376 |
| 2 | Clean aluminium | 1398 |
| 3 | Dross 1 | 1435 |
| 4 | Dross 1 | 1483 |
| 5 | Clean aluminium + Dross 1 | 1447 |
| 6 | Clean aluminium + Dross 2 | 1467 |

Figure 4.13 shows a scanning electron microscopy (SEM) image of the metal phase, denoted Silicon in Figure 4.11. It is evident from the image that the metal consists of two main phases – one dark and one light phase. Both phases were analysed using EPMA, and from the results it is evident that the dark phase is silicon while the light phase is a Si-Ca-Al alloy. In Tables 4.4 and 4.5, the silicon, aluminium and calcium fractions are presented for the light and dark phase, respectively.

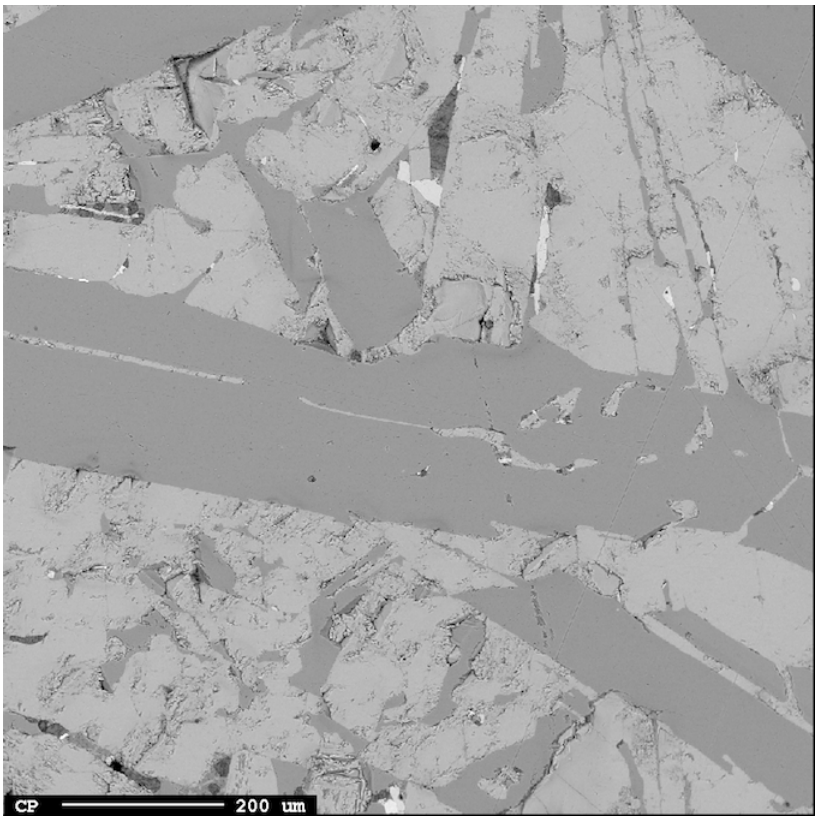


Figure 4.13: SEM image of the metal phase from the first experiment using clean aluminium at 100X magnification

Table 4.4: Composition of Si, Al and Ca in the light metal phase from EPMA

| Reducing material | %Si | %Al | %Ca |
|---|---|---|---|
| Clean Al | 37.02 ± 2.10 | 37.10 ± 0.76 | 23.92 ± 0.26 |
| Dross 1 | 37.53 ± 0.76 | 36.79 ± 0.29 | 24.31 ± 0.05 |
| Clean Al + Dross 1 | 37.02 ± 0.62 | 36.68 ± 0.39 | 23.69 ± 0.65 |
| Clean Al + Dross 2 | 37.46 ± 0.10 | 36.44 ± 0.09 | 23.57 ± 0.11 |

Table 4.5: Composition of Si, Al and Ca in the dark metal phase from EPMA

| Reducing material | %Si | %Al | %Ca |
|---|---|---|---|
| Clean Al | 96.87 ± 2.76 | 0.20 ± 0.77 | 0.15 ± 0.52 |
| Dross 1 | 98.11 ± 4.60 | 0.28 ± 0.82 | 0.22 ± 0.56 |
| Clean Al + Dross 1 | 97.44 ± 1.22 | 0.51 ± 0.49 | 0.32 ± 0.31 |
| Clean Al + Dross 2 | 99.06 ± 0.47 | 0.32 ± 0.19 | 0.02 ± 0.01 |

Using ImageJ [79], the volume fraction of the metal phase was analysed. Table 4.6 presents the volume fractions of the two phases. The analysed images are found in Appendix C. Using these fractions and compositions of the two phases, the total silicon, aluminium and calcium contents in the metal can be calculated. Table 4.7, shows the total composition of the

metal phase from EPMA, while Table 4.8 shows the results of ICP-MS analyses. The complete analyses can be found in Appendices A and B.

Table 4.6: Volume fractions of phases in the metal

| Reducing material | Volume fraction light phase [%] | Volume fraction dark phase [%] |
|---|---|---|
| Clean Al | 47.4 ± 5.2 | 50.8 ± 5.9 |
| Dross 1 | 44.5 ± 0.3 | 51.1 ± 0.9 |
| Clean Al + Dross 1 | 35.4 | 59.9 |

Table 4.7: Composition of Si, Al and Ca in the metal phase from EPMA

| Reducing material | %Si | %Al | %Ca | Remaining [wt%] |
|---|---|---|---|---|
| Clean Al | 66.8 | 17.7 | 11.4 | 4.1 |
| Dross 1 | 66.8 | 17.5 | 10.9 | 3.7 |
| Clean Al + Dross 1 | 71.4 | 13.3 | 8.4 | 6.9 |

Table 4.8: Composition of Si, Al and Ca in the metal phase from ICP-MS

| Reducing material | %Si | %Al | %Ca | Remaining [wt%] |
|---|---|---|---|---|
| Clean Al | 61.9 ± 3.3 | 22.5 ± 2.1 | 14.8 ± 3.7 | 0.9 |
| Dross 1 | 62.9 ± 2.4 | 21.5 ± 2.8 | 11.9 ± 7.9 | 3.7 |
| Clean Al + Dross 1 | 59.1 ± 4.0 | 24.2 ± 2.7 | 14.4 ± 2.2 | 2.3 |

The slag phase was also analysed by EPMA. As seen from the SEM image in Figure 4.14, the slag seems to consist of only one main phase. The spheres in the image are the metallic phase. The CaO, $Al_2O_3$ and $SiO_2$ contents of the slag can be found in Table 4.9. The complete results are found in Appendix A.

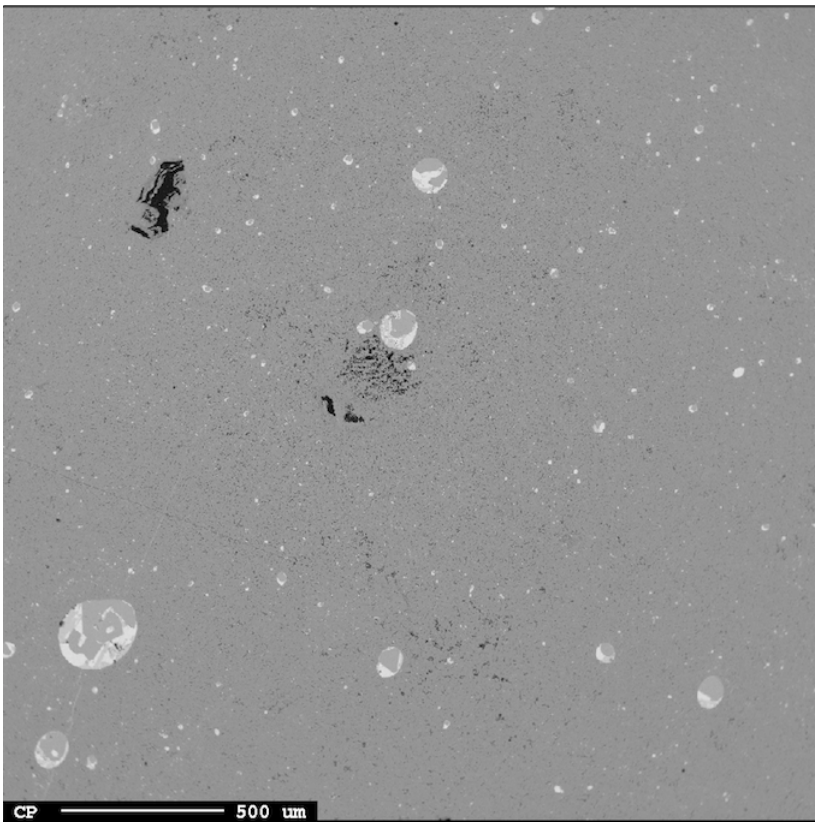


Figure 4.14: SEM image of the slag phase from the first experiment using clean aluminium at 200X magnification

Table 4.9: Composition of CaO, $Al_2O_3$ and $SiO_2$ in the slag phase from EPMA

| Experiment no. | Reducing material | %CaO | %$Al_2O_3$ | %$SiO_2$ |
|---|---|---|---|---|
| 1 | Clean Al | 36.21 ± 0.80 | 62.45 ± 0.85 | 0.12 ± 0.30 |
| 2 | Dross 1 | 36.17 ± 0.05 | 61.32 ± 0.78 | 0.002 ± 0.028 |
| 3 | Clean Al + Dross 1 | 36.22 ± 0.03 | 61.67 ± 0.06 | 0.29 ± 0.09 |
| 4 | Clean Al + Dross 2 | 36.08 ± 0.22 | 48.87 ± 0.11 | 11.936 ± 0.463 |

To model the equilibrium concentrations of slag and metal at 1600°C, FactSage [13] was used. Figure 4.15 shows the equilibrium fractions of the phases present at 1600°C as function of the partial pressure of oxygen. One can see that in addition to a slag and metal phase, a solid $CaAl_4O_7$ phase should be present at equilibrium between $10^{-20}$ and $10^{-17}$ atm. This phase is present in the $Al_2O_3$-CaO rich region of the $Al_2O_3$-CaO-$SiO_2$ phase diagram, highlighted by the red area in Figure 4.16.

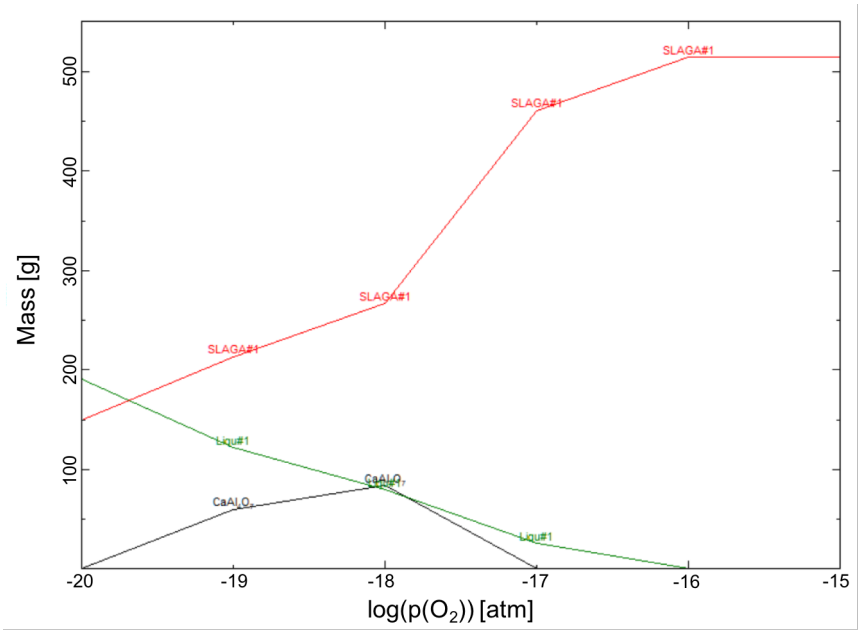


Figure 4.15: Equilibrium fractions of phases at 1600°C as function of the partial pressure of oxygen

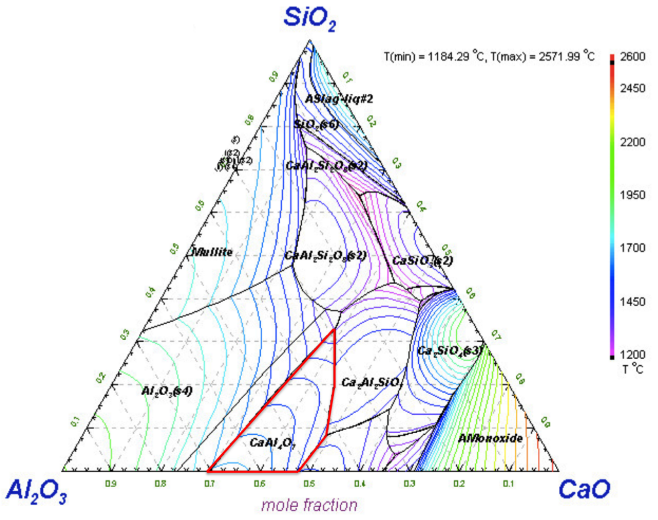


Figure 4.16: $Al_2O_3$-CaO-$SiO_2$ phase diagram [73]. The red area indicated the $CaAl_4O_7$ phase

A closer study of the composition of the metal phase as function of oxygen partial pressure, reveals that the silicon concentration in the metal decreases upon decreasing partial pressures. Similarly, the $SiO_2$ content will also decrease with lower partial pressure. In Figures 4.17 and 4.18, the equilibrium concentrations of elements in the metal and slag phases are shown, respectively.

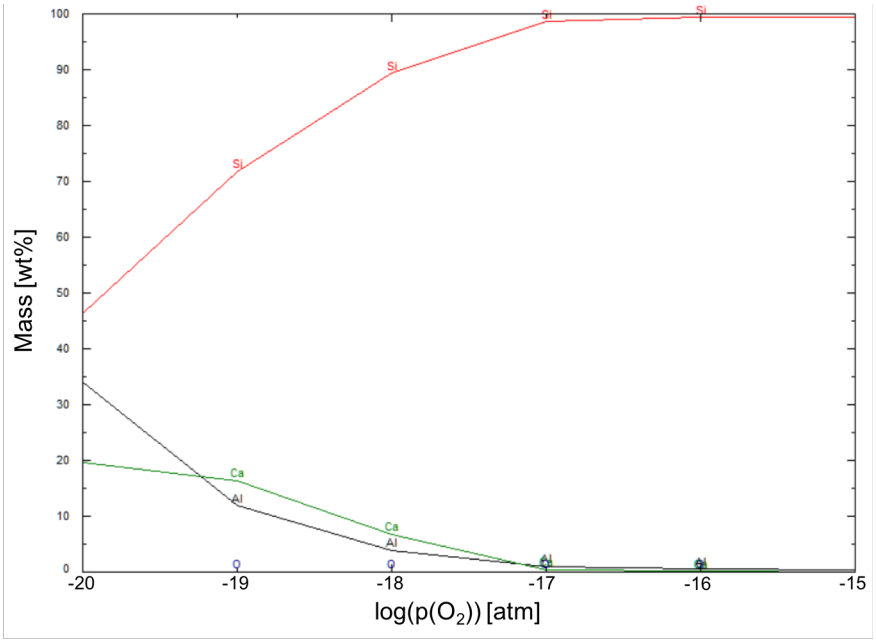


Figure 4.17: Equilibrium fractions of the metal phase at 1600°C as function of the partial pressure of oxygen

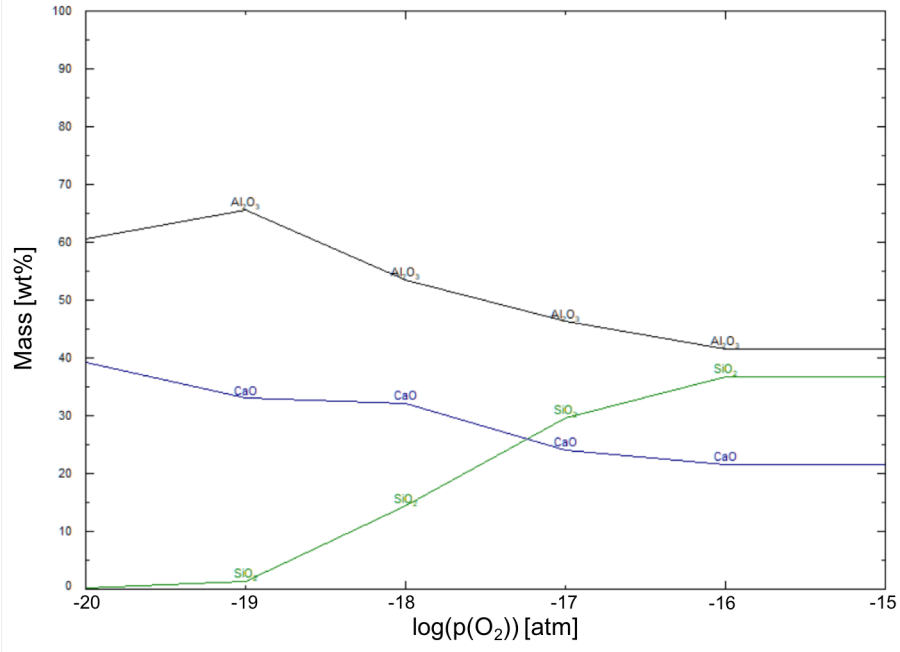


Figure 4.18: Equilibrium fractions of the slag phase at 1600°C as function of the partial pressure of oxygen

If the cooling is assumed to follow the Scheil-Gulliver equation, the solidification should be as shown in Figures 4.19 and 4.20 for the metal and slag, respectively. Both $CaSi_2$ and $CaAl_2Si_2$ should be present in the metal phase at room temperature in addition to pure silicon. In the slag phase, melilite (50wt% $Ca_2AlSi_2O_7$, 50wt% $Ca_2Al_3O_7$) and $CaAl_4O_7$ will be present at

high concentrations at room temperature. The concentration of each when solidified can be calculated from the figures. In Appendix G, the phase transitions and resulting phases are shown. In Table 4.10, the compositions as shown.

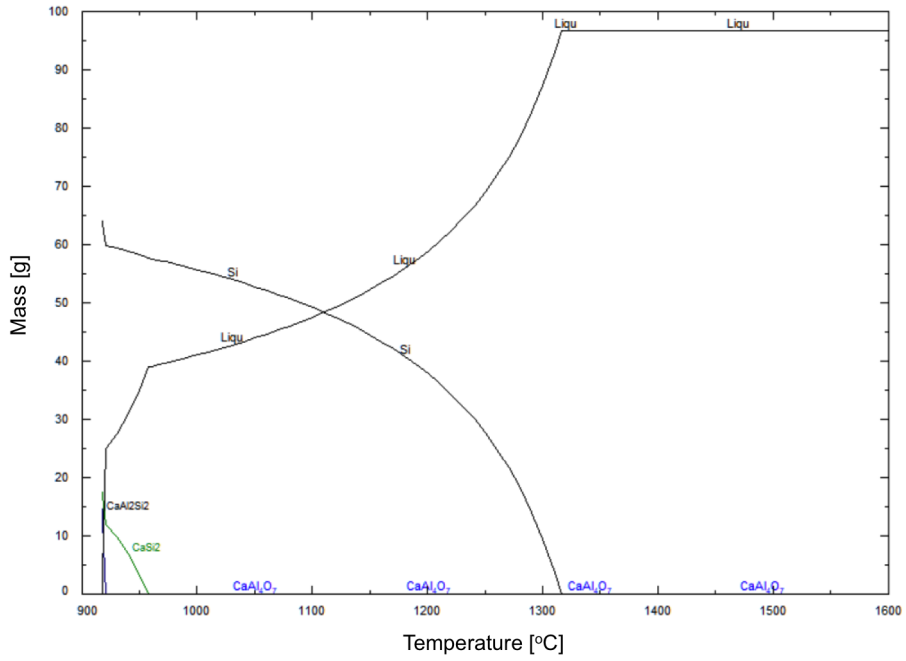


Figure 4.19: Composition of elements in metal phase upon cooling from 1600° assuming Scheil-Gulliver cooling

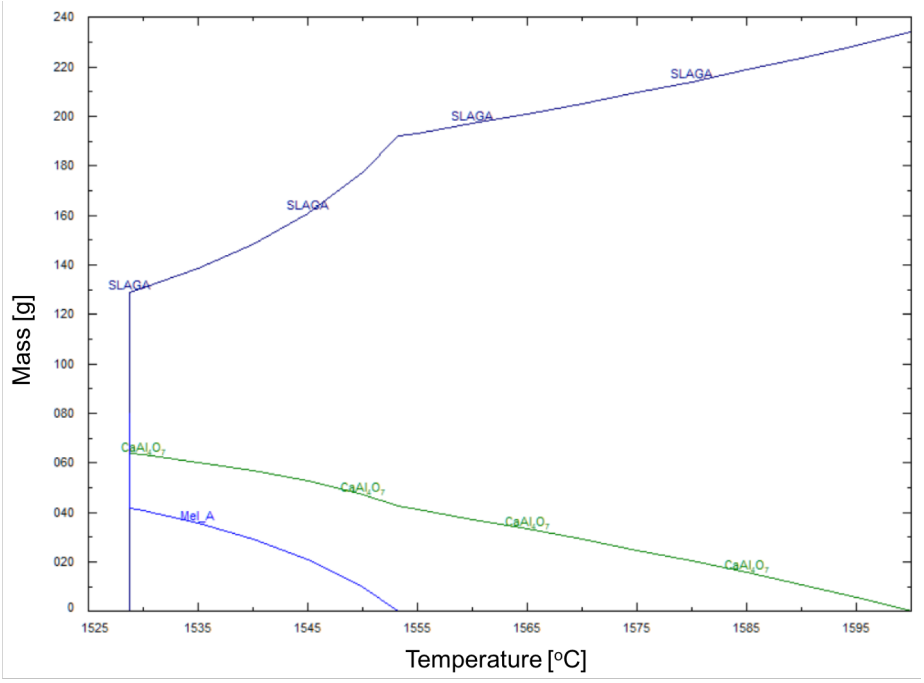


Figure 4.20: Composition of elements in slag phase upon cooling from 1600° assuming Scheil-Gulliver cooling. The $CaAl_2O_4$ phase is not shown in the figure, but should be present according to values in Appendix G

Table 4.10: Theoretical concentrations of phases in metal and slag at room temperature

| | | |
|---|---|---|
| Metal | wt% Si | 66.5 |
| | wt% $CaSi_2$ | 18.3 |
| | wt% $CaAl_2Si_2$ | 15.2 |
| Slag | wt% melilite | 34.3 |
| | wt% $CaAl_2O_4$ | 35.2 |
| | wt% $CaAl_4O_7$ | 30.5 |

# Chapter 5

# Discussion

In this chapter, the results obtained are discussed and evaluated. An evaluation of the salts and scraps will be performed, and deviations will be discussed. The chemical compositions of slag and metal phases obtained by EPMA and ICP-MS will be compared to one another and to thermodynamic data calculated by FactSage [13].

## 5.1 Investigation of coalescence behaviour

### 5.1.1 Scrap materials

As the results clearly show, the UBCs did not produce satisfactory results using this setup. A reason for why the material did not melt properly and coalesce might be due to the coating surrounding the UBCs. The six UBC pieces used in the experiments (shown in Figure 3.8) are not single pieces. The small pieces consist of many UBC layers, with each layer being covered in coating on both sides. Therefore, melting is expected to be more difficult than having one whole coated aluminium piece. This was observed in the experiments, as the aluminium was molten, but was kept in its original form due to the coating layer. Further, even though the cans are compressed, they are not fully compacted. Figure 5.1 shows a SEM image of the cross section of the compressed UBCs. The red area, representing the UBCs, accounts for 79.9% of the image. The rest can be categorised as porosity. Having 20% porosity decreases the density of the material, resulting in it floating on the top and oxidising when exposed to air. However, the bulk density of the incinerator raw material is lower than that for UBCs, as seen in Table 3.3. The reason for them not floating to the top is most likely that they will coalesce upon melting, increasing the density of the material. Clearly, the hindering of coalescence by the coating layers is significant.

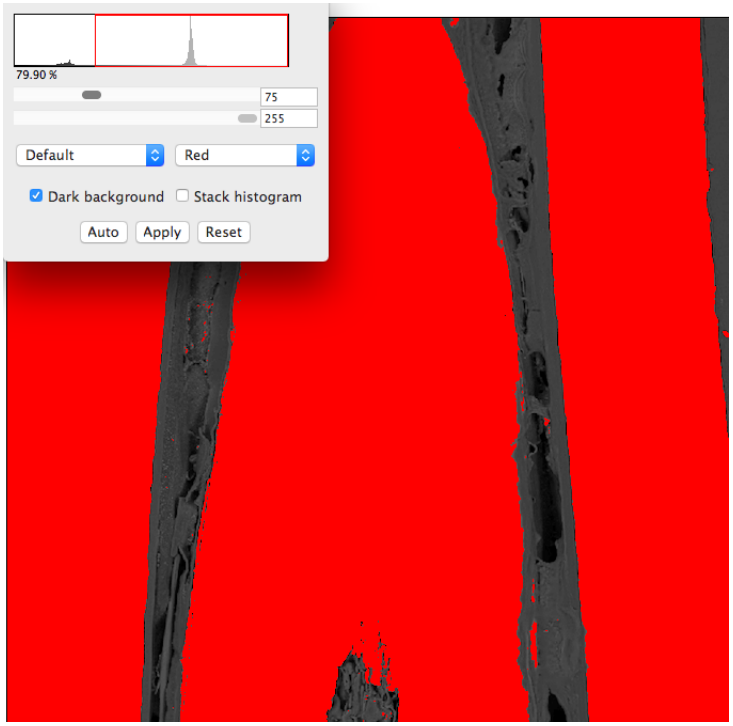


Figure 5.1: SEM picture of the cross section of compressed UBCs at 100X magnification. The red area is UBCs, corresponding to 79.9% of the image

The obtained results from the UBC material indicate that the number of compressed pieces added is not of great importance. The individual layers of UBC seem to have a greater effect on the results, as the metal within the pieces has not coalesced. On the other hand, some coalesced aluminium is observed on some of the UBC pieces. A theory is that the coalescence starts on the edges of the cut pieces, where un-coated aluminium is exposed to the molten salt. Figure 5.2 shows an extracted piece, where the original shape is clearly visible. The picture is taken from above, as in Figure 3.8. Some coalescence has occurred on one corner where aluminium is exposed. As a consequence, the size of the pieces could be of importance, as more un-coated aluminium is exposed the smaller the pieces are.

Figure 5.2: Extracted UBC piece after coalescence experiment seen from above. The red square indicates the original form of the material

If this is the case, the discussion on whether pre-treatment steps should be applied becomes relevant. As described in Section 2.2.2, thermal de-coating to decompose the coating on the UBCs should improve the coalescence as the aluminium sheets are able to find each other more easily. This was also shown experimentally by Capuzzi et al. [34]. It is also partly confirmed in this study, by the incinerator metal being much more easily coalesced while not have any coating.

The recyclability of incinerator metal seems to be as high as for the UBCs, if not higher. Therefore, an acceptable yield would be expected in industry. There is no doubt that the material should be recycled, but it is important to minimise the aluminium content ending up as incinerator metal. Even though a high yield can be obtained during the actual recycling process, metal losses occur in other parts of the life cycle, as illustrated in Figure 2.26. Due to the low total yield of this material, a lot more aluminium is lost than for the UBCs, illustrated in Figure 2.27.

Since the incinerator metal produces high metal yield and coalesce relatively easily, the oxide layer does not seem to hinder coalescence. Figure 5.3 shows a SEM image of one incinerated aluminium piece. The dark layer on the right hand side of the image is the oxide layer. For this sample, the layer ranges from below 25$\mu$m to 100$\mu$m. The analysed piece was 3 mm wide at the cross section where the image is taken. Assuming an average oxide layer thickness of 50 $\mu$m on both sides, the total oxidation is less than 3.5%. This is less than the reported 10% from Raadal et al.[55]. However, one piece is not enough to determine the overall oxidation

rate of incinerator metal. One theory is that the oxide layer thickness is independent of the size of the incinerator metal pieces, meaning a small piece has an equally thick oxide layer as a large pieces. This results in small pieces being more oxidised than larger pieces. This will need to be further investigated to draw any conclusions about the general oxide thickness of the incinerator metal.

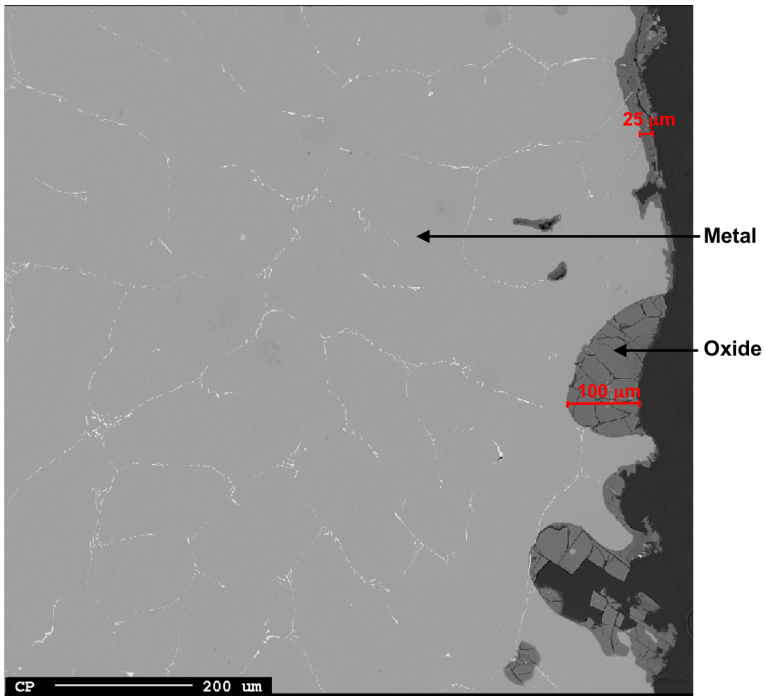


Figure 5.3: SEM image of incinerator raw material at 100X magnification. The oxide layer is seen to the right in the image

The profitability of recycling the incinerator metal depends on several factor. Firstly, the recycling process and resulting yield is of high importance. If one can skip processing steps, like melting the materials directly in a melting furnace instead of melting it in a rotary furnace first, the process will become more profitable if the same yield is obtained. If the incinerator metal can be bought for the same price as UBCs, then the profitability of the incinerator metal would be higher assuming the same yield. However, this is hardly the case. Usually a compromise has to be made between yield and cost as more processing steps often increase the yield and quality while simultaneously increasing the cost. The same can be said the pre-treament procedures, which will increase the cost but potentially increase the yield so much that the process becomes profitable.

### 5.1.2 Salt types

Since only one salt was used for the UBCs, the salts were only compared using the incinerator metal. As Figure 5.4 shows, the recycled salt coalesce the incinerator metal much more

efficiently than the industrial salt. An uncertainty with the recycled salt is the chemical composition. The fact that it is recycled means the composition is not necessarily the same for each batch. It is possible that the batch used in these experiments was a good batch, while other batches might not be. One example is two recycled salt batches received for this work. Both were sent from Hydro Aluminium Rolled Products AS in Holmestrand after they received the salts from Befesa S.A. One salt visibly contains more moist than the other. In the experiments, the "dry" salt was used. The moisture can create problems with reactivity of the salt, leading to burning and flaming due to the moisture being in contact with liquid aluminium. A reason for why the moisture content is varying, could be that KCl is hygroscopic, *i.e.* it absorbs moisture [80]. Therefore, storing time and environment will most likely affect the moisture content of the salts.

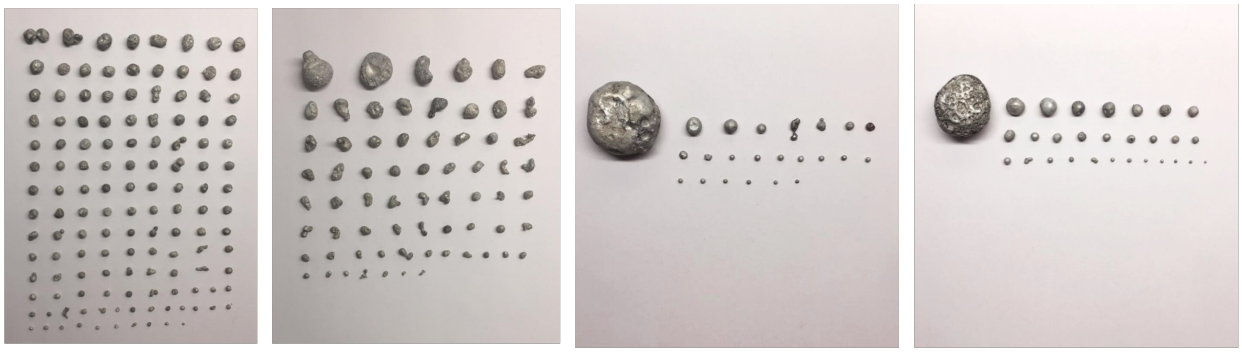


Figure 5.4: Incinerator metal with salts containing 2wt% $CaF_2$

The effect of fluorine content seems significant. Comparing results using recycled salt with no $CaF_2$ and 2wt% $CaF_2$ (Figure 4.2), one can conclude that the expected effect of fluorine is present. However, increasing the fluorine content from 2wt% to 4wt%, as was done for the industrial salt (Figure 4.1), the same effect is not observed. This supports the results from Besson et al [38], who found that the coalescence effect increases dramatically from 0 wt% to 1 wt% cryolite ($Na_3AlF_6$) addition, but the effect slows down with increasing additions above 1 wt%.

There are several potential reasons for why the recycled salt performs better than the industrial one. Firstly, the size distribution of the salts are different, as Figure 2.15 shows. The industrial salt is the salt containing 2wt% $CaF_2$ in the figure. Clearly, the industrial salt has higher average particle size than the recycled salt. In addition, the size distribution is wider for the industrial salt. This could have an affect on the coalescence efficiency of the salt, but this needs to be further investigated.

Secondly, the chemical composition of the salts could be of importance. As Table 3.4 shows, the NaCl:KCl ratios are different for the two salts. While the recycled salt have nearly as much KCl and NaCl, the industrial salt consist of over 3/4 NaCl. This means that the recycled salt has a lower melting point than the industrial salt, leading to decreased viscosity and better

coalescence efficiency as explained in Section 2.2.3.

### 5.1.3 Comparison to industrial procedures

A significant difference in these experiments compared to industry, is the amount of stirring. In industry, where rotary furnaces are usually used to melt UBCs, the stirring greatly contributes to mixing the materials, illustrated in Figure 2.8. In these lab-scale experiments though, the amount of stirring was minimal. A small induction coil was used, leading to some magnetic stirring, but nowhere near the mechanical stirring obtained in a rotary furnace. The fact that the coated UBC scrap did not coalesce when melted in a salt flux with practically no stirring is after all not particularly surprising.

Another significant difference is the salt to scrap ratio. In these experiments, twice the amount of salt as scrap was used, whereas only around 15–20% is used in industry [78]. The reason for this is mainly the scale and amount of stirring. 20% salt would hardly cover any of the scrap when physical stirring is not applied. Also, when the scale is small, the ratios used in industry would not give desirable results during lab-scale experiments. As a consequence, the results might not be directly comparable to industry. However, they give an indication of the expected performance of the salts and recyclability of the scraps.

## 5.2 Melting aluminium scrap under a salt flux

As Figure 4.9 shows, the difference between the two parallels are varying. For UBCs with industrial salt and incinerator metal with recycled salt, the differences are relatively small. For the incineration metal with industrial salt however, the difference between the two parallels are 26.7%. The first run produces a material yield of 83%, while the second only gives 56%. There can be several reason for this difference, as will be discussed later.

As in the coalescence experiments, twice the amount of salt as scrap was used. Therefore, the yields obtained here is not directly comparable to the yields obtained in industry. The purpose of experiments were to compare incinerator metal to UBCs, and recycled salt to industrial salt, not to compare the results to industry. By comparing the scraps, incinerator metal seems to be a highly recyclable material, as it performs in the same region as the UBCs which is profitably being recycled in Norway today.

### 5.2.1 Effect of temperature

In Figure 5.5, the temperature profiles of the two parallels with the largest difference (incinerator metal + industrial salt) explained above, are shown. The maximum temperature during

the first parallel was 819°C, while it was only 771°C for the second parallel. This is clearly the lowest maximum temperature for all eight experiments, see Table F.2 in Appendix F. All temperature profiles can be found in Appendix D. Assuming the NaCl:KCl ratio defines the melting temperature of the salts, one can find from the phase diagram (Figure 2.12) that the melting temperature of the industrial salt should be somewhere around 750°C. Therefore, a maximum temperature of 771° might not be high enough for the flux to perform optimally. As stated by Majidi , the flux' refining properties are not particularly good if the operating temperature is too close to the flux' solidification temperature [40]. Therefore, a temperature well above 800°C should increase the yield. However, temperatures over 900° do not seem to have any effect on the yield. Figure 5.6 shows the maximum temperature plotted against material yield for all eight experiments. There is no relation between temperature and yield, and it seems that temperature is not a decisive factor as long as it is high enough.

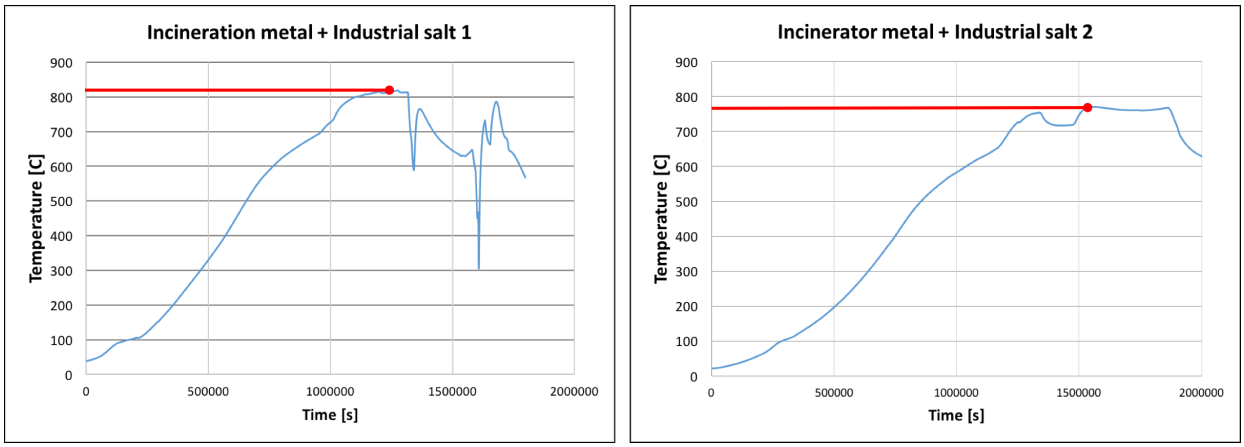


Figure 5.5: Temperature profiles of experiments melting incinerator metal with industrial salt

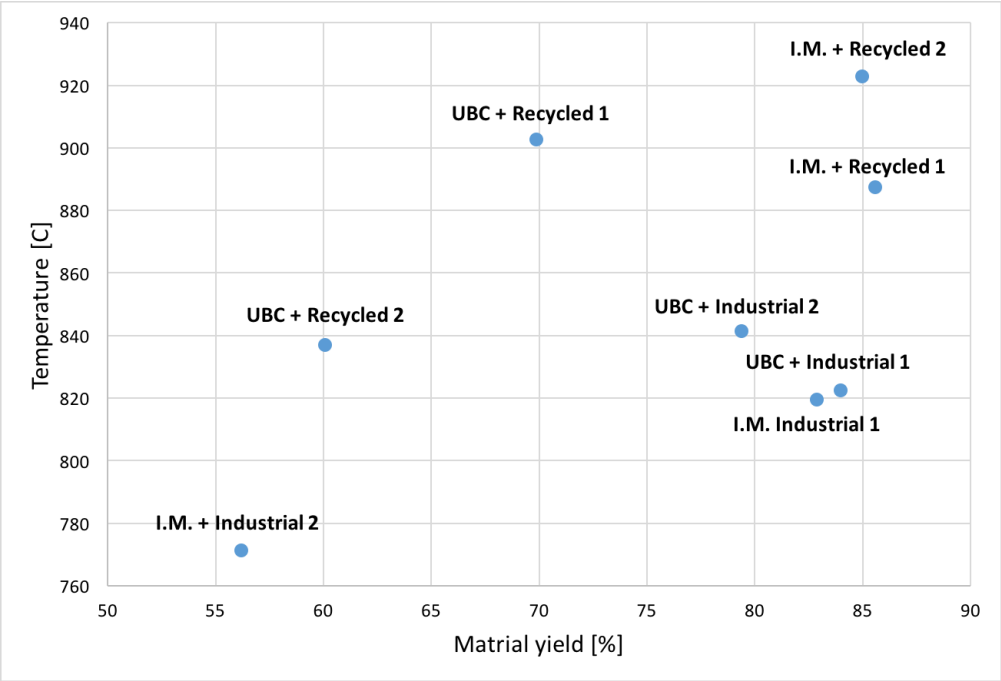


Figure 5.6: Maximum temperature vs. material yield for all eight experiments

### 5.2.2 Effect of stirring

Since an induction furnace is used, magnetic stirring will occur due to metallic aluminium being present in the crucible at all times. The power was higher in these experiments compared to the coalescence experiments, leading to better stirring. From comparing the results using UBCs in these two experimental setups, it is clear that the extra stirring is able to remove the coating layer and coalesce the aluminium in the UBCs.

A large difference between the two salts is not observed in the yield experiments, as opposed to in the coalescence experiments. One explanation to this might be that the temperature distribution is better when having more stirring, meaning the effect of the different melting temperatures might not be that crucial. As long as the temperature is well above the melting temperature of the salt, the scraps coalesce well, as discussed in Section 5.2.1.

It is believed that an important contributor to the large deviations in the results is the amount of manual stirring. A graphite tube was used to stir the materials and check that the materials were molten before casting. As the amount of stirring was not measured in these experiments, it is difficult to know the full effect of the stirring. Anyhow, this could have affected the yield significantly, as mechanical stirring in the rotary furnace is very important for melting the materials.

### 5.2.3 Effect of time

The times could also affect the results. In Table 5.1 the total time of the experiments, from the furnace was turned on until casting, is presented. The times vary a lot, from approximately 20 to 90 minutes. During the experiments, the time was not considered. The materials were heated and cast when properly molten. Generally, the experiments using UBCs took longer time due to heavy smoking between 400°C and 500°C, most likely due to the coating burning off. The power was lowered in this period, before it was increased again when the smoking stopped. This decrease in power, leading to a lower temperature gradient, is visible in the temperature profile plots, shown in Appendix D. One example curve is shown in Figure 5.7, for the second parallel using UBCs and industrial salt.

Table 5.1: Total time of experiments for yield experiments

| Exp. no. | Scrap materials | Salt type | Experiment time [s] |
|---|---|---|---|
| 1 | UBC | Recycled | 1250 |
| 2 | UBC | Recycled | 3800 |
| 3 | UBC | Industrial | 5300 |
| 4 | UBC | Industrial | 3800 |
| 5 | I.M. | Recycled | 1700 |
| 6 | I.M. | Recycled | 1950 |
| 7 | I.M. | Industrial | 1650 |
| 8 | I.M. | Industrial | 1850 |

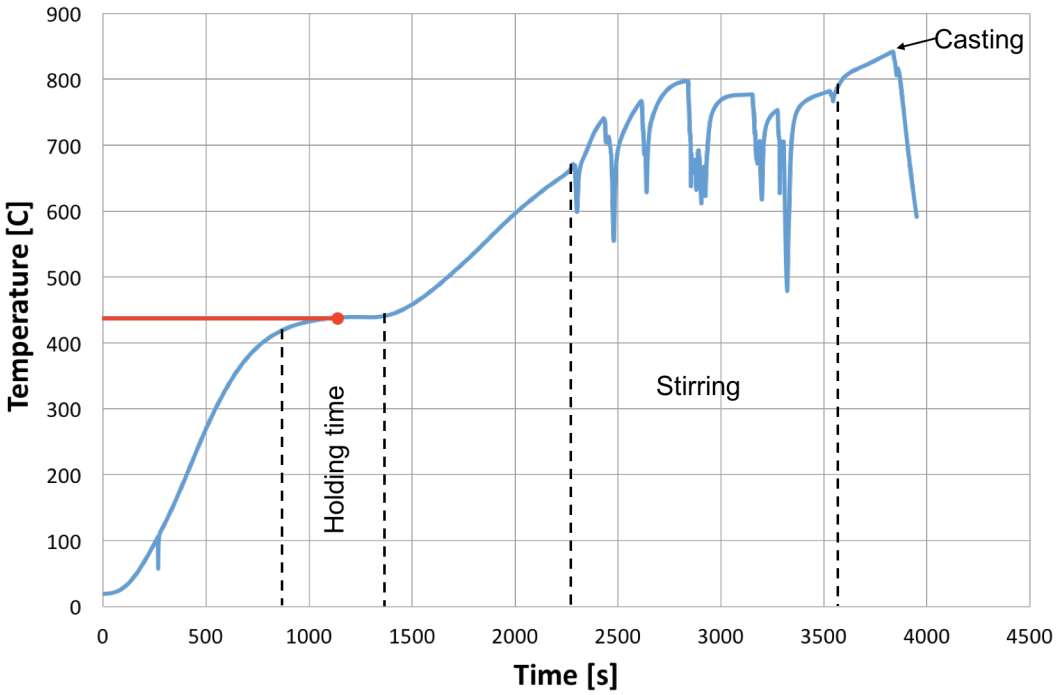


Figure 5.7: Temperature profile for UBCs with industrial salt. Holding time at 400-500°C is highlighted with red line

If the experiment times are plotted against the obtained material yield, see Figure 5.8, it seems a correlation between the times and yields does not exist.

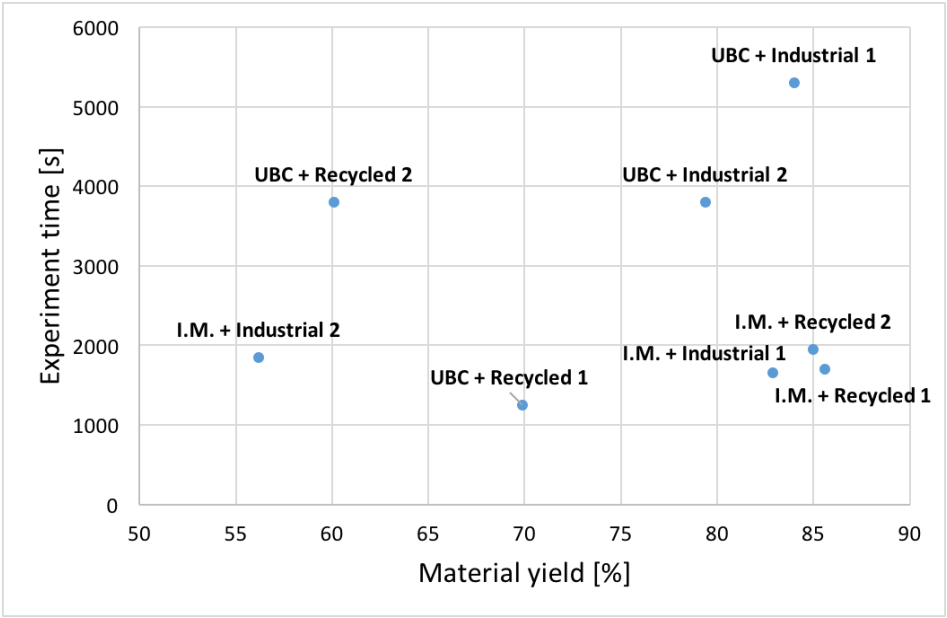


Figure 5.8: Total time of experiment vs. material yield for all eight experiments

### 5.2.4 Effect of initial temperature

Another possible reason for the large difference between the two parallels with incinerator metal and industrial salt, is that in the first trial the crucible was placed into an already hot furnace while the furnace was heated from room temperature in the second parallel. This lead to faster heating rate for the first parallel, and a decreased time from experiment start to end, as seen in Figure 5.5. An increased heating rate leads to the aluminium reaching its melting temperature faster, potentially decreasing the degree of oxidation. On the other hand, oxidation might start earlier as a results of the rapid heating, leading to oxidation before the metal reacts with the salt.

### 5.2.5 Chemistry of resulting metal

The uncertainty in the chemical analyses of the incinerator metal is large. As seen from the ICP-MS analysis in Table 3.2, the deviations are in the range of the average values for the trace elements. From the complete chemical analysis in Appendix B, one can clearly see that the values vary a lot. This confirms that the incinerator metal is inhomogeneous, and it is difficult to obtain a reliable chemical analysis.

According to chemical analyses obtained by EPMA and listed in Table 4.1, the light phase in the SEM images (Appendix C) have aluminium amounts ranging from 58wt% to 75wt%. As seen from Table 4.2, the phase has high iron contents. The metal extracted from experiments using incinerator metal contains significantly higher iron amounts. However, the incinerator raw material does not seem to have higher iron contents than UBCs, as can be seen in Table 5.2. The content in the UBCs is calculated from the alloy compositions in Table 3.1, and the assumption that the can body weighs 3.4 times more than the lid [56]. A reason for why the iron content in the light phase is different for UBCs and incinerator metal, might be due to the concentration of other trace elements resulting in different phases.

Table 5.2: Iron contents of UBCs and incinerator metal

| Material | wt% Fe |
|---|---|
| UBC | 0.70 |
| Incinerator metal (OES) | 0.55 |
| Incinerator metal (ICP-MS) | 0.76 |

### 5.2.6 Contaminations

Small amounts of lead are found in the cast aluminium using incinerator metal. Figure 5.9 shows a mapping of the lead content in the first parallel using incinerator metal and recycled

salt. The points highlighted with a red circle indicate areas with relatively high lead contents, and this amount is similar for all experiments using incinerator metal. This indicates that the raw material contains lead, which comes from other scrap being incinerated together with the aluminium waste. Table 5.3 shows lead content obtained by ICP-MS analyses. As three analyses were conducted on the incinerator metal, three lead values are obtained. The values vary a lot, ranging from 4 to over 400 ppm. This confirms the inhomogeneity of the material, and that lead is present in relatively large amounts. Lead is undesirable as it is hazardous for the human body and environment [81]. Therefore, the acceptable limits are very low, and the product will not be saleable if large lead contents are present.

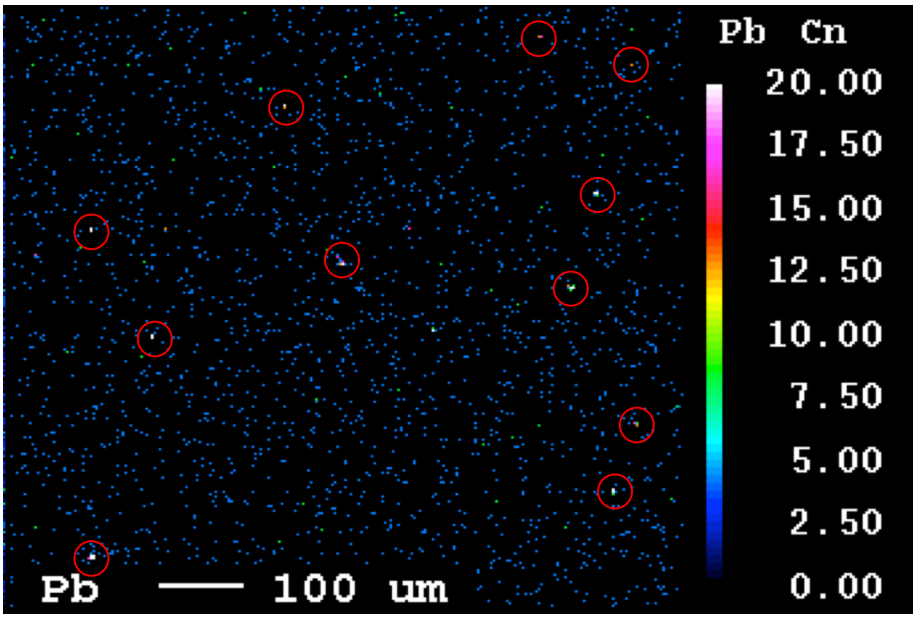


Figure 5.9: Pb mapping of experiment using incinerator metal and recycled salt. The red circles indicate areas with high Pb concentrations

Table 5.3: Lead contents of the incinerator metal

| Analysis number | Pb [ppm] |
|---|---|
| 1 | 422.6 |
| 2 | 4.3 |
| 3 | 30.0 |

Other heavy metals and trace elements might also be detrimental for the finished product. These should be thoroughly investigated to know the real recyclability of the incinerator metal. Even though a high yield might be obtained, the material will not be recycled if the products are not within acceptable quality standards.

### 5.2.7 Comparison to industry

Interestingly, the constellation of scrap and salt used today by Hydro Aluminium Rolled Products in Holmestrand, i.e. UBCs and industrial salt, produces the product with the lowest aluminium content, which is illustrated in Figure 5.10. In addition, it has the lowest volume fraction of the aluminium rich phase (darkest phase in Figure 4.10), seen in Table 4.1.

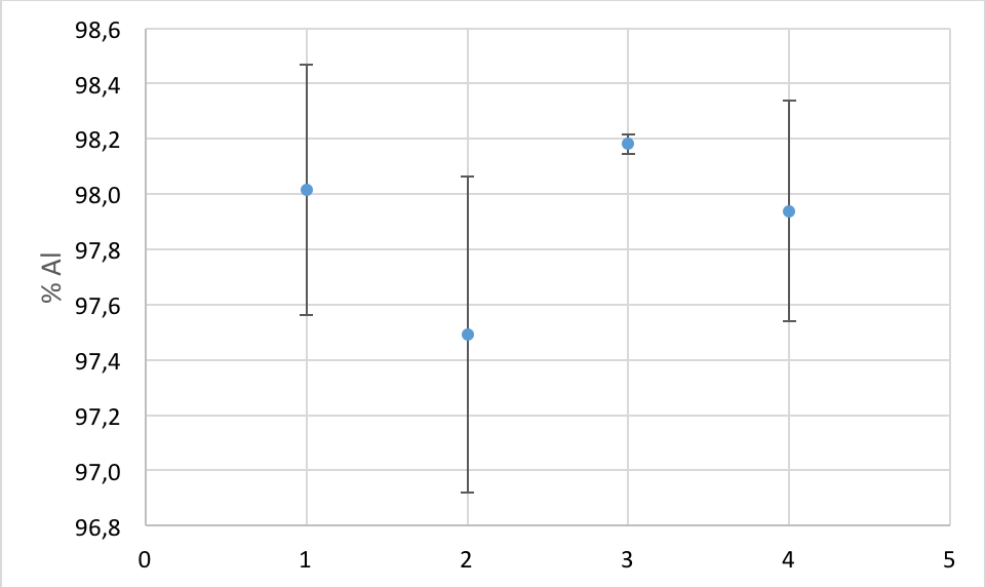


Figure 5.10: %Al in the dark phase for the four experiments. 1 = UBC + Recycled, 2 = UBC + Industrial, 3 = I.M. + Recycled, 4 = I.M. + Industrial

The addition of $CaF_2$ was done slightly differently in these small scale experiments compared to industry. In these experiments, $CaF_2$ was added separately to the batches of salts used in each experiment to ensure the same amount of $CaF_2$ every time. However, in industry the $CaF_2$ is added to a large batch of salts. Therefore, you have the possibility of insufficient mixing, hence inhomogeneous distribution of the $CaF_2$ within the salt.

## 5.3 Aluminothermic production of silicon

### 5.3.1 Raw materials

The quality of the raw materials is expected to have a large effect on the purity of the resulting silicon. Using dross or end-of-life scrap will most likely not produce high-purity silicon. Therefore, an option is to use these materials to make silicon alloys instead. Also, refining can be applied to obtain high purity silicon. However, looking at the chemistry of the resulting metal, which was analysed by EPMA and ICP-MS (Tables 4.7 and 4.8), using dross

as reducing material produce approximately the same silicon, aluminium and calcium contents in the metal as using clean aluminium. As dross contains a lot of impurities, the results might indicate that the purity of the reducing material is not of great importance for the purity of the resulting metal. However, trace elements might have a dramatic effect on the possible use of end product, as some impurities are very hard to get rid of. From ICP-MS analyses shown in Appendix B, the experiments using dross contains higher iron and copper contents than using clean aluminium, but other elements are quite similar. As iron and copper are more noble than silicon, they are hard to get rid of during refining. Therefore, one would expect that the iron and copper contents in the dross would be lower than in the clean aluminium. The effect of trace elements should be studied more thoroughly to draw any conclusions, but from this preliminary study dross seems highly possible to use for this purpose.

Another way of obtaining high-purity silicon is to put the resulting silicon back into the process, i.e. a production loop. Figure 5.11 shows a loop where the resulting silicon is melted again in a new slag. The resulting product will be more pure, i.e. more silicon in the metal and more $Al_2O_3$ in the slag.

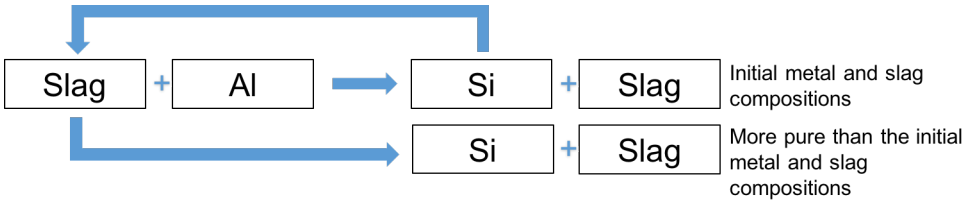


Figure 5.11: Continous process for increased purity of phases

As Section 3.2.3 explains, the synthetic slag contains less CaO than expected. The reason for this is most likely that CaO lumps floated on top of the molten slag, as seen in the red circles in Figure 5.12. Even though the slag was melted twice, all the CaO did not melt properly, leading to lower CaO contents in the analysed slag material.

Figure 5.12: Synthetic slag after crushing in agate mortar. Red circles indicate areas containing CaO pieces

An additional reason for the low CaO contents in the slag might be that pre-reduction of $SiO_2$ occurs. Since the materials are melted in a graphite crucible, carbon might reduce some of the $SiO_2$. Since an elemental analysis was performed, it is assumed that all silicon and calcium is in the form of oxides. However, if $SiO_2$ has been reduced, the calculations will give higher $SiO_2$ contents than realistic.

If the resulting slag compositions are assessed, one can observe that the remaining $SiO_2$ content in the experiment using clean aluminium and Dross 2 is very high compared to the other experiments. The values are plotted in Figure 5.13. Since the aluminium content of this dross was unknown, the high $SiO_2$ content indicates that the dross contained less aluminium than the assumed 50wt%, meaning there is not enough aluminium to reduce all the $SiO_2$. This is emphasised by the low $Al_2O_3$ of the slag and the low silicon content in the metal, see Tables 4.9 and 4.8. An over-stoichiometric concentration of aluminium is desirable to decrease the $SiO_2$ amounts, i.e. increasing the amount of silicon in the metal. Therefore, it is very important to know the composition of the raw materials to utilise them optimally.

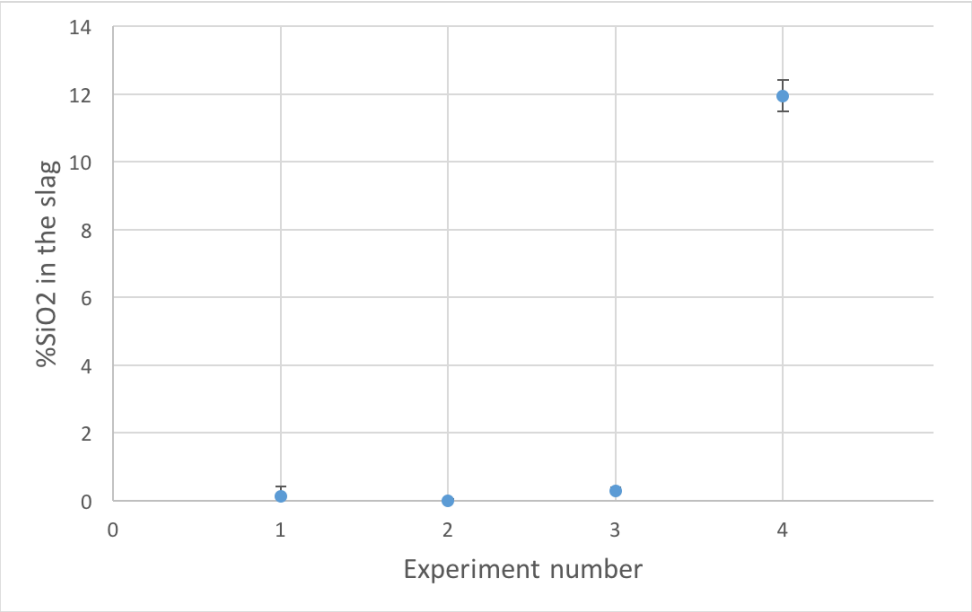


Figure 5.13: %$SiO_2$ in the slag phase from EPMA

### 5.3.2 Charging procedure

The addition of solid aluminium into the molten slag is expected to be one of the most important steps in this experimental procedure. Since the crucibles were small, it was difficult to get the charged aluminium beneath the molten slag surface. This might have led to some oxidation of the aluminium being exposed to air, meaning more $Al_2O_3$ and less silicon being produced. The $Al_2O_3$ contents of the slag is quite similar the three stoichiometric experiments, either indicating a low or same degree of oxidation during charging.

Since the reaction occuring after aluminium addition (Equation 2.10) is exothermic, the temperature is expected to increase upon addition of aluminium. However, the temperature instead decreases as shown in Table 4.3 and Appendix D.2. A probable reason for this is that the experiments are conducted in an open furnace in small scale. In an industrial process on the other hand, where the scale is larger, it is expected that the actual reaction will generate heat, leading to a decreased energy consumption as the materials heat themselves in a continuous process.

### 5.3.3 Thermodynamic modelling

As the thermodynamic calculations indicate, presented in Section 4.3 and shown in Figure 4.15, a $CaAl_4O_7$ phase should be present at 1600°C between $10^{-20}$ and $10^{-17}$ atm. However, this solid phase is not observed during any of the experiments. Therefore, the oxygen partial pressure is most likely above $10^{-17}$ or below $10^{-20}$ atm.

In the above discussion, no carbon is assumed present in the system. However, the graphite crucible will introduce carbon. According to thermodynamics, SiC will start to form immediately when carbon is present, see Figure 5.14. However, large amounts of SiC are not observed during the experiments. One theory is that silicon will react with the carbon on the crucible walls, forming a thin SiC layer on the interface between molten material and crucible. This layer will have a protective effect, hindering the graphite from coming into contact with silicon in the melt, i.e. hindering further SiC generation. To check this theory, light optical microscopy (LOM) images were taken of the interface between the slag and crucible. It is worth mentioning that only the slag touched the crucible walls. One image is seen in Figure 5.15. One might see a thin SiC layer on the interface, but this is difficult to say for certain without chemical analyses.

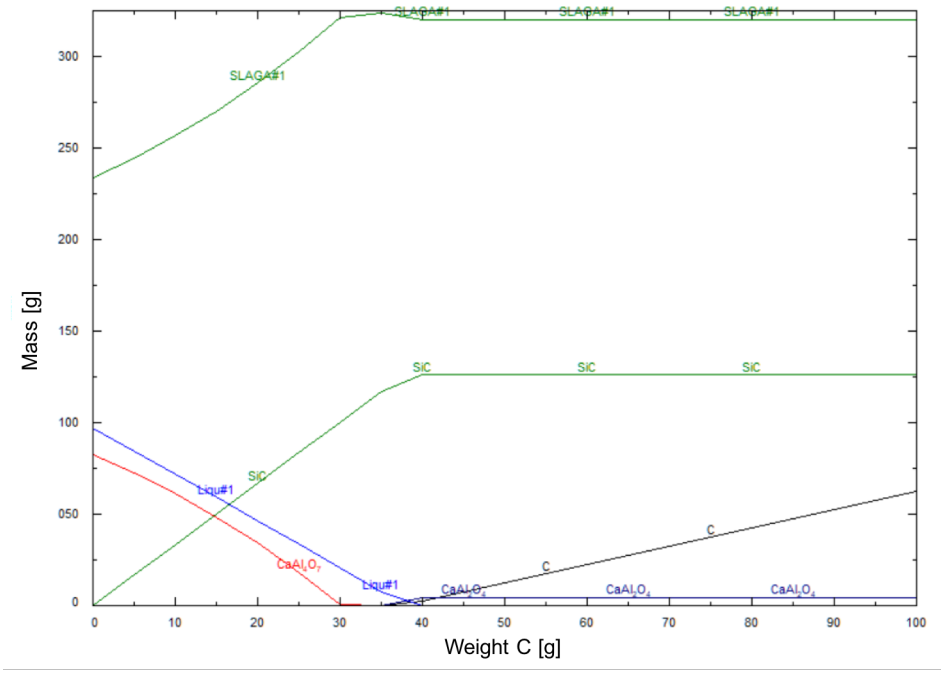


Figure 5.14: Equilibrium fractions of the phases at 1600° as function of carbon content

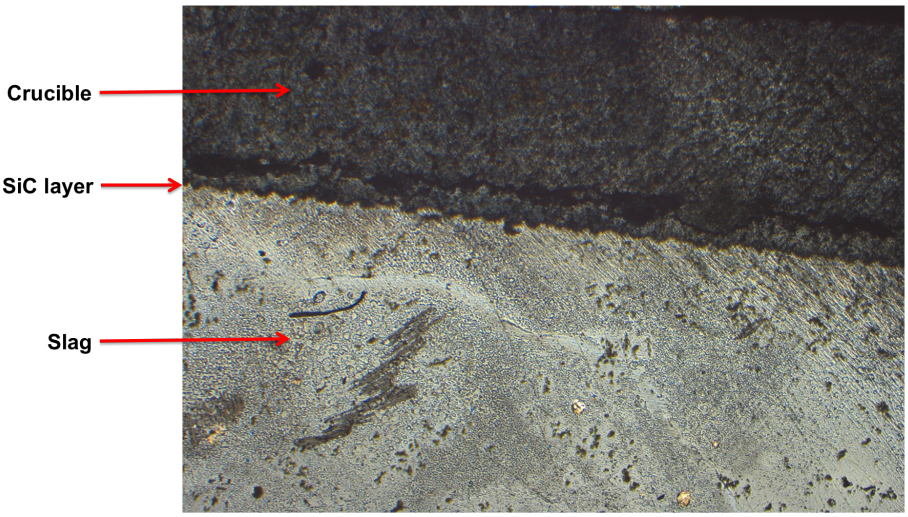


Figure 5.15: LOM image of slag-crucible interface

In Figure 5.16, the equilibrium concentration of the slag obtained by FactSage [13] is plotted into the $Al_2O_3$-CaO-$SiO_2$ phase diagram. As the $SiO_2$ concentrations are very low, the ico-concentration lines are not present in the range of the composition. However, one can see that at such low $SiO_2$ contents, the aluminium and calcium equilibrium concentrations in the metal will be high.

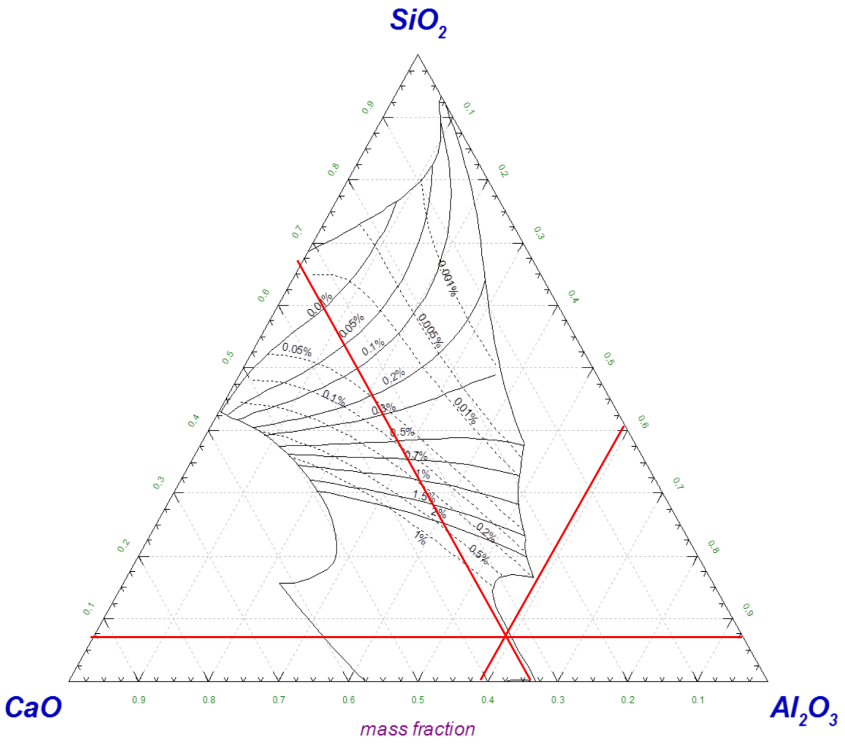


Figure 5.16: $Al_2O_3$-CaO-$SiO_2$ phase diagram with lines indicating the equilibrium concentration at 1600°C

Comparing the experimental results with the thermodynamic calculations, the values deviate quite a lot. Since ICP-MS analyses are more reliable for small concentrations, the ICP-MS results are used for the comparison of the metal phase. In Table 5.4, the silicon, aluminium and calcium contents of the experiments are listed together with the theoretical values at room temperature, while the results are shown graphically in Figure 5.17. The concentrations of silicon, calcium and aluminium are relatively similar for all experiments. As the values deviate between two an eight percent within the samples as indicated by the error bars, the deviations between the experiments are quite low taken that into consideration.

Table 5.4: Chemical composition of metal phase at room temperature from ICP-MS

| | Clean Al | Dross 1 | Clean Al + Dross 1 | Theoretical |
|---|---|---|---|---|
| wt% Si | 61.9 | 62.9 | 59.1 | 82.9 |
| wt% Al | 22.5 | 21.5 | 24.2 | 5.46 |
| wt% Ca | 14.8 | 11.9 | 14.4 | 11.68 |

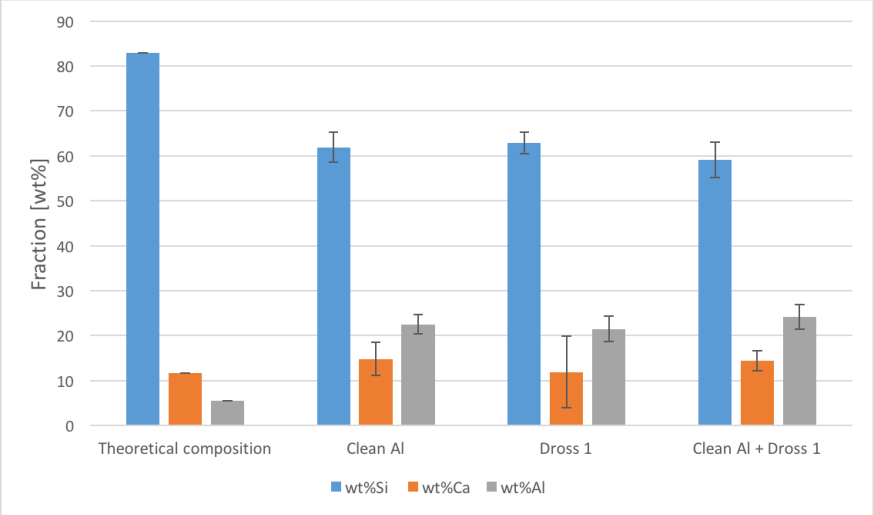


Figure 5.17: Silicon, aluminium and calcium contents for the different reducing materials plotted together with the theoretical composition

However, comparing the ICP-MS results to the results obtained by thermodynamic modelling, the resulting compositions vary quite a lot. According to theory, the metal phase should consist of over 80wt% silicon, while during the experiments approximately 60wt% is obtained. A likely reason for the low silicon contents is the solidification time. If the materials are cooled slowly, the metal phase will most likely be more pure, i.e. have higher silicon contents. At slow solidification times, the solidification will follow the solidus and liquidus lines in the phase diagram, resulting in equilibrium concentrations at room temperature. When cooling is not controlled, as was the case in these experiments, one will not have control of this very important parameter.

For the slag composition, a similar comparison was made. As seen from Figure 5.18, the equilibrium concentration of the elements in the slag are relatively constant. Table 5.5 lists the contents of $SiO_2$, $Al_2O_3$ and CaO in the slag together with the theoretical composition, while Figure 5.19 shows the results graphically. The CaO contents are very constant, while the $SiO_2$ contents vary a lot. A lower $SiO_2$ content than equilibrium concentration indicates that an over-stoichiometric composition of aluminium has been used.

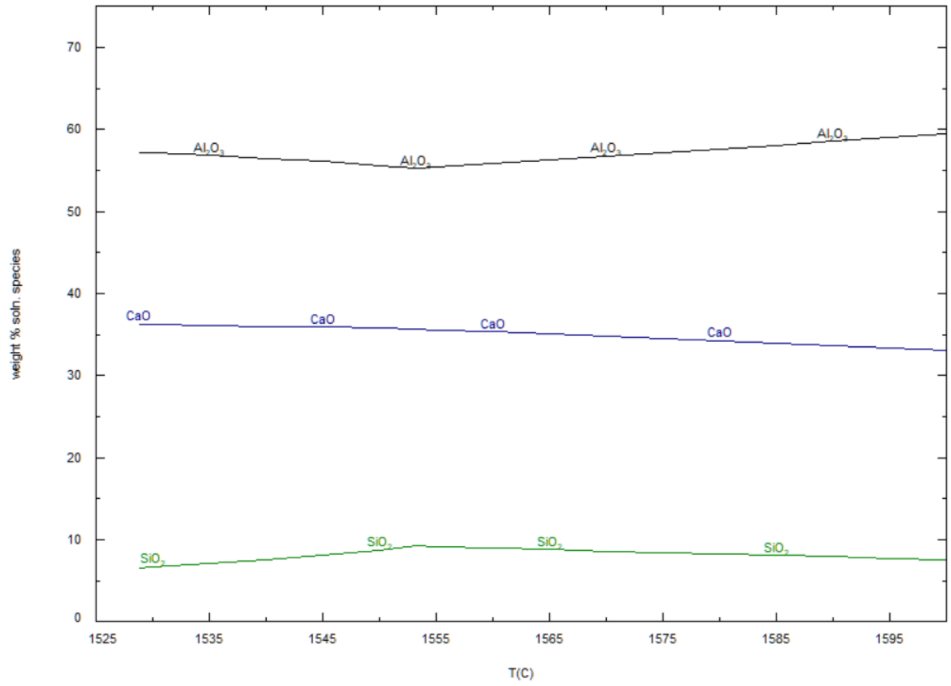


Figure 5.18: Equilibrium concentration of slag component upon cooling from 1600°C

Table 5.5: Chemical composition of slag phase at room temperature from EPMA

| | Clean Al | Dross 1 | Clean Al + Dross 1 | Al + Dross 2 | Theoretical |
|---|---|---|---|---|---|
| wt% $Al_2O_3$ | 62.5 | 61.3 | 61.7 | 48.9 | 57 |
| wt% CaO | 36.2 | 36.2 | 36.2 | 36.1 | 36 |
| wt% $SiO_2$ | 0.12 | 0.002 | 0.29 | 11.9 | 7 |

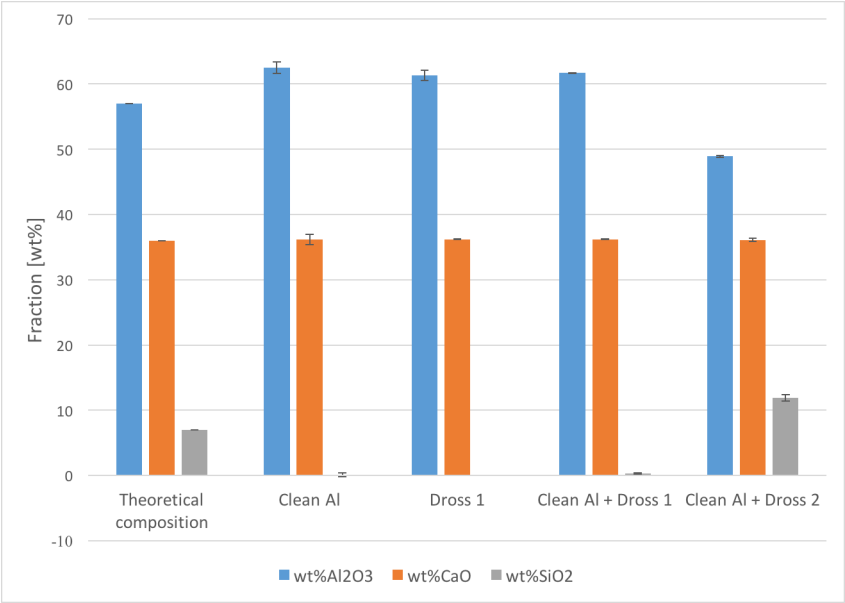


Figure 5.19: $SiO_2$, $Al_2O_3$ and CaO contents for the different reducing materials plotted together with the theoretical composition

### 5.3.4 Evaluation of experimental setup

The experimental setup seems to work well. The desired reaction, seen in Equation 2.10, has clearly taken place as silicon is visible in the crucibles. Except for the experiment having an unknown aluminium content, the reaction seems to have gone to completion. This shows that the setup works, and it can be tailored for future experiments of the same kind.

No violent reaction was observed upon addition of solid aluminium to the liquid slag. Therefore, increasing the scale should be possible. However, increasing the amount of materials increases the energy of the reaction, so up-scaling should be done gradually.

The charging procedure might not be optimal. Manually charging the aluminium pieces introduce uncertainties and variations in the experiments. Also, the added pieces were not necessarily the same shape and size. It may be more comparable if all pieces were the same. In addition, large aluminium pieces were added. A dense lump of aluminium is expected to be easier to melt than small and thin pieces, due to the possibility of them floating on top of the melt. The geometry of the added aluminium might be a significant contributor to the resulting yield.

The chosen temperature of 1600°C seems to be high enough, as the materials are properly molten. Lowering the temperature might be interesting to see if one can operate below 1600°C. Due to the energy consumption, it is desirable to operate at as low temperatures as possible, while at the same time not lowering the yield or quality of the product. It might also be interesting to investigate higher temperatures, to see if it can improve the resulting

product.

As a holding time of 30 minutes was chosen after addition of aluminium, it seems the reaction needs less than the tested 30 minutes to complete, as no metallic aluminium is observed in the stoichiometric experiments.

# Chapter 6

# Conclusions

In this study, the recyclability of used beverage cans and incinerator metal has been evaluated. In addition, the efficiency of two different salt fluxes has been compared, and important contributing factors have been established. Further, the possibility of utilising dross as reducing material for aluminothermic reduction was investigated through comparing the resulting metal phases of using dross and clean aluminium as reducing materials.

The recyclability of incinerator metal seems to be as high as for the UBCs, if not higher. The incinerator metal performs significantly better in the coalescence experiments, as the UBCs were not able to coalesce. In the yield experiments, the UBCs and incinerator metal produced yields in the same range. Therefore, an acceptable yield would be expected in industry. However, contaminations might be very detrimental for the industrial recyclability of the scrap. Lead was found in the incinerator raw material ranging from 4 to 400 ppm, which results in high lead concentrations in the cast metal. There is no doubt that the material should be recycled, but it is important to minimise the aluminium content ending up as incinerator metal due to losses in the process and introduction of contaminants.

Large differences between the salts were observed in the coalescence experiments, where the recycled salt performed significantly better. Over 85% of the extracted weight of the pieces were over 2 cm using the recycled salt, while no pieces over 2 cm were found using the industrial salt. However, the same difference was not observed in the yield experiments, as the salt performed equally good. It is believed that amount of stirring and operating temperature is very important for the performance of the salts, as more stirring is applied in the yield experiments and temperature close to the salt solidification temperature was found to produce low yields.

From this preliminary study, dross seems like a suitable material for use in aluminothermic reduction of $SiO_2$, as approximately the same composition of silicon, aluminium and calcium is found in the metal using dross and clean aluminium. However, the compositions deviate from that obtained by thermodynamic calculations. According to thermodynamics,

the metal phase should contain over 80% silicon, while the obtained results give approximately 60%. This difference is most likely due to the solidification being too rapid.

# Future Work

## Recycling

Firstly, due to the large deviations in the yield experiments, more parallels should be conducted.

Concerning the raw materials, the oxide layer of the incinerator metal should be studied more extensively, including variations as function of size and treatment at the incineration facility. Also, thorough chemical characterisation of the incinerator raw material should be conducted to map the extent of contaminants in the raw material. To compliment this, large scale experiments using incinerator metal, measuring yield and chemical composition, should be conducted to further understand the recyclability of the material.

As for the salt fluxes, one should study the mechanisms and effect of particle size and particle size distribution on the metal yield. An evaluation of the importance of these parameters compared to chemical composition of the salts should be done.

In addition, the full effect of stirring and temperature on the yield for recycling end-of-life alumininum scrap should be investigated by controlling amount of stirring and operating temperature carefully.

## Aluminothermic reduction

As dross has proven to be useful as reducing material in the aluminothermic process, a wider range of drosses could be tested. In addition, challenging end-of-life aluminium products, e.g. UBCs and incinerator metal, should be tested to see if high silicon contents can be achieved also for these materials.

Further, controlled solidification of the materials should be performed and the resulting silicon content in the metal should be analysed.

Similarly to the recycling experiments, larger scale experiments should be conducted to get a better understanding of how much heat is generated due to the exothermic reaction taking place.

# Bibliography


[1] European Aluminium. URL: https://www.european-aluminium.eu/data/.

[2] Royal Society of Chemistry. *Periodic Table - Aluminium*. 2017. URL: http://www.rsc.org/periodic-table/element/13/aluminium.

[3] M. Tangstad. *Metal production in Norway*. Trondheim, Norway: Akademika Publishing, 2013.

[4] NVE. *Energintensiv industri – en beskrivelse og økonomisk analyse av energiintensiv industri i Norge*. Tech. rep. 2013.

[5] BBC. *Aluminium Extraction*. 2014. URL: http://www.bbc.co.uk/schools/gcsebitesize/science/add_aqa/electrolysis/electrolysisrev3.shtml.

[6] S.K. Das, W.J. Long, and H.W. Hayden et al. "Energy implications of the changing world of aluminium metal supply." In: *JOM* 56.8 (2004), pp. 14–17. DOI: https://doi.org/10.1007/s11837-004-0175-6.

[7] S.K. Das and W. Yin. "The worldwide aluminium economy: The current state of the industry." In: *JOM* 59.11 (2007), pp. 57–63. DOI: https://doi.org/10.1007/s11837-007-0142-0.

[8] A. Ulus, H. Ekici, and E. Guler. "Optimization of Recovery Efficiency of Briquetted Aluminium Chips up to Briquetting Parameters." In: *Light Metals 2017* (2017), pp. 925–932. DOI: https://doi.org/10.1007/978-3-319-51541-0_111.

[9] J. Henryson and M. Goldman. *Återvunnen råvara - en god affär för klimatet*. Tech. rep. 2007.

[10] Hydro. *Recycling*. URL: https://www.hydro.com/en/about-aluminium/Aluminium-life-cycle/Recycling/.

[11] *Ducker Worldwide Study: Aluminium content in cars (public summary)*. URL: http://www.ducker.com/news-insights/ducker-worldwide-study-aluminum-content-cars-public-summary.

[12] "Internal sketch, SINTEF Materials and Chemistry." 2017.

[13] FactSage7.2. URL: factsage.com.

[14] World Aluminium. *Primary aluminium production*. 2018. URL: http://www.world-aluminium.org/statistics/#linegraph.

[15] World aluminium. *Global aluminium cycle 2016*. URL: http://www.world-aluminium.org/statistics/massflow/.

[16] World Aluminium. *Global Aluminium Cycle 2016*. 2017. URL: http://www.world-aluminium.org/statistics/massflow/.

[17] European Aluminium. *EU exports destination of aluminium scrap*. 2016. URL: https://www.european-aluminium.eu/data/recycling-data/eu-exports-destination-of-aluminium-scrap/.

[18] European Commission. *Towards a circular economy*. URL: https://ec.europa.eu/commission/priorities/jobs-growth-and-investment/towards-circular-economy_en.

[19] European Aluminium Association. *Environmental Profile Report for the European Aluminium Industry*. Tech. rep. 2011.

[20] P.A. Plunkert. *Aluminium Recycling in the United States in 2000*. Tech. rep.

[21] R.D. Peterson. *Aluminium Recycling: Can We be Zero Emissions and Zero Waste?* 2018.

[22] Melting Solutions. *Tilting rotary furnaces*. URL: http://www.meltingsolutions.com/tilting-rotary-furnace.

[23] B. Zhou et al. "Modelling of aluminium scrap melting in a rotary furnace." In: *Minerals Engineering* 19.3 (2005), pp. 299–308. DOI: https://doi.org/10.1016/j.mineng.2005.07.017.

[24] A. Morris. *Minimizing melt loss in aluminium recycling*. URL: https://www.industrialheating.com/articles/91516-minimizing-melt-loss-in-aluminum-recycling?v=preview.

[25] T.A. Engh. *Principles of metal refining*. New York, United States: Oxford University Press Inc., 1992, Chapter 3.

[26] U. Boin, M.A. Reuter, and T. Probst. "Understanding the Aluminium Scrap Melting Processes Inside a Rotary Furnace". In: *World of Metallurgy – ERZEMETALL* (2004), pp. 264–269.

[27] A. Kvithyld, D. Dispinar, and A. Nordmark. "Quality of Remelted Sheet and Cast Aluminium." In: *Proceedings - European Metallurgical Conference, EMC 2011* (2011), pp. 839–852.

[28] G. Tranell, A. Kvithyld, and E. Gumbmann. "Aluminium resirkulering". PowerPoint presentation.

[29] J. Steglich et al. "Dross Formation Mechanisms of Thermally Pre-Treated Used Beverage Can Scrap Bales with Different Density." In: *Light Metals* (2017), pp. 1105–1113. DOI: 10.1007/978-3-319-51541-0_133.

[30] R. Dittrich et al. "Understanding of Interactions Between Pyrolysis Gases and Liquid Aluminium and Their Impact on Dross Formation." In: *Light Metals* (2017), pp. 1457–1464. DOI: 10.1007/978-3-319-51541-0_174.

[31] B. Jaroni et al. “Conditions of Pyrolythis Processes in Multi Chamber Furnaces for Aluminium Recycling.” In: 2011.

[32] S. Rumpel. “Die autotherme Wirbelschichtpyrolyse zur Erzegung heizwertreicher Stützbrennstoffe.” PhD thesis. Karlsruhe, Germany, 2000.

[33] A. Kvithyld, C.E.M.Meskers, and S. Gaal et al. “Recycling Light Metals: Optimal Thermal De-coating.” In: *JOM* 60.8 (2008), pp. 47–51. DOI: https://doi.org/10.1007/s11837-008-0107-y.

[34] S. Capuzzi et al. “Coalescence of clean, coated and de-coated aluminium for various salts and salt-scrap ratio.” In: (2017).

[35] T. Danbolt. “Aluminium Recycling, Tubes for Food Packaging.” 2017.

[36] R. Narayanan and Y. Sahai. “Metal Loss in Remelting of Aluminium Alloys in Molten Salt Fluxes.” In: *Light Metals 1995* (1995), pp. 803–807.

[37] T.A. Utigard et al. “The Properties and Uses of Fluxes in Molten Aluminium Processing.” In: *JOM* 50.11 (1998), pp. 38–43. DOI: https://doi.org/10.1007/s11837-998-0285-7.

[38] S. Besson et al. “Improving Coalescence in Al-Recycling by Salt Optimization.” In: *World of Metallurgy* (2011), pp. 759–774.

[39] K.J. Friesen et al. “Coalescence behaviour of aluminium droplets under a molten salt flux cover.” In: *Light Metals 1997* (1997), pp. 857–864.

[40] O. Majidi et al. “Study of fluxing temperature in molten aluminum refining process.” In: *Journal of Materials Processing Technology* 182.1–3 (2007), pp. 450–455. DOI: https://doi.org/10.1016/j.jmatprotec.2006.09.003.

[41] S. Capuzzi. “Optimization of the aluminium refining process”. PhD thesis. 2017.

[42] J. Herbert and M. Collins. “The art of dross management – Part Two.” In: *Aluminium Times* ().

[43] factsage.cn. URL: http://www.factsage.cn/fact/phase_diagram.php?file=KCl-NaCl.jpg&dir=FTsalt.

[44] T. Klug et al. “Repetitorium zur Reinigung von Aluminiumschmelzen mit Salzpräparaten.” In: *Giesserei* (2016), pp. 50–61.

[45] I. Meling. “Recycling of Aluminium – Salt fluxing.” 2017.

[46] J. Herbert. “The art of dross management.” In: *Aluminium Times* (2007), pp. 44–45.

[47] I. Meling. “Recycling of Aluminium – Salt fluxing and utilisation of scrap”. 2017.

[48] P. Baumli, J. Sytchev, and G. Kaptay. “Prefect wettability of carbon by liquid aluminium achieved by a multifunctional flux.” In: *Journal of Materials Science* 45.19 (2010), pp. 5177–5190.

[49] World Aluminium. *Global Mass Flow Model 2016 (2017)*. 2017. URL: http://www.world-aluminium.org/publications/tagged/mass%5C%20flow/.

[50] T. Karoliussen. *Aluminium – Et regnestykke der svaret er resirkulering*. URL: https://infinitummovement.no/resirkulere-aluminium/.

[51] Befesa. *Salt slags and SPL recycling services*. URL: http://www.befesaaluminium.es/web/en/nuestros-procesos/detalle/Salt-slags-and-SPL-Recycling-Services/.

[52] Waste management resources. *Incineration*. URL: http://www.wrfound.org.uk/articles/incineration.html.

[53] "Internal sketch, SINTEF Industry." 2018.

[54] D. Hogg, T. Elliot, and S. Croasdell et al. *Options and Feasibility of a European Refund System for Metal Beverage Cans*. Tech. rep. 2011.

[55] H.L. Raadal, I.S. Modahl, and O.M.K. Iversen. *Comparison of recycling and incineration of aluminium cans*. Tech. rep. 2017.

[56] D.A. Doutre. "LiMCA and its Contribution to the Development of the Aluminium Beverage Container and UBC Recycling." In: 2011, pp. 319–321.

[57] D. Dispinar and J. Campbell. "Use of bilim index as an assesment of liquid metal quality." In: *International Journal of Cast Metals Research vol. 19* (2006), pp. 5–17.

[58] Miljødirektoratet. *Kontrollerer alle forbrenningsanlegg for avfall*. 2009. URL: http://www.miljodirektoratet.no/no/Nyheter/Nyheter/Old-klif/2009/Oktober_2009/Kontrollerer_alle_forbrenningsanlegg_for_avfall/.

[59] LOOP - Stiftelsen for Kildesortering og Gjenvinning. *Forbrenningsanlegg*. 2018. URL: https://snl.no/forbrenningsanlegg.

[60] A.J. Chandler, T.T.Eighmy, and J. Hartlén et al. *Muncipal Solid Waste Incinerator Residues*. Amsterdam, The Netherlands: Elsevier, 1997.

[61] A. Schei, J.K. Tuset, and H. Tveit. *Production of High Silicon Alloys*. Trondheim, Norway: Tapir forlag, 1998.

[62] European Commission. *Communication from the commission to the European parliament, the council, the European economic and social committee and the committee of the regions*. 2014. URL: http://eur-lex.europa.eu/legal-content/EN/TXT/PDF/?uri=CELEX:52014DC0297&from=EN.

[63] CRM Alliance. *Silicon Metal*. 2017. URL: http://criticalrawmaterials.org/silicon-metal/.

[64] Jim Clark. *Giant covalent structures*. 2000. URL: https://www.chemguide.co.uk/atoms/structures/giantcov.html.

[65] Southern Africa Analysis Smelting. URL: http://www.southernas.com/indexd52f.html?ac=article&at=list&tid=57.

[66] L. Ozturk and R.J. Fruehan. "The rate of formation of SiO by the reaction of CO or $H_2$ with silica and silicate slags." In: *Metallurgical Transactions B* (1985), pp. 801–806.

[67] M. Hasegawa. “Treatise on Process Metallurgy – Chapter 3.3”. In: Elsevier, 2014.

[68] M.B. Djurdjevic et al. “Calculation of Liquidus Temperature for Aluminum and Magnesium Alloys Applying Method of Equivalency - Scientific Figure on ResearchGate”. In: (2013). URL: https://www.researchgate.net/The-Al-Si-phase-diagram-6_fig6_258390327%20[accessed%2010%20Jun,%202018.

[69] *Silicon production with low environmental impact using secondary aluminium and silicon product streams*. 2017. URL: Application%20for%20EU%20project.

[70] J. Dietl and C. Holm. “New Aspects in Aluminothermic Reduction of SiO2”. In: *Seventh E.C. Photovoltaic Solar Energy Conference*. Ed. by A. Goetzberger, W. Palz, and G. Willeke. Dordrecht: Springer Netherlands, 1987, pp. 726–730. DOI: 10.1007/978-94-009-3817-5_129.

[71] NPL. URL: http://resource.npl.co.uk/mtdata/dgox1.htm.

[72] Huahai Mao, Malin Selleby, and Bo Sundman. “A re-evaluation of the liquid phases in the CaO–Al2O3 and MgO–Al2O3 systems”. In: 28 (2004), pp. 307–312.

[73] Centre for Research in Computational Thermochemistry. URL: http://www.crct.polymtl.ca/factsage/fs_polythermal_proj.php.

[74] *Private communication with professor Gabriella Tranell*. 2018.

[75] J. Liu et al. “Phase field simulation study if the dissolution behaviour of $Al_2O_3$ into CaO-$Al_2O_3$-$SiO_2$ slags.” In: *Computational Materials Science vol. 119* (2016), pp. 9–18.

[76] V.L. Cherginets et al. “Solubility of $Al_2O_3$ in Some Chloride-Fluoride Melts.” In: *Inorganic chemistry vol. 45* (2006), pp. 7367–7371.

[77] MakeItFrom. *Material Properties Database*. URL: https://www.makeitfrom.com/material-group/Aluminum-Alloy.

[78] Norsk Hydro. *Data provided by personal meeting and e-mail correspondence with André Granå and Eva Gumbmann*. 2018.

[79] *ImageJ*. URL: https://imagej.nih.gov/ij/index.html.

[80] Wikipedia the free encyclopedia. *Potassium chloride*. URL: https://en.wikipedia.org/wiki/Potassium_chloride.

[81] Lenntech BV. *Lead - Pb*. URL: https://www.lenntech.com/periodic/elements/pb.htm.

# Appendix A

# EPMA analyses

In this appendix, the results from EPMA analyses are presented for the yield experiments and aluminothermic reduction experiments. Three or six analyses were performed for each phase in each sample. In Table A.1, the compositions of the UBC and incinerator raw materials are listed. The compositions of the dark and light phase in the cast metal from yield experiments are listed in Tables A.2 and A.3, respectively. Table A.4 list the composition of the phases in the metal phase of aluminothermic reduction, while Table A.5 list the slag compositions for the same experiments.

Table A.1: EPMA analysis of UBCs and incinerator metal in wt%

| Si | Mg | Ti | Fe | Al | Cr | Cu | Mn | Zn | Comment |
|---|---|---|---|---|---|---|---|---|---|
| 0.013 | 5.419 | 0.007 | 0.082 | 95.568 | 0.0 | 0.042 | 0.455 | 0.0 | |
| 0.0 | 6.020 | 0.0 | 0.029 | 94.957 | 0.0 | 0.042 | 0.508 | 0.033 | UBC dark phase |
| 0.0 | 5.415 | 0.0 | 0.034 | 95.368 | 0.0 0.0 | 0.351 | 0.041 | | |
| 5.433 | 0.193 | 0.011 | 14.996 | 67.127 | 0.100 | 0.344 | 12.804 | 0.0 | |
| 5.649 | 0.458 | 0.000 | 15.220 | 65.791 | 0.040 | 0.334 | 12.351 | 0.0 | UBC light phase |
| 5.467 | 0.159 | 0.0 | 15.418 | 66.264 | 0.041 | 0.333 | 12.745 | 0.054 | |
| 0.039 | 0.0 | 0.0 | 0.057 | 98.255 | 0.001 | 0.0 | 0.094 | 0.001 | |
| 0.070 | 0.0 | 0.003 | 0.018 | 98.714 | 0.0 | 0.0 | 0.175 | 0.000 | I.M. dark phase 0.052 |
| 0.0 | 0.032 | 0.032 | 98.357 | 0.0 | 0.005 | 0.082 | 0.0 | | |
| 0.736 | 0.0 | 0.0 | 35.113 | 61.310 | 0.0 | 0.058 | 0.223 | 0.0 | |
| 6.612 | 0.0 | 0.0 | 27.849 | 62.734 | 0.0 | 0.178 | 0.131 | 0.013 | I.M. light phase |
| 0.976 | 0.002 | 0.0 | 26.998 | 74.379 | 0.0 | 0.0 | 0.082 | 0.0 | |

Table A.2: EPMA analysis of dark phase of cast aluminium from yield experiments in wt%

| Si | Mg | Ti | Fe | Al | Cr | Cu | Mn | Zn | Comment |
|---|---|---|---|---|---|---|---|---|---|
| 0.044 | 0.927 | 0.044 | 0.036 | 98.277 | 0.0 | 0.068 | .0897 | 0.063 | |
| 0.068 | 1.148 | 0.0 | 0.009 | 97.791 | 0.0 | 0.060 | 0.782 | 0.019 | UBC + Recycled 1 |
| 0.029 | 1.027 | 0.032 | 0.011 | 97.980 | 0.0 | 0.022 | 0.736 | 0.0 | |
| 0.103 | 1.304 | 0.0 | 0.070 | 97.903 | 0.046 | 0.119 | 0.867 | 0.045 | |
| 0.085 | 1.298 | 0.016 | 0.054 | 97.999 | 0.057 | 0.102 | 0.845 | 0.058 | UBC + Recycled 2 |
| 0.017 | 0.886 | 0.019 | 0.0 | 98.144 | 0.007 | 0.061 | 0.768 | 0.059 | |
| 0.018 | 0.206 | 0.0 | 0.035 | 97.802 | 0.026 | 0.044 | 0.840 | 0.100 | |
| 0.031 | 0.209 | 0.013 | 0.035 | 97.462 | 0.014 | 0.070 | 0.827 | 0.048 | UBC + Industrial 1 |
| 0.050 | 0.223 | 0.050 | 0.046 | 97.049 | 0.017 | 0.078 | 0.819 | 0.0 | |
| 0.160 | 0.708 | 0.0 | 0.042 | 97.481 | 0.042 | 0.079 | 0.875 | 0.0 | |
| 0.129 | 0.757 | 0.0 | 0.057 | 97.794 | 0.057 | 0.177 | 1.006 | 0.018 | UBC + Industrial 2 |
| 0.125 | 0.718 | 0.002 | 0.031 | 97.366 | 0.0 | 0.140 | 0.592 | 0.013 | |
| 0.629 | 0.009 | 0.0 | 0.034 | 97.722 | 0.029 | 0.357 | 0.398 | 0.585 | |
| 0.462 | 0.015 | 0.093 | 0.037 | 98.035 | 0.027 | 0.239 | 0.332 | 0.530 | I.M. + Recycled 1 |
| 0.569 | 0.001 | 0.0 | 0.04 | 98.197 | 0.015 | 0.368 | 0.490 | 0.472 | |
| 0.265 | 0.0 | 0.044 | 0.048 | 98.574 | 0.030 | 0.186 | 0.326 | 0.400 | |
| 0.497 | 0.000 | 0.035 | 0.045 | 98.094 | 0.000 | 0.441 | 0.397 | 0.488 | I.M. + Recycled 2 |
| 0.320 | 0.001 | 0.077 | 0.068 | 98.461 | 0.024 | 0.217 | 0.370 | 0.369 | |
| 0.300 | 0.000 | 0.000 | 0.060 | 97.652 | 0.039 | 0.349 | 0.329 | 0.301 | |
| 0.308 | 0.000 | 0.049 | 0.005 | 97.255 | 0.008 | 0.328 | 0.258 | 0.426 | I.M. + Industrial 1 |
| 0.265 | 0.000 | 0.006 | 0.001 | 97.515 | 0.000 | 0.241 | 0.444 | 0.362 | |
| 0.417 | 0.010 | 0.035 | 0.000 | 98.053 | 0.045 | 0.572 | 0.323 | 0.433 | |
| 0.213 | 0.0 | 0.082 | 0.016 | 98.507 | 0.018 | 0.392 | 0.414 | 0.400 | I.M. + Industrial 2 |
| 0.278 | 0.000 | 0.064 | 0.021 | 98.647 | 0.020 | 0.496 | 0.431 | 0.467 | |

Table A.3: EPMA analysis of light phase of cast aluminium from yield experiments in wt%

| Si | Mg | Ti | Fe | Al | Cr | Cu | Mn | Zn | Comment |
|---|---|---|---|---|---|---|---|---|---|
| 0.134 | 0.080 | 0.000 | 14.174 | 75.871 | 0.027 | 0.173 | 10.469 | 0.0 | |
| 0.121 | 0.071 | 0.000 | 13.838 | 75.796 | 0.049 | 0.156 | 10.668 | 0.0 | UBC + Recycled 1 |
| 0.168 | 0.116 | 0.0 | 16.147 | 75.409 | 0.0 | 0.443 | 7.867 | 0.047 | |
| 0.267 | 0.132 | 0.0 | 16.388 | 75.036 | 0.011 | 0.695 | 8.015 | 0.088 | |
| 0.207 | 0.173 | 0.016 | 16.462 | 74.822 | 0.000 | 1.176 | 7.369 | 0.011 | UBC + Recycled 2 |
| 0.119 | 0.138 | 0.021 | 15.216 | 75.462 | 0.007 | 0.443 | 8.828 | 0.0 | |
| 0.282 | 0.015 | 0.001 | 15.069 | 74.434 | 0.007 | 0.440 | 9.085 | 0.033 | |
| 0.168 | 0.000 | 0.025 | 14.966 | 74.183 | 0.012 | 0.290 | 9.170 | 0.0 | UBC + Industrial 1 |
| 2.124 | 0.057 | 0.022 | 17.120 | 71.394 | 0.007 | 1.075 | 6.758 | 0.022 | |
| 0.259 | 0.069 | 0.000 | 15.059 | 74.684 | 0.0 | 0.334 | 9.297 | 0.021 | |
| 0.200 | 0.066 | 0.011 | 14.315 | 74.733 | 0.012 | 0.263 | 8.937 | 0.021 | UBC + Industrial 2 |
| 0.241 | 0.059 | 0.0 | 16.056 | 74.314 | 0.011 | 0.613 | 8.020 | 0.067 | |
| 7.822 | 0.0 | 0.0 | 23.029 | 61.439 | 0.101 | 1.778 | 5.467 | 0.254 | |
| 8.966 | 0.0 | 0.0 | 24.814 | 59.668 | 0.017 | 3.164 | 3.111 | 0.319 | I.M. + Recycled 1 |
| 8.942 | 0.007 | 0.0 | 24.872 | 59.230 | 0.028 | 3.352 | 3.102 | 0.324 | |
| 7.882 | 0.0 | 0.0 | 22.106 | 61.955 | 0.120 | 1.467 | 6.304 | 0.165 | |
| 8.967 | 0.0 | 0.0 | 24.696 | 59.499 | 0.021 | 3.834 | 3.415 | 0.293 | I.M. + Recycled 2 |
| 8.101 | 0.0 | 0.030 | 21.960 | 61.922 | 0.131 | 1.754 | 6.247 | 0.218 | |
| 8.079 | 0.0 | 0.0 | 22.700 | 61.100 | 0.080 | 3.185 | 5.444 | 0.140 | |
| 8.274 | 0.003 | 0.0 | 23.330 | 60.411 | 0.033 | 4.041 | 4.080 | 0.243 | I.M. + Industrial 1 |
| 8.009 | 0.0 | 0.0 | 23.326 | 60.202 | 0.028 | 3.340 | 4.405 | 0.254 | |
| 8.096 | 0.0 | 0.0 | 22.615 | 60.607 | 0.052 | 4.002 | 4.654 | 0.247 | |
| 0.171 | 0.0 | 0.0 | 0.783 | 46.381 | 0.0 | 55.187 | 0.360 | 0.374 | I.M + Industrial 2 |
| 7.966 | 0.0 | 0.0 | 21.840 | 61.130 | 0.121 | 3.625 | 5.561 | 0.266 | |

Table A.4: EPMA analysis of metal phases from aluminothermic reduction experiments in wt%

| Si | Mg | Ca | Mn | Al | Fe | Comment |
|---|---|---|---|---|---|---|
| 96.724 | 0.009 | 0.346 | 0.0 | 0.403 | 0.036 | |
| 97.152 | 0.003 | 0.391 | 0.019 | 0.507 | 0.012 | |
| 97.735 | 0.021 | 0.409 | 0.018 | 0.527 | 0.023 | Clean Al 1, dark phase |
| 96.725 | 0.0 | 0.066 | 0.0 | 0.114 | 0.032 | |
| 97.374 | 0.009 | 0.094 | 0.012 | 0.103 | 0.0 | |
| 96.568 | 0.002 | 0.071 | 0.033 | 0.086 | 0.0 | |
| 37.061 | 0.293 | 23.912 | 0.019 | 37.083 | 0.000 | |
| 37.426 | 0.267 | 24.005 | 0.000 | 37.152 | 0.000 | |
| 38.445 | 0.392 | 23.786 | 0.007 | 37.273 | 0.019 | Clean Al 1, light phase |
| 36.075 | 0.180 | 24.261 | 0.000 | 37.200 | 0.025 | |
| 37.027 | 0.244 | 23.768 | 0.000 | 37.264 | 0.038 | |
| 36.984 | 0.191 | 23.834 | 0.005 | 37.186 | 0.000 | |
| 97.494 | 0.003 | 0.108 | 0.002 | 0.128 | 0.000 | |
| 98.097 | 0.009 | 0.130 | 0.000 | 0.132 | 0.000 | |
| 95.167 | 0.004 | 0.073 | 0.000 | 0.145 | 0.006 | Clean Al 2, dark phase |
| 95.551 | 0.016 | 0.043 | 0.009 | 0.105 | 0.042 | |
| 96.860 | 0.014 | 0.022 | 0.000 | 0.078 | 0.026 | |
| 96.965 | 0.019 | 0.103 | 0.000 | 0.113 | 0.041 | |
| 37.082 | 0.476 | 24.128 | 0.000 | 36.826 | 0.023 | |
| 36.888 | 0.315 | 23.643 | 0.003 | 36.945 | 0.039 | |
| 37.249 | 0.531 | 24.102 | 0.000 | 36.747 | 0.000 | Clean Al 2, light phase |
| 36.812 | 0.292 | 23.807 | 0.017 | 37.234 | 0.008 | |
| 36.618 | 0.277 | 23.607 | 0.014 | 36.888 | 0.058 | |
| 36.598 | 0.200 | 24.142 | 0.000 | 37.409 | 0.081 | |
| 98.682 | 0.011 | 0.463 | 0.000 | 0.449 | 0.000 | |
| 98.296 | 0.014 | 0.439 | 0.000 | 0.559 | 0.000 | |
| 98.463 | 0.021 | 0.451 | 0.000 | 0.569 | 0.027 | Dross 1 1, dark phase |
| 99.263 | 0.000 | 0.061 | 0.043 | 0.052 | 0.000 | |
| 99.275 | 0.000 | 0.030 | 0.023 | 0.106 | 0.004 | |
| 99.139 | 0.001 | 0.018 | 0.005 | 0.075 | 0.026 | |
| 37.323 | 0.360 | 24.381 | 0.000 | 36.722 | 0.013 | |
| 37.631 | 0.351 | 24.327 | 0.000 | 36.627 | 0.011 | |
| 37.627 | 0.376 | 24.246 | 0.000 | 36.642 | 0.029 | Dross 1 1, light phase |
| 37.731 | 0.126 | 24.182 | 0.032 | 37.138 | 0.000 | |
| 37.778 | 0.152 | 24.400 | 0.008 | 37.118 | 0.038 | |
| 37.823 | 0.133 | 24.289 | 0.009 | 36.984 | 0.034 | |
| 96.100 | 0.016 | 0.241 | 0.000 | 0.275 | 0.002 | |
| 95.851 | 0.002 | 0.301 | 0.006 | 0.317 | 0.026 | |
| 95.913 | 0.000 | 0.269 | 0.000 | 0.265 | 0.011 | Dross 1 2, dark phase |
| 98.900 | 0.009 | 0.081 | 0.042 | 0.197 | 0.011 | |
| 98.669 | 0.000 | 0.106 | 0.007 | 0.198 | 0.000 | |
| 98.762 | 0.011 | 0.160 | 0.013 | 0.284 | 0.000 | |

| Si | Mg | Ca | Mn | Al | Fe | Comment |
|---|---|---|---|---|---|---|
| 38.015 | 0.584 | 24.264 | 0.011 | 36.390 | 0.017 | |
| 37.089 | 0.417 | 24.232 | 0.001 | 36.383 | 0.000 | |
| 36.985 | 0.572 | 24.496 | 0.016 | 36.555 | 0.007 | Dross 1 2, light phase |
| 37.507 | 0.182 | 24.352 | 0.038 | 36.980 | 0.000 | |
| 37.496 | 0.194 | 24.276 | 0.022 | 36.982 | 0.004 | |
| 37.381 | 0.172 | 24.303 | 0.025 | 37.018 | 0.000 | |
| 97.294 | 0.015 | 0.771 | 0.000 | 1.316 | 0.000 | |
| 96.115 | 0.011 | 0.664 | 0.009 | 1.047 | 0.000 | |
| 96.785 | 0.006 | 0.392 | 0.000 | 0.340 | 0.007 | Clean Al + Dross 1, dark phase |
| 97.056 | 0.004 | 0.004 | 0.000 | 0.053 | 0.001 | |
| 97.410 | 0.009 | 0.029 | 0.000 | 0.224 | 0.162 | |
| 99.999 | 0.009 | 0.036 | 0.007 | 0.098 | 0.001 | |
| 35.790 | 0.214 | 22.369 | 0.018 | 36.036 | 0.000 | |
| 37.057 | 0.204 | 24.367 | 0.023 | 37.015 | 0.022 | |
| 36.812 | 0.306 | 24.100 | 0.000 | 36.888 | 0.022 | Clean Al + Dross 1, light phase |
| 37.247 | 0.209 | 23.533 | 0.004 | 36.269 | 0.174 | |
| 37.513 | 0.146 | 24.005 | 0.024 | 37.051 | 0.000 | |
| 37.692 | 0.172 | 23.760 | 0.005 | 36.820 | 0.035 | |
| 99.323 | 0.000 | 0.412 | 0.045 | 0.414 | 0.018 | |
| 99.477 | 0.014 | 0.396 | 0.002 | 0.406 | 0.015 | |
| 98.138 | 0.018 | 0.416 | 0.037 | 0.655 | 0.000 | Clean Al + Dross 2, dark phase |
| 99.483 | 0.019 | 0.019 | 0.028 | 0.144 | 0.029 | |
| 99.099 | 0.000 | 0.025 | 0.031 | 0.169 | 0.000 | |
| 98.868 | 0.000 | 0.000 | 0.020 | 0.129 | 0.004 | |
| 37.296 | 0.149 | 23.409 | 0.007 | 36.500 | 0.020 | |
| 37.422 | 0.110 | 23.650 | 0.009 | 36.314 | 0.044 | Clean Al + Dross 2, light phase |
| 37.656 | 0.145 | 23.653 | 0.040 | 36.519 | 0.029 | |

Table A.5: EPMA analysis of slag phase from aluminothermic reduction experiments in wt%

| $SiO_2$ | MgO | CaO | MnO | $Al_2O_3$ | FeO | Comment |
|---|---|---|---|---|---|---|
| 0.154 | 0.063 | 36.069 | 0.006 | 62.427 | 0.000 | |
| 0.225 | 0.057 | 36.218 | 0.000 | 62.337 | 0.000 | Clean Al 1 |
| 0.049 | 0.065 | 35.784 | 0.052 | 62.542 | 0.021 | |
| 0.296 | 0.181 | 36.883 | 0.023 | 62.109 | 0.000 | |
| 0.000 | 0.081 | 36.225 | 0.000 | 62.779 | 0.015 | Clean Al 2 |
| 0.001 | 0.105 | 36.055 | 0.000 | 62.477 | 0.000 | |
| 0.000 | 0.059 | 36.071 | 0.000 | 61.188 | 0.021 | |
| 0.000 | 0.071 | 36.269 | 0.016 | 61.347 | 0.000 | Dross 1 1 |
| 0.000 | 0.059 | 36.005 | 0.000 | 61.337 | 0.000 | |
| 0.000 | 0.052 | 36.327 | 0.025 | 61.168 | 0.000 | |
| 0.013 | 0.214 | 36.293 | 0.000 | 61.175 | 0.000 | Dross 1 2 |
| 0.000 | 0.107 | 36.051 | 0.011 | 61.693 | 0.010 | |
| 0.404 | 0.045 | 36.188 | 0.075 | 61.669 | 0.030 | |
| 0.293 | 0.083 | 36.253 | 0.042 | 61.611 | 0.023 | |
| 0.183 | 0.052 | 36.219 | 0.020 | 61.736 | 0.000 | Clean Al + Dross 1 |
| 2.583 | 1.215 | 37.238 | 0.000 | 55.883 | 0.000 | |
| 3.693 | 1.014 | 38.561 | 0.000 | 53.678 | 0.027 | |
| 3.030 | 1.121 | 38.386 | 0.000 | 54.990 | 0.018 | |
| 11.362 | 1.338 | 36.233 | 0.000 | 49.026 | 0.000 | |
| 11.949 | 1.373 | 36.240 | 0.031 | 48.779 | 0.041 | Clean Al + Dross 2 |
| 12.497 | 1.328 | 35.766 | 0.050 | 48.802 | 0.006 | |

# Appendix B

# ICP-MS analyses

This chapter presents results from ICP-MS analyses run on the different materials. The analyses were performed by Syverin Lierhagen, while the solutions were prepared by Torild Krogstad. ICP-MS analyses were performed on the incinerator raw material and the salt and metal fraction from two recycling experiments. In addition, analyses were performed on the metal phases produced in the aluminothermic production, in addition to the synthetic slag. The values listed are concentrations with the unit of $\mu$g/g, corresponding to ppm.

Table B.1: ICP-MS analysis in $\mu$g/g

| Na | Mg | Al | Si | P | S | K | Ca | Ti | V | Cr | Mn | Fe | Co | Sr |
|---|---|---|---|---|---|---|---|---|---|---|---|---|---|---|
| 65.2 | 5320.6 | 193.0 | 252881.6 | 18.0 | 107.7 | 114.4 | 225912.4 | 35.2 | 1.5 | 2.5 | 9.3 | 127.2 | 5.8 | 87.8 |

| B | Se | Y | Zr | Sn | Pb | U | Na | Mg | Al | Si | P | S | K | Comment | |
|---|---|---|---|---|---|---|---|---|---|---|---|---|---|---|---|
| -0,3636 | 1,7847 | 0,1192 | 50,5956 | 139,3310 | 422,6329 | 0,7103 | 112,1928 | 561,7332 | 870694,9743 | 48786,6467 | 19,8056 | 134,8284 | 19,1960 | I.M. | Yield experiments |
| -1,0435 | 1,6422 | 0,0013 | 7,5520 | 20,7000 | 4,3183 | 0,5599 | -41,3411 | 1,4062 | 883974,4071 | 3431,6995 | 5,4691 | 30,4714 | -13,8896 | I.M. | |
| -4,2451 | 1,4997 | 0,0537 | 15,6639 | 10,8276 | 30,0470 | 0,5999 | 0,9828 | 488,1295 | 913982,2363 | 4954,8634 | 15,0320 | 154,8700 | 1,0528 | I.M. | |
| -7,4591 | 1,6485 | 0,0819 | 16,3269 | 16,0070 | 13,1476 | 0,5163 | 7,8461 | 9993,6206 | 993055,9177 | 1276,6205 | 6,7036 | -95,1493 | -13,2351 | UBC + Recycled, Al | |
| -9,0402 | 1,9543 | 0,0704 | 15,6433 | 7,9393 | 16,9749 | 0,5130 | -49,0248 | 5098,8133 | 968880,9299 | 1516,4536 | 12,0058 | 18,2483 | -10,7993 | UBC + Industrial, Al | |
| 3,8422 | 1,5208 | 0,0370 | 7,4981 | -0,0931 | 0,6469 | 0,0568 | 273359,3155 | 4488,7675 | 14058,1826 | -50,4453 | 19,0154 | 2938,6160 | 152440,4758 | UBC + Industrial, salt | |
| 17,1851 | 2,0182 | 0,4700 | 6,5216 | 0,9079 | 2,5474 | 0,0280 | 235312,8335 | 2239,4095 | 19190,9179 | -736,2530 | 30,2867 | 664,0957 | 160314,5958 | UBC + Recycled, salt | |
| 6,7507 | 1,7847 | 1,0963 | 48,2652 | 1,2753 | 28,3219 | 1,7391 | 30,6773 | 5887,3982 | 214230,9510 | 590108,4301 | 9,1161 | -26,7195 | -19,5569 | Clean Al, 1 | Aluminothermic reduction experiments |
| 52,3762 | 1,7996 | 0,9479 | 837,4928 | 13,3268 | 13,6479 | 1,7738 | 68,5509 | 6259,5267 | 201138,3237 | 588280,9093 | 78,8759 | -13,3779 | -3,0015 | Dross 1, 1 | |
| 36,4736 | 1,5937 | 1,1685 | 576,5826 | 7,8827 | 20,0355 | 1,6983 | 25,4844 | 5902,5792 | 244497,9461 | 597901,4548 | 23,8581 | -27,8266 | -6,4078 | Clean Al + Dross 1 | |

| Ca | Ti | V | Cr | Mn | Fe | Co | Ni | Cu | Zn | Sr | Mo | Ba | Comment | |
|---|---|---|---|---|---|---|---|---|---|---|---|---|---|---|
| 596,392 | 445,925 | 80,256 | 194,812 | 2068,797 | 14699,693 | 5,827 | 308,962 | 12031,942 | 8937,895 | 1,698 | 5,313 | 6,136 | I.M. | Yield experiments |
| -36,869 | 101,886 | 66,235 | 19,081 | 1088,005 | 2676,304 | 1,294 | 48,932 | 740,313 | 806,227 | 0,126 | 1,975 | -0,062 | I.M. | |
| 117,776 | 222,855 | 108,150 | 71,975 | 4150,768 | 5346,725 | 2,936 | 61,413 | 1146,102 | 1276,952 | 0,446 | 2,264 | 1,064 | I.M. | |
| 54,864 | 180,733 | 106,542 | 143,765 | 8631,573 | 5043,657 | 2,592 | 58,031 | 1850,388 | 458,169 | 0,008 | 3,303 | 0,232 | UBC + Recycled, Al | |
| -26,595 | 167,905 | 101,114 | 140,805 | 8341,863 | 4677,406 | 2,925 | 58,811 | 1645,799 | 337,167 | 0,025 | 2,790 | -0,004 | UBC + Industrial, Al | |
| 4295,027 | 128,750 | 1,313 | 9,624 | 84,036 | 133,153 | 0,141 | 0,787 | 23,167 | 1,800 | 38,440 | 0,100 | 4,643 | UBC + Industrial, salt | |
| 1877,948 | 72,541 | 2,915 | 5,636 | 152,586 | 246,311 | 0,445 | 1,973 | 43,130 | 10,398 | 3,124 | 0,484 | 15,121 | UBC + Recycled, salt | |
| 140947,903 | 265,012 | 147,130 | 18,600 | 46,572 | 1760,218 | 2,941 | 59,541 | 10,689 | 6,104 | 90,714 | 2,524 | 7,515 | Clean Al, 1 | Aluminothermic reduction experiments |
| 110793,636 | 1308,070 | 119,057 | 37,239 | 9739,312 | 3330,127 | 2,180 | 55,574 | 12620,944 | 55,728 | 64,456 | 3,548 | 7,349 | Dross 1, 1 | |
| 145371,922 | 934,457 | 134,278 | 31,622 | 6098,046 | 3322,299 | 2,227 | 56,655 | 6270,038 | 35,142 | 85,837 | 3,374 | 8,558 | Clean Al + Dross 1 | |

Figure B.1: ICP-MS analyses in $\mu$g/g

# Appendix C

# Image analyses

Here the pictures used to calculate area fraction of the phases are presented. It is assumed that the area fraction equals the volume fraction. ImageJ [79] was used to calculate the area fractions of the phases in SEM pictures. The pictures are presented in figures together with the area fractions in the top left corners.

## C.1 Yield experiments

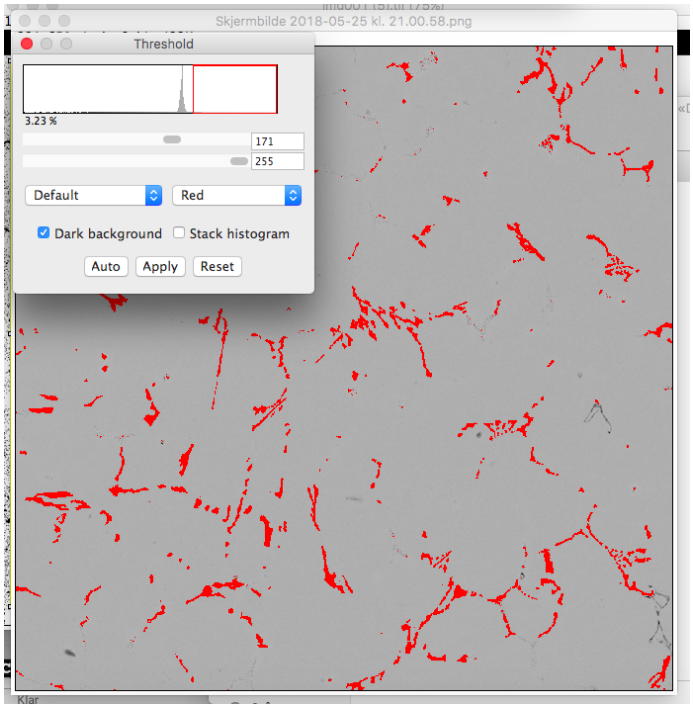


Figure C.1: UBC + Recycled salt 1 (3.23% of red phase)

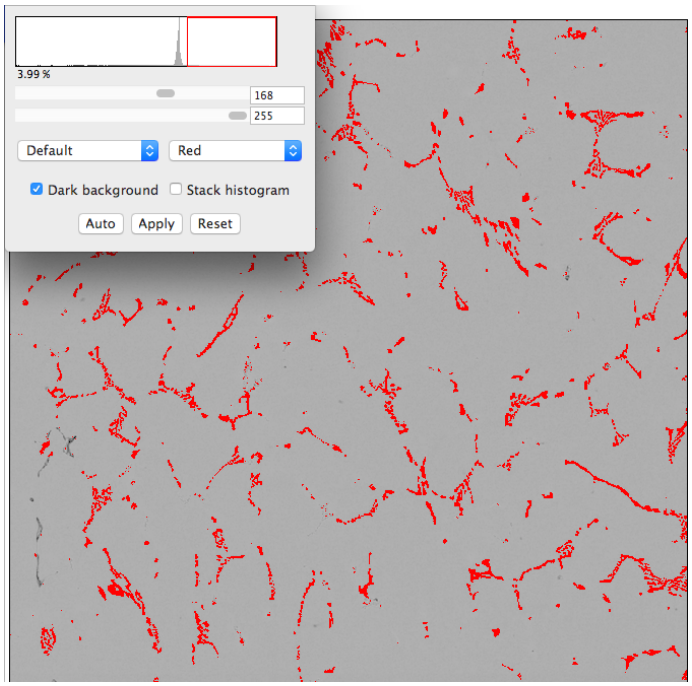


Figure C.2: UBC + Recycled salt 2 (3.99% of red phase)

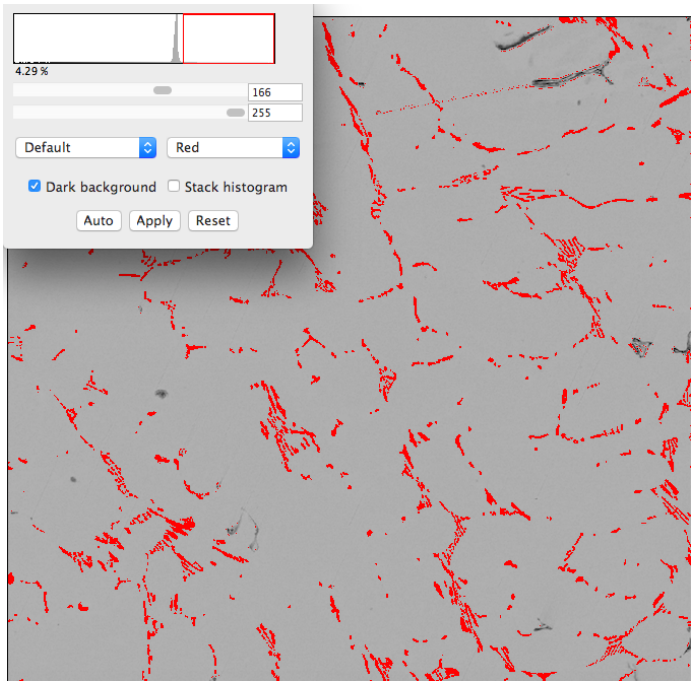


Figure C.3: UBC + Industrial salt 1 (4.29% of red phase)

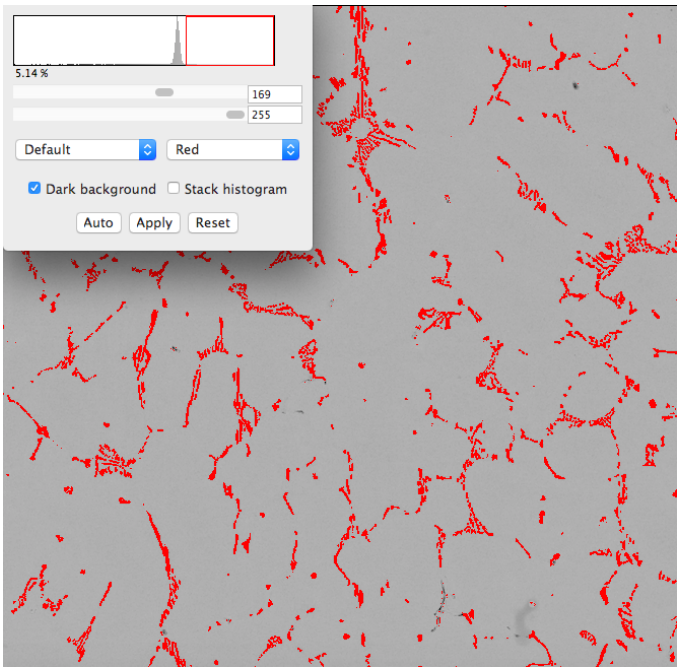


Figure C.4: UBC + Industrial salt 2 (5.14% of red phase)

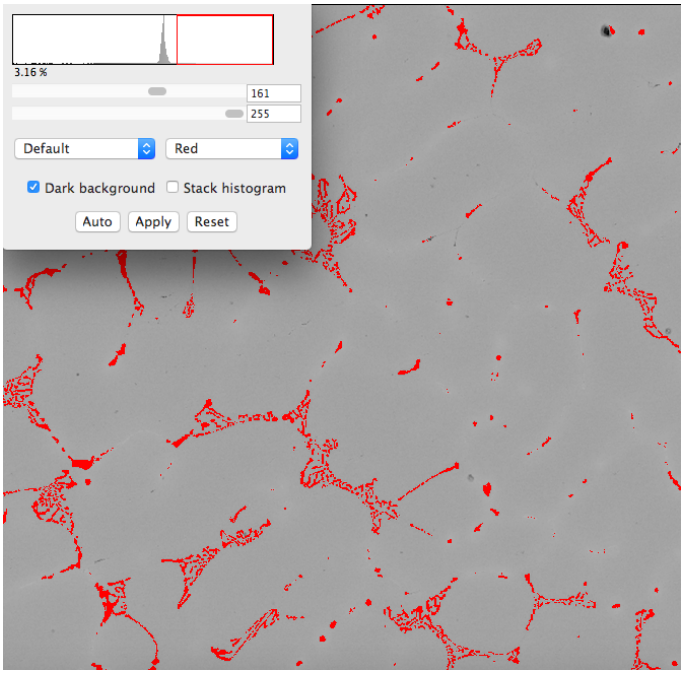


Figure C.5: Incinerator metal + Recycled salt 1 (3.16% of red phase)

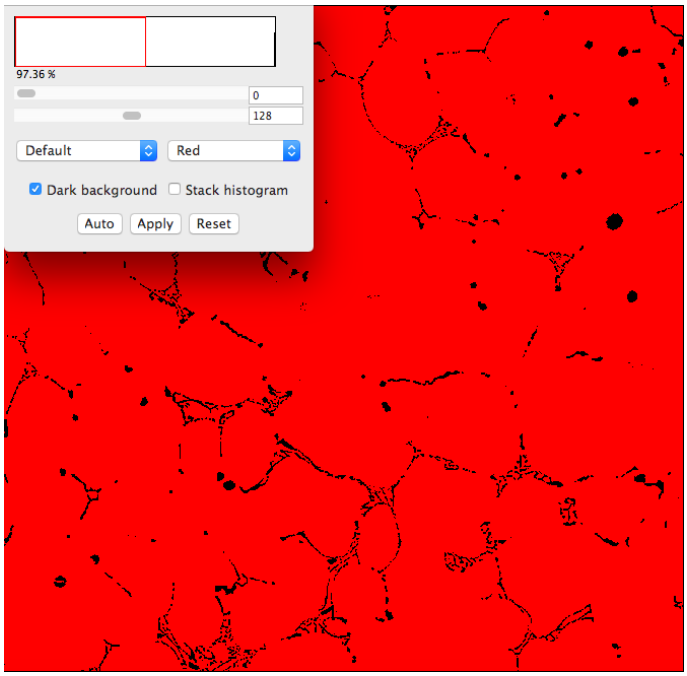


Figure C.6: Incinerator metal + Recycled salt 2 (97.36% of red phase)

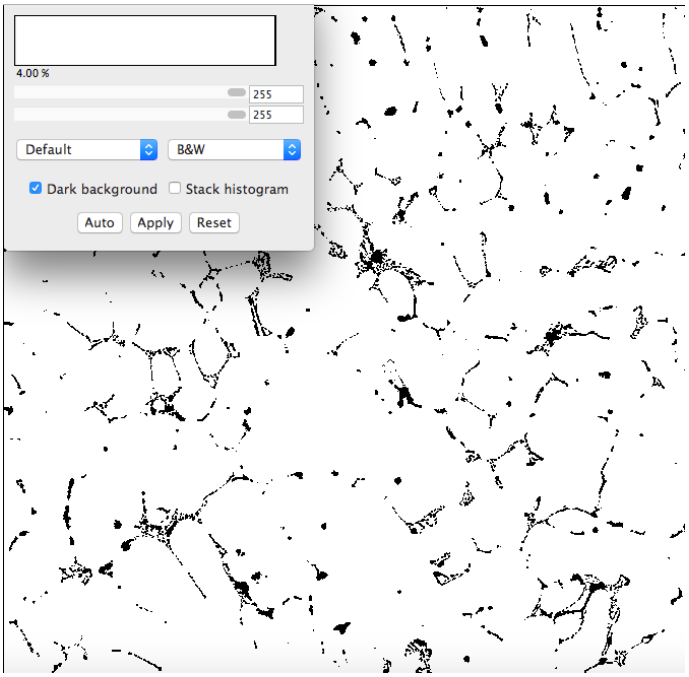


Figure C.7: Incinerator metal + Industrial salt 1 (4.00% of black phase)

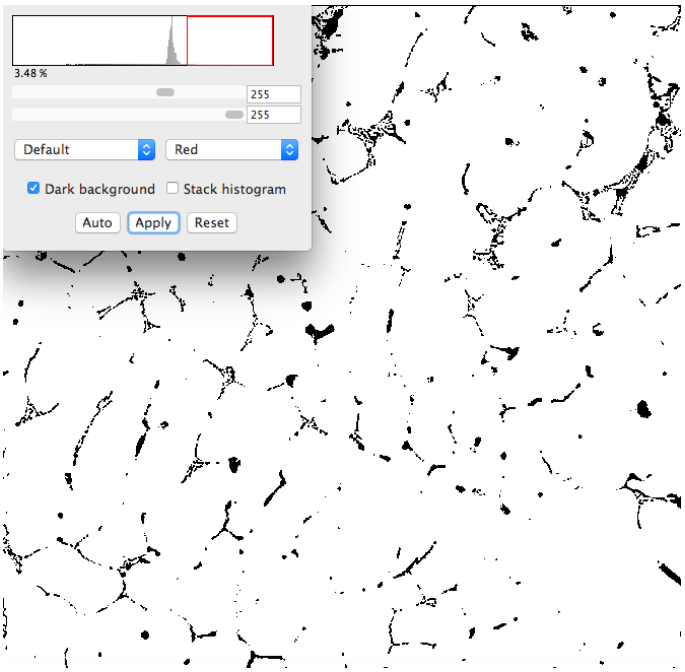


Figure C.8: Incinerator metal + Industrial salt 2 (3.48% of black phase)

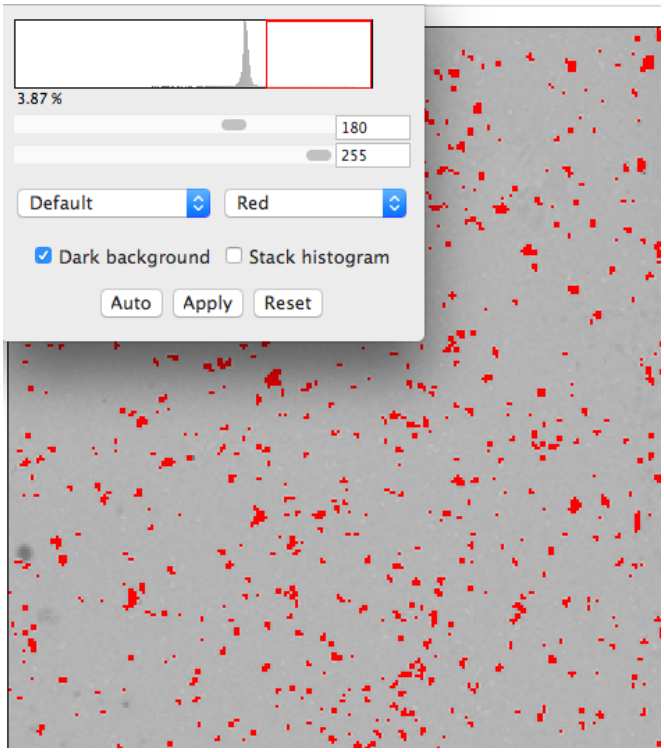


Figure C.9: UBC raw material (3.87% of red phase)

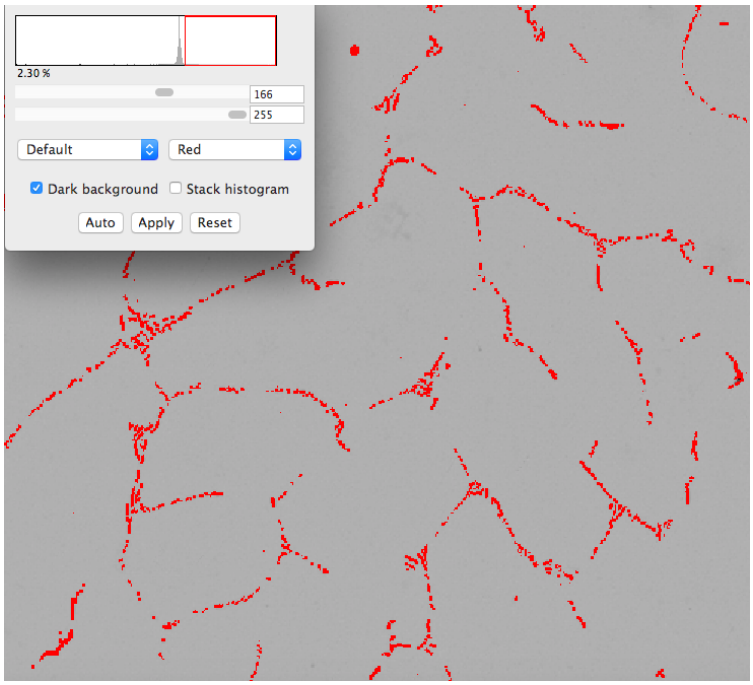


Figure C.10: Incinerator metal raw material (2.30% of red phase)

## C.2 Aluminothermic production of silicon

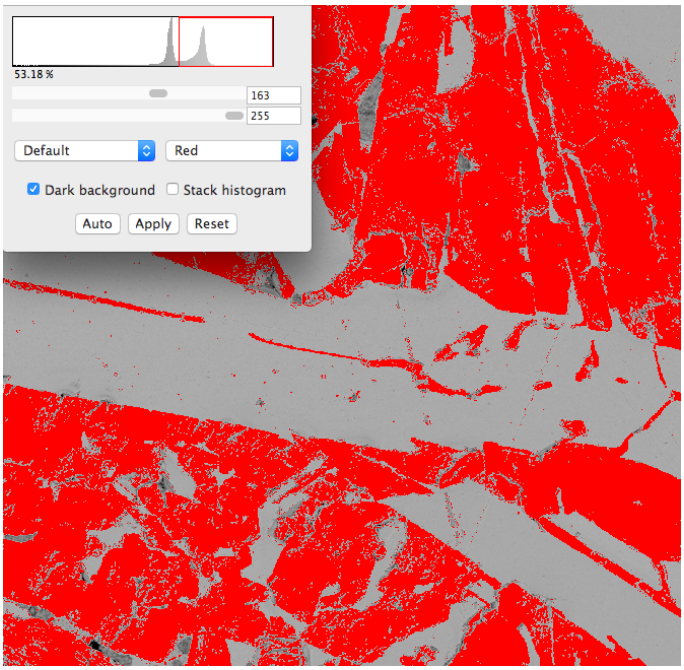


Figure C.11: Clean aluminium 1

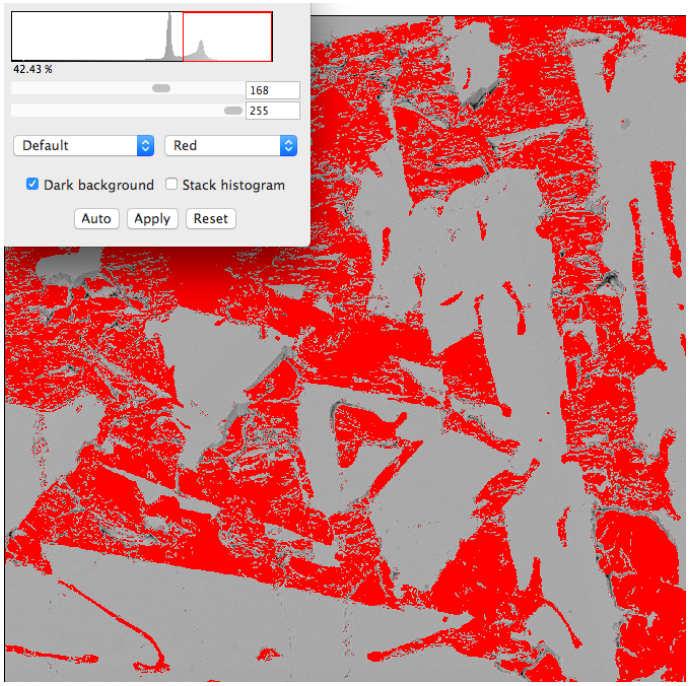


Figure C.12: Clean aluminium 2

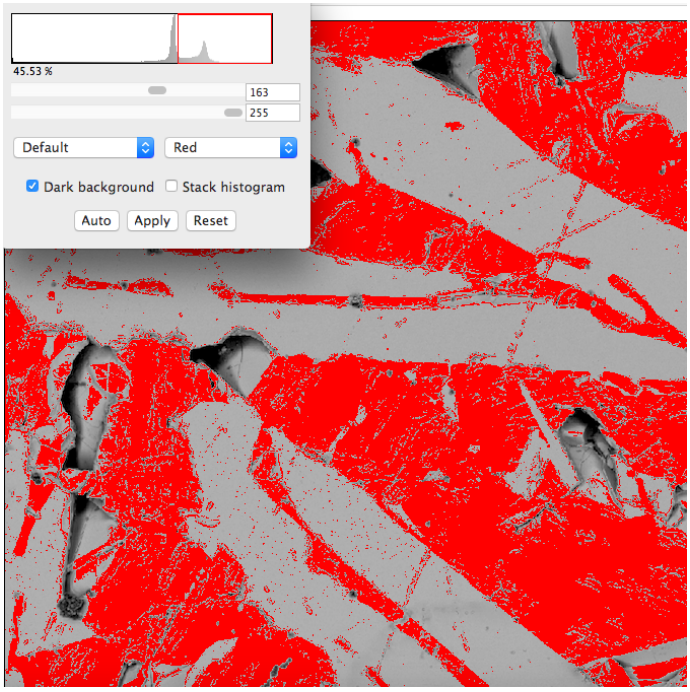


Figure C.13: Dross 1, 1

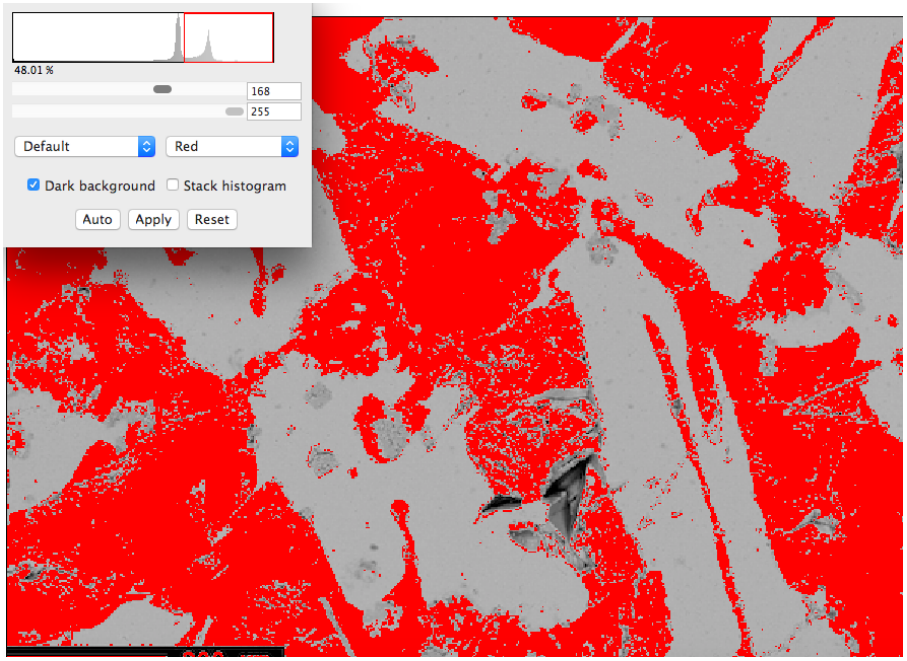


Figure C.14: Dross 1, 2

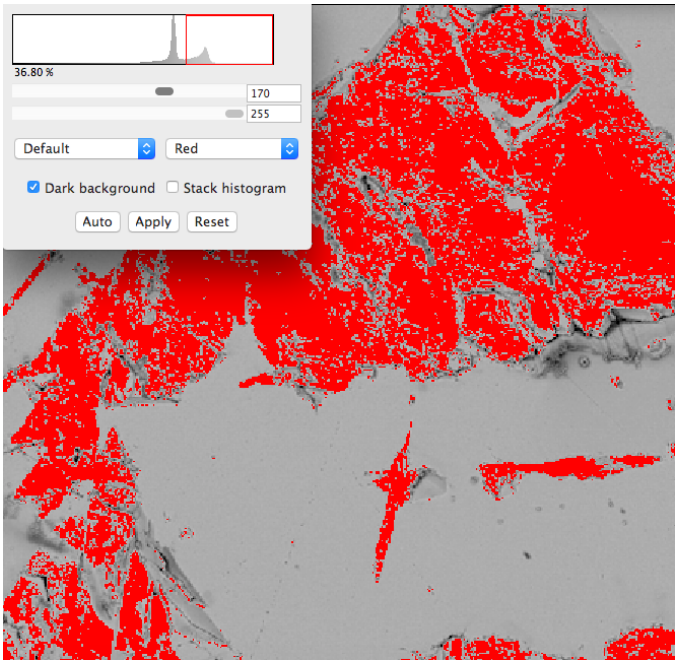


Figure C.15: Clean aluminium + Dross 1

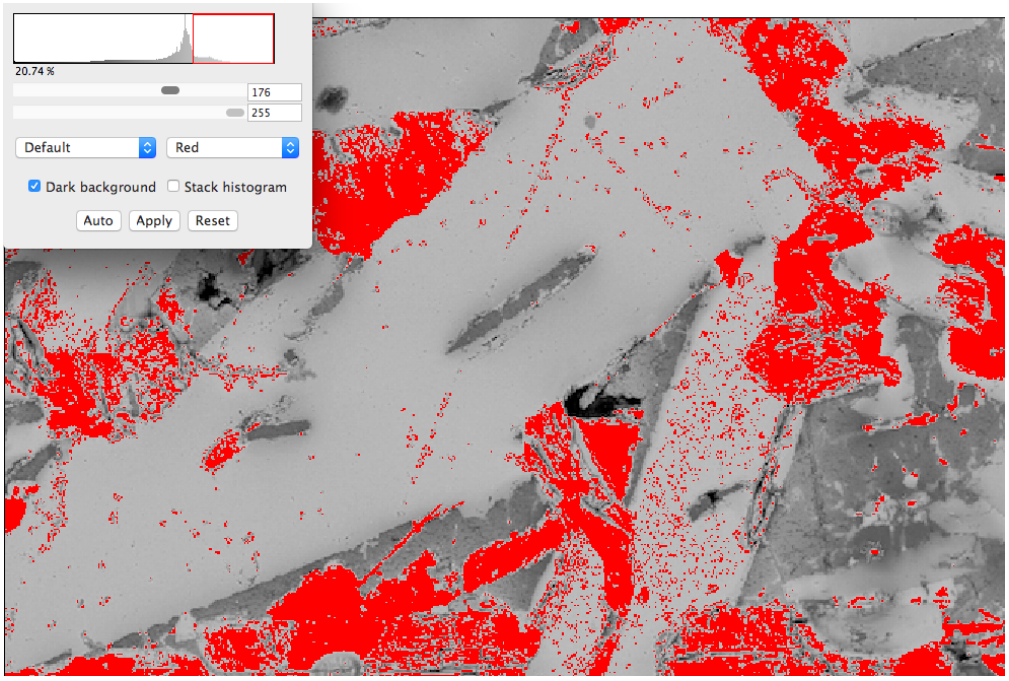


Figure C.16: Clean aluminium + Dross 2

# Appendix D

# Temperature profiles

The temperature profiles from the eight yield experiments and six aluminothermic reduction experiments are presented. It is worth noting that the temperature values are suddenly radically dropping at high temperatures for a few seconds. This is due to the fact that the graphite tube with the thermocouple was used to stir the materials, resulting in temperature fluctuations as the thermocouple is moved up to a colder region during stirring. Also in some experiments, where the temperature fluctuates up and down, the thermocouple was worn out and had to be changed.

## D.1 Yield experiments

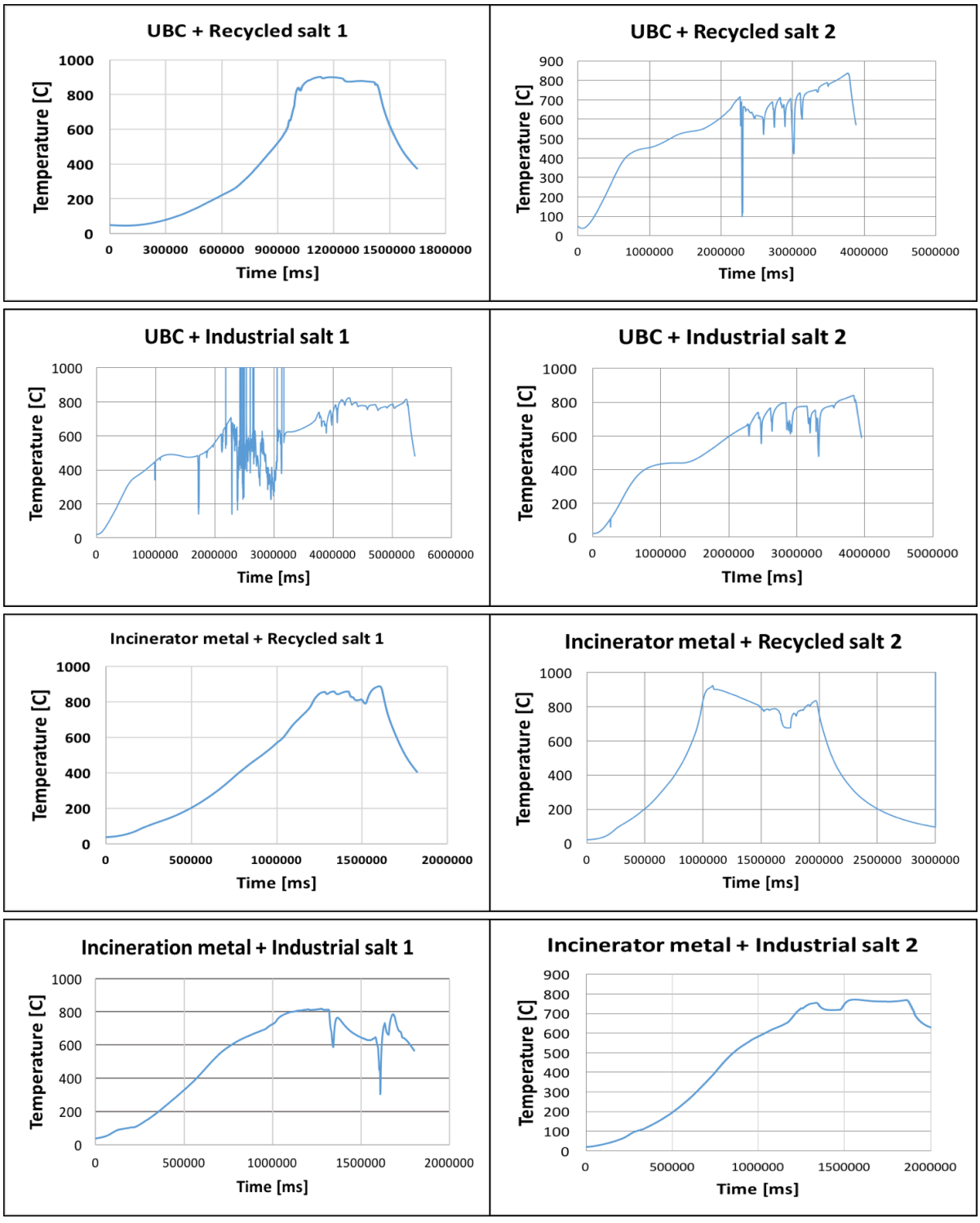

## D.2 Aluminothermic production of Si

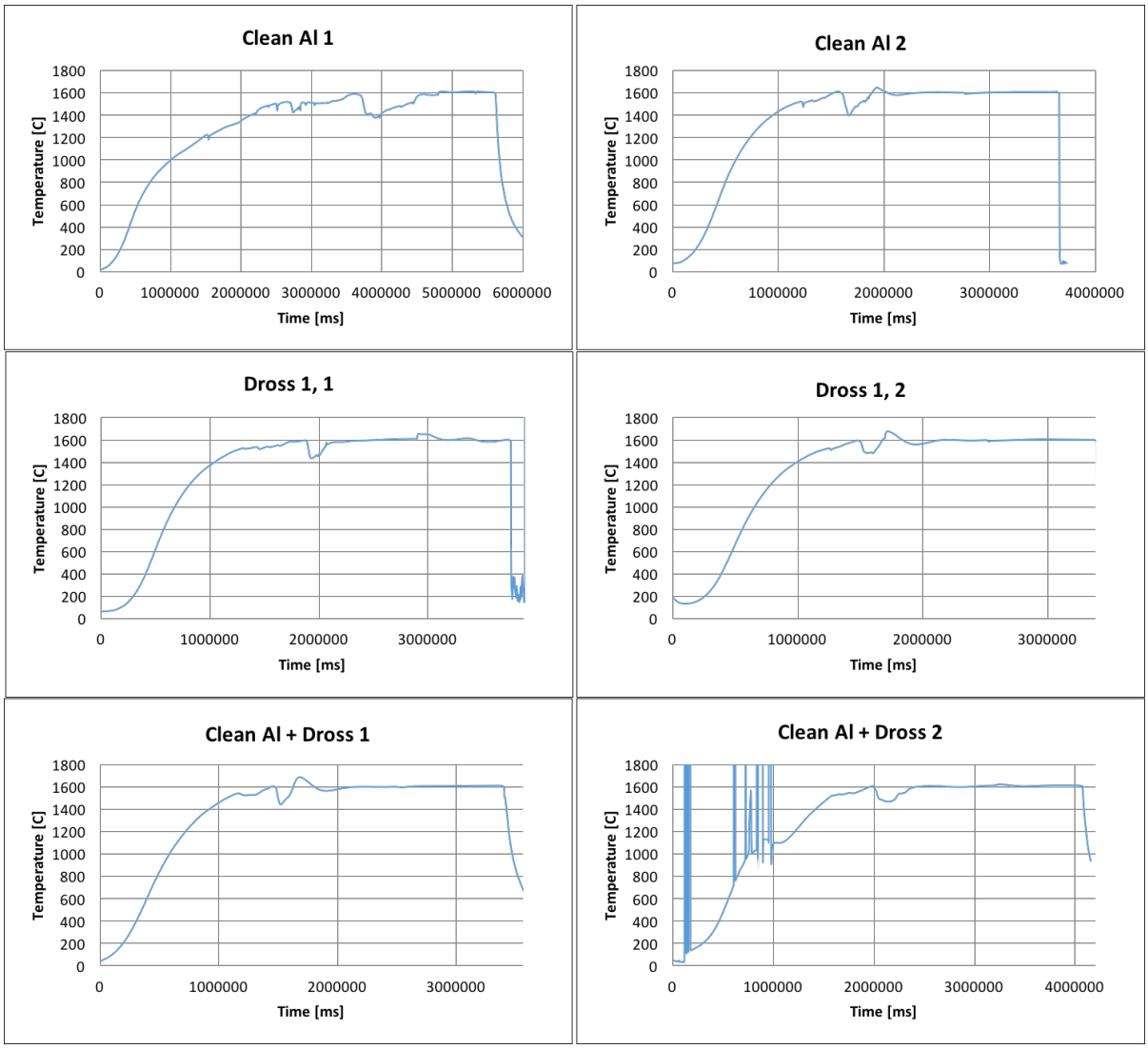

# Appendix E

# Statistical analysis

Statistical analyses on the chemical analyses from EPMA and ICP-MS were conducted. A student-t distribution with a confidence interval of 95% was used. The results are written as average values plus/minus the calculated deviation. Assuming a normal distribution of the data, the upper and lower confidence limits (UCL and LCL) can be written as follows:

$$UCL_{1-\alpha} = \overline{X}_n + t_{n-1,\frac{\alpha}{2}} * \frac{S_n}{\sqrt{n}} \tag{E.1}$$

$$LCL_{1-\alpha} = \overline{X}_n - t_{n-1,\frac{\alpha}{2}} * \frac{S_n}{\sqrt{n}} \tag{E.2}$$

Here, $\overline{X}_{\mathrm{n}}$ denotes the average value of the observations, while the t value is found from the t-distribution table. n denotes the number of observations and $\alpha$ denotes the chosen confidence interval. $S_{\mathrm{n}}$ is the standard deviation.

## Example calculation

To illustrate the how the statistical analyses were performed, the calculation of the silicon content in the dark phase using clean aluminium as the reducing matrial for aluminothermic reduction from EPMA is shown. The input data is shown in the table below. Six analyses were performed for the phases in each sample, denoted analysis number in the table.

| Analysis number | $X_1$ | $\overline{X}_1$ | $S_1$ | $X_2$ | $\overline{X}_2$ | $S_2$ |
|---|---|---|---|---|---|---|
| 1 | 96.73 | 97.05 | 0.41 | 95.55 | 96.69 | 1.03 |
| 2 | 97.37 | | | 96.86 | | |
| 3 | 96.57 | | | 96.97 | | |
| 4 | 96.72 | | | 97.49 | | |
| 5 | 97.15 | | | 98.10 | | |
| 6 | 97.74 | | | 95.17 | | |

As two parallels are analysed, the value of n is two. The average between the two parallels is 96.87, while the standard deviation is 0.307. From the t distribution table, one can find that with n = 2 and $\alpha$ = 0.05, the t value becomes 12.706.

Inserting these values into the formulas for upper and lower confidence limits, one gets that the concentration of silicon in the experiment using clean aluminium as the reducing material is 96.87 $\pm$ 2.76 according to EPMA analysis.

# Appendix F

# Various results from yield experiments

Here, the material yields and maximum temperatures for all eight yield experiments are listed in tables. The same results are presented in Figures 4.9 and 5.6.

Table F.1: Remelting experiments under a salt flux

| Exp. no. | Scrap type | Salt type | Charged scrap[g] | Weight of extracted metal [g] | Material yield [%] |
|---|---|---|---|---|---|
| 1 | UBC | Recycled | 820 | 573 | 69.9 |
| 2 | UBC | Recycled | 710 | 427 | 60.1 |
| 3 | UBC | Industrial | 746 | 627 | 84.0 |
| 4 | UBC | Industrial | 742 | 586 | 79.4 |
| 5 | I.M. | Recycled | 828 | 709 | 85.6 |
| 6 | I.M. | Recycled | 822 | 699 | 85.0 |
| 7 | I.M. | Industrial | 820 | 680 | 82.9 |
| 8 | I.M. | Industrial | 812 | 456 | 56.2 |

Table F.2: Maximum temperatures reached during yield experiments

| Exp. no. | Scrap materials | Salt type | Maximum temperature [°C] |
|---|---|---|---|
| 1 | UBC | Recycled | 902.6 |
| 2 | UBC | Recycled | 836.9 |
| 3 | UBC | Industrial | 822.3 |
| 4 | UBC | Industrial | 841.3 |
| 5 | I.M. | Recycled | 887.4 |
| 6 | I.M. | Recycled | 922.8 |
| 7 | I.M. | Industrial | 819.4 |
| 8 | I.M. | Industrial | 771.2 |

# Appendix G

# Phase transitions upon cooling

In this appendix, the modelled phase transitions from FactSage [13] upon cooling the metal and slag phase during aluminothermic reduction are presented.

## Metal phase

```
REACTION BETWEEN 1600 C AND 1315.65 C

Liquid -> CaAl4O7_solid(s)

REACTANTS
                          TOTAL CHANGE/g.atom TOTAL CHANGE/gram
Liquid                        -5.3190E-08        -1.1517E-06

PRODUCTS (Constituent 1)
CaAl4O7_solid(s)
                                  TOTAL AMT/g.atom TOTAL AMT/gram
                                     5.3150E-08      1.1516E-06

CONSTITUENTS AND PHASES AT 1315.65 C

CONS. PHASE                       TOTAL AMT/g.atom TOTAL AMT/gram
  1   1 CaAl4O7_solid(s)             5.3150E-08      1.1516E-06
TOTAL:                              5.3150E-08      1.1516E-06

                                  TOTAL AMT/g.atom TOTAL AMT/gram
CaAl4O7_solid(s)                    5.3150E-08      1.1516E-06

REACTION BETWEEN 1315.65 C AND 971.82 C

Liquid -> Si_diamond_A4(s)

REACTANTS
                          TOTAL CHANGE/g.atom TOTAL CHANGE/gram
Liquid                        -2.0309E+00        -5.7038E+01

PRODUCTS (Constituent 2)
Si_diamond_A4(s)
                                  TOTAL AMT/g.atom TOTAL AMT/gram
                                     2.0309E+00      5.7038E+01

CONSTITUENTS AND PHASES AT 971.82 C

CONS. PHASE                       TOTAL AMT/g.atom TOTAL AMT/gram
  1   1 CaAl4O7_solid(s)             5.3150E-08      1.1516E-06
TOTAL:                              5.3150E-08      1.1516E-06

  2   1 Si_diamond_A4(s)             2.0309E+00      5.7038E+01
TOTAL:                              2.0309E+00      5.7038E+01

                                  TOTAL AMT/g.atom TOTAL AMT/gram
Si_diamond_A4(s)                    2.0309E+00      5.7038E+01
CaAl4O7_solid(s)                    5.3150E-08      1.1516E-06
```

```
REACTION BETWEEN 971.82 C AND 957.49 C

Liquid -> Si_diamond_A4(s) + CaAl2O4_solid(s)

REACTANTS
                          TOTAL CHANGE/g.atom TOTAL CHANGE/gram
Liquid                        -2.3510E-02        -6.6030E-01

PRODUCTS (Constituent 3)
Si_diamond_A4(s)
                                TOTAL AMT/g.atom TOTAL AMT/gram
                                   2.3510E-02      6.6030E-01
CaAl2O4_solid(s)
                                TOTAL AMT/g.atom TOTAL AMT/gram
                                   1.6801E-09      3.7931E-08

CONSTITUENTS AND PHASES AT 957.49 C

CONS. PHASE                     TOTAL AMT/g.atom TOTAL AMT/gram
  1   1 CaAl4O7_solid(s)           5.3150E-08      1.1516E-06
TOTAL:                            5.3150E-08      1.1516E-06

  2   1 Si_diamond_A4(s)           2.0309E+00      5.7038E+01
TOTAL:                            2.0309E+00      5.7038E+01

  3   1 Si_diamond_A4(s)           2.3510E-02      6.6030E-01
  3   2 CaAl2O4_solid(s)           1.6801E-09      3.7931E-08
TOTAL:                            2.3510E-02      6.6030E-01

                                TOTAL AMT/g.atom TOTAL AMT/gram
Si_diamond_A4(s)                  2.0544E+00      5.7698E+01
CaAl2O4_solid(s)                  1.6801E-09      3.7931E-08
CaAl4O7_solid(s)                  5.3150E-08      1.1516E-06


REACTION BETWEEN 957.49 C AND 917.24 C

Liquid -> Si_diamond_A4(s) + CaSi2_C12_hR18_R-3m(s) + CaAl2Si2_P3m1(s) + CaAl4O7_solid(s)

REACTANTS
                          TOTAL CHANGE/g.atom TOTAL CHANGE/gram
Liquid                        -1.1614E+00        -3.5555E+01

PRODUCTS (Constituent 4)
Si_diamond_A4(s)
                                TOTAL AMT/g.atom TOTAL AMT/gram
                                   2.1278E-01      5.9760E+00
CaSi2_C12_hR18_R-3m(s)
                                TOTAL AMT/g.atom TOTAL AMT/gram
                                   5.2882E-01      1.6966E+01
CaAl2Si2_P3m1(s)
                                TOTAL AMT/g.atom TOTAL AMT/gram
                                   4.1984E-01      1.2613E+01
CaAl4O7_solid(s)
                                TOTAL AMT/g.atom TOTAL AMT/gram
                                   1.5971E-08      3.4603E-07

CONSTITUENTS AND PHASES AT 917.24 C

CONS. PHASE                     TOTAL AMT/g.atom TOTAL AMT/gram
  1   1 CaAl4O7_solid(s)           5.3150E-08      1.1516E-06
TOTAL:                            5.3150E-08      1.1516E-06

  2   1 Si_diamond_A4(s)           2.0309E+00      5.7038E+01
TOTAL:                            2.0309E+00      5.7038E+01

  3   1 Si_diamond_A4(s)           2.3510E-02      6.6030E-01
  3   2 CaAl2O4_solid(s)           1.6801E-09      3.7931E-08
TOTAL:                            2.3510E-02      6.6030E-01

  4   1 Si_diamond_A4(s)           2.1278E-01      5.9760E+00
  4   2 CaSi2_C12_hR18_R-3m(s)     5.2882E-01      1.6966E+01
  4   3 CaAl2Si2_P3m1(s)           4.1984E-01      1.2613E+01
  4   4 CaAl4O7_solid(s)           1.5971E-08      3.4603E-07
TOTAL:                            1.1614E+00      3.5555E+01

                                TOTAL AMT/g.atom TOTAL AMT/gram
Si_diamond_A4(s)                  2.2672E+00      6.3674E+01
CaSi2_C12_hR18_R-3m(s)            5.2882E-01      1.6966E+01
CaAl2Si2_P3m1(s)                  4.1984E-01      1.2613E+01
CaAl2O4_solid(s)                  1.6801E-09      3.7931E-08
CaAl4O7_solid(s)                  6.9121E-08      1.4976E-06
```

# Slag phase

```
REACTION BETWEEN 1600.00 C AND 1553.22 C

Slag-liq -> CaAl4O7_solid(s)

REACTANTS
                          TOTAL CHANGE/g.atom TOTAL CHANGE/gram
Slag-liq                      -1.9518E+00        -4.2289E+01

PRODUCTS (Constituent 1)
CaAl4O7_solid(s)
                                TOTAL AMT/g.atom TOTAL AMT/gram
                                   1.9518E+00      4.2289E+01

CONSTITUENTS AND PHASES AT 1553.22 C

CONS. PHASE                     TOTAL AMT/g.atom TOTAL AMT/gram
  1   1 CaAl4O7_solid(s)           1.9518E+00      4.2289E+01
TOTAL:                            1.9518E+00      4.2289E+01

                                TOTAL AMT/g.atom TOTAL AMT/gram
CaAl4O7_solid(s)                  1.9518E+00      4.2289E+01
```

REACTION BETWEEN 1553.22 C AND 1528.66 C

Slag-liq -> Melilite + CaAl4O7_solid(s)

REACTANTS

| | TOTAL CHANGE/g.atom | TOTAL CHANGE/gram |
|---|---|---|
| Slag-liq | -2.8106E+00 | -6.3054E+01 |

PRODUCTS (Constituent 2)
Melilite

| | MOLE FRACTION | MASS FRACTION |
|---|---|---|
| Ca | 1.6667E-01 | 2.9233E-01 |
| Si | 8.3333E-02 | 1.0243E-01 |
| Al | 1.6667E-01 | 1.9680E-01 |
| O | 5.8333E-01 | 4.0845E-01 |
| e(Melilite) | -5.5559E-16 | -1.3338E-20 |
| | TOTAL AMT/g.atom | TOTAL AMT/gram |
| | 1.8234E+00 | 4.1666E+01 |

CaAl4O7_solid(s)

| | TOTAL AMT/g.atom | TOTAL AMT/gram |
|---|---|---|
| | 9.8717E-01 | 2.1389E+01 |

CONSTITUENTS AND PHASES AT 1528.66 C

| CONS. | PHASE | TOTAL AMT/g.atom | TOTAL AMT/gram |
|---|---|---|---|
| 1 | 1 CaAl4O7_solid(s) | 1.9518E+00 | 4.2289E+01 |
| TOTAL: | | 1.9518E+00 | 4.2289E+01 |
| 2 | 1 Melilite | 1.8234E+00 | 4.1666E+01 |
| 2 | 2 CaAl4O7_solid(s) | 9.8717E-01 | 2.1389E+01 |
| TOTAL: | | 2.8106E+00 | 6.3054E+01 |

| | TOTAL AMT/g.atom | TOTAL AMT/gram |
|---|---|---|
| Melilite | 1.8234E+00 | 4.1666E+01 |
| CaAl4O7_solid(s) | 2.9390E+00 | 6.3678E+01 |

CONSTITUENTS AND PHASES AT 1528.66 C
(temperature of final disappearance of Slag-liq)

| CONS. | PHASE | TOTAL AMT/g.atom | TOTAL AMT/gram |
|---|---|---|---|
| 1 | 1 CaAl4O7_solid(s) | 1.9518E+00 | 4.2289E+01 |
| TOTAL: | | 1.9518E+00 | 4.2289E+01 |
| 2 | 1 Melilite | 1.8234E+00 | 4.1666E+01 |
| 2 | 2 CaAl4O7_solid(s) | 9.8717E-01 | 2.1389E+01 |
| TOTAL: | | 2.8106E+00 | 6.3054E+01 |
| 3 | 1 Melilite | 1.6857E+00 | 3.8517E+01 |
| 3 | 2 CaAl2O4_solid(s) | 3.6517E+00 | 8.2444E+01 |
| 3 | 3 CaAl4O7_solid(s) | 3.5777E-01 | 7.7517E+00 |
| TOTAL: | | 5.6951E+00 | 1.2871E+02 |